UNIVERSITY OF CALIFORNIA, SAN DIEGO

Functionally Labeled Polymers And Nanoparticles: Synthetic Strategies And *In Vivo* Analysis

A dissertation submitted in partial satisfaction of the requirements for the degree Doctor of Philosophy

in

Chemistry

by

Lyndsay M. Randolph

Committee in charge:

Professor Nathan C. Gianneschi, Chair
Professor Robert F. Mattrey
Professor Michael J. Sailor
Professor James K. Whitesell
Professor Jerry Yang

2014

The Dissertation of Lyndsay M. Randolph is approved, and it is acceptable in quality and form for publication on microfilm and electronically:

_____

_____

_____

_____

_____

Chair

University of California, San Diego

2014

DEDICATION

For my parents and Geoffrey Show.

TABLE OF CONTENTS

LIST OF SYMBOLS AND ABBREVIATIONS

^{13}C-NMR	Carbon nuclear magnetic resonance
^{1}H NMR	Proton nuclear magnetic resonance
A	Alanine (amino acid)
α	Alpha
Å	Ångström; 10^{-10} m
A_{λ}	Absorbance at wavelength λ
Ac	Acetyl
ACN	Acetonitrile
AFM	Atomic force microscopy
BF-STEM	Bright field scanning transmission electron microscopy
br	Broad peak (NMR)
C	Concentration (Beer's Law)
C57Bl/6	Inbred strain of black laboratory mice
CAC	Critical aggregation concentration
CD	β-cylodextran
CMC	Critical micelle concentration
Cy5	2-[(1E,3E,5Z)-5-(1,3-dihydroindol-2-ylidene)penta-1,3 dienyl]-3H-indol-1-ium, Cyanine dye
δ	Chemical shift; ppm
d	Doublet (NMR)

D–A	Donor-Acceptor
DABCYL	[4 - ((4 - (dimethylamino)phenyl)azo)benzoic acid]
DCC	N,N'-dicyclohexylcarbodiimide
DCM	Dichloromethane
dd	Doublet of doublets (NMR)
D_h	Hydrodynamic diameter
DIPEA	*N,N*-Diisopropylethylamine
DLS	Dynamic light scattering
DMF	Dimethylformamide
DMSO	Dimethylsulfoxide
DNA	Deoxyribonucleic acid
DOTA	1,4,7,10-tetraazacyclododecane-1,4,7,10-tetraacetic acid
DOX	Doxorubicin
DP	Degree of polymerization
DTPA	Diethylenetriaminepentaacetic
ε	Extinction coefficient
Ebes	4-((2-(2-(2-aminoethoxy)ethoxy)ethyl)amino)-4-oxobutanoic acid
EDANS	(5-((2-Aminoethyl)amino)naphthalene-1-sulfonic acid)
EDCI	1-Ethyl-3-(3-dimethylaminopropyl)carbodiimide
EDS	Energy dispersive X-ray spectroscopy
EG	End group
Em	Emission

ESI-MS	Electrospray ionization mass spectrometry
EtOAc	Ethyl acetate
EtOH	Ethanol
EVE	Ethyl vinyl ether
Ex	Excitation
F	Phenylalanine (amino acid)
FA	Folic acid
FDA	Food and Drug Administration
FMN	Fibril micellar nanoparticle
Fmoc	Fluorenylmethyloxycarbonyl
FRET	Förster resonance energy transfer
G	Glycine
Gd or Gd^{3+}	Gadolinium
Gd-DTPA	Gadolinium-diethylenetriaminepentaacetic
Gd-DOTA	Gadolinium-1,4,7,10-tetraazacyclododecane-1,4,7,10-tetraacetic acid
Gd-DOTA-MA	Gd-1,4,7,10-tetraazacyclododecane-1,4,7,10-tetraacetic monomethyl amide
Gly	Glycine
GOx	Glucose oxidase
HAADF-STEM	High angle annular dark field scanning transmission electron microscopy
HATU	(1-[Bis(dimethylamino)methylene]-1H-1,2,3-triazolo[4,5-b]pyridinium 3-oxid hexafluorophosphate)

HBTU	*N,N,N',N'*-Tetramethyl-O-(1H-benzotriazol-1-yl)uronium hexafluorophosphate
HeLa	Cervical cancer cell line
HPLC	High performance liquid chromatography
HRMS	High resolution mass spectrometry
HT-1080	Fibrosarcoma cell line
I	Intensity
ICP-MS	Inductively coupled plasma mass spectrometry
ICP-OES	Inductively coupled plasma optical emission spectrometry
IP	Intraperitoneal
IS	Inner hydration sphere
IV	Intravenous
K	Lysine (amino acid)
KB	Oral carcinoma cell line
k_{ex}	Water exchange rate
λ	Wavelength
L	Leucine (amino acid)
LRMS	Low resolution mass spectrometry
m	Multiplet (NMR)
MBHA	4-Methylbenzhydrylamine
MeOD	Deuterated methanol
MeOH	Methanol
MHz	Megahertz

mM	millimolar
µM	micromolar
MMP	Matrix metalloproteinase
M_n	Number average molecular weight
MRI	Magnetic resonance imaging
MTT	3-(4,5-dimethylthiazol-2-yl)-2,5-diphenyltetrazolium bromide
MWCO	Molecular weight cut off
M_w/M_n	Polymer dispersity (weight average molecular weight/number average molecular weight)
m/z	Mass-to-charge ratio
na	Not applicable
NHS	*N*-hydroxysuccinimide
NMR	Nuclear magnetic resonance
NMRD	Nuclear magnetic resonance dispersion
Norb	Norbornene
NP(s)	Nanoparticle(s)
OAc	Acetate
OEG	Oligoethylene glycol
OS	Outer hydration sphere
P	Proline
PAA	Poly-(acrylic acid)
PBS	Phosphate buffered saline
PCL	Poly-(ε-caprolactone)

PDI	Poly dispersity index
PEG	Poly-(ethylene glycol)
PEI	Poly-(ethyleneimine)
PEO	Poly-(ethylene oxide)
PET	Positron emission tomography
PHPMA	Poly-(methacrylamide)
PLA	Poly-(lactide)
PLG	Poly-($_{L}$-glutamic acid)
PLGA	Poly-($_{D,L}$-lactide-co-glycolide)
PMA	Poly-(methyl acrylate)
PMI	Perylene monoidimide
POEGMA	Poly-(oligo(ethylene glycol) monomethyl ether methacrylate)
PPA(s)	Peptide polymer amphiphile(s)
PPE	Poly-(p-phenyleneethylene)
ppm	Parts per million
PPS	Poly-(propylene sulfide)
P(*r*)	Probability function
Pro	Proline
r	Mean distance between fluorophores
R_0	Förster distance between donor and acceptor
r_1	Longitudinal relaxation rate equal to reciprocal of T_1 relaxation time multiplied by the inverse of Gd^{3+} concentration in mM

r_{1p}	Proton relaxation rate (NMRD)
RI	Refractive index
ROMP	Ring opening metathesis polymerization
RP-HPLC	Reverse phase high performance liquid chromatography
rt	Room temperature
s	Singlet (NMR)
SBM	Solomon-Bloembergen-Morgan
sec	Second
SEC-MALS	Size exclusion chromatography coupled with multi-angle light scattering
SMN	Spherical micellar nanoparticle
SP	Solvated polymer
SPECT	Single-photon emission computed tomography
STEM	Scanning transmission electron microscopy
τ_D	Lifetime decay of donor
τ_{DA}	Lifetime decay between donor and acceptor
τ_M	Residence lifetime
τ_R	Rotational correlation time
τ_{RG}	Global rotation time
τ_{RL}	Local rotational lifetime
T	Threonine (amino acid)
T	Tesla (when following a number)
T_1	Spin-spin relaxation time (longitudinal relaxation)

T_2	Spin-lattice relaxation time
t	Triplet (NMR)
TA	Termination agent
TEA	Triethylamine
TEM	Transmission electron microscopy
TFA	Trifluoroacetic acid
THF	Tetrahydrofuran
Tris	2-Amino-2-hydroxymethyl-propane-1,3-diol
UV-VIS	Ultraviolet-visible
V	Valine (amino acid)

LIST OF FIGURES

LIST OF TABLES

ACKNOWLEDGMENTS

I would like to acknowledge the chair of my committee, Professor Nathan Gianneschi, for all of his guidance and support throughout my graduate career. I would also like to acknowledge Dr. Matthew Thompson and Dr. Michael Hahn for all of their invaluable assistance throughout the last five and a half years. Without them, my research would have taken much longer to complete. Additionally, I would like to recognize the rest of the Gianneschi lab, past and present, for all of their support. My fellow lab members have taught me a great deal about becoming a research scientist and a better person. Lastly, I want to thank all of my friends and family for their support and understanding.

Chapter 1, in part, is a reprint of Randolph, Lyndsay M., Chien, Miao-Ping, and Gianneschi, Nathan C. “Biological stimuli and biomolecules in the assembly and manipulation of nanoscale polymeric particles.” *Chem. Sci.* ***3,*** 1363-1380 (2012). The dissertation author was the primary author of this paper.

The material in chapter 2, in part, is a reprint of Hahn, Michael E., Randolph, Lyndsay M., Adamiak, Lisa, Thompson, Matthew P. and Gianneschi, Nathan C. “Polymerization of a peptide-based enzyme substrate.” *Chem. Commun.* **49**, 2873-2875 (2013). The dissertation author was the secondary author of this paper.

Chapter 3, in full, is a reprint of the material as found in Thompson, Matthew P., Randolph, Lyndsay M., James, Carrie R., Davalos, Ashley N., Hahn, Michael E., and Gianneschi, Nathan C. “Labelling polymers and micellar

nanoparticles via initiation, propagation and termination with ROMP." *Polym. Chem.* **5**, 1954-1964 (2014). The dissertation author is the secondary author of this publication.

Chapter 4, in part, and chapter 5, in full, has been submitted for publication: Randolph, Lyndsay M., LeGuyader, Clare L. M., Hahn, Michael E., Andolina, Christopher M., Mattrey, Robert F., Millstone, Jill E., Botta, Mauro, Scadeng, Miriam, and Gianneschi, Nathan C. "*In Vivo* MRI reveals Morphology Dependent Biodistribution of Nanoparticles Versus Small Molecule Contrast Agents." *submitted* (2014). The dissertation author is the primary author of this manuscript.

VITA

Education

University of California, San Diego 2014
Doctor of Philosophy, Chemistry
Advisor: Assistant Professor Nathan C. Gianneschi

University of California, San Diego 2010
Master of Science, Chemistry
Advisor: Assistant Professor Nathan C. Gianneschi

University of California, San Diego 2006
Bachelor of Science, Chemistry

Professional Experience

Graduate Student Researcher
University of California, San Diego, La Jolla, CA 2008 - 2014
Research Experience:

- Synthesized and characterized small molecule dyes and contrast agents
- Synthesized and characterized complex polymers and polymeric nanomaterials
- Characterized small molecules, polymers and nanomaterials using HPLC, NMR, ESI, MALDI size exclusion chromatography multi-angle light scattering (SEC-MALS), static light scattering (SLS), dynamic light scattering (DLS), and transmission electron microscopy (TEM)
- Studied assembly behavior of nanomaterials *via* Förster resonance energy transfer (FRET, fluorescence lifetime and spectroscopy) and changes in T_1 relaxation with nuclear magnetic resonance (NMR) spectroscopy and/or magnetic resonance imaging (MRI)
- Developed novel MRI contrast agents and studied them *in vitro* utilizing 3T and 7T MRI instruments and *in vivo* in mouse models using a 7T MRI scanner

Teaching Experience:

- Assisted in writing syllabi, quizzes, and lecture plans for introductory organic chemistry laboratories and lectures
- Tutorial Instructor for Introductory Organic Chemistry (Winter 2009), Organic Chemistry II: Methods of Analysis and Chemistry of Hydrocarbons and Carbonyls (Spring 2009), Honors Organic Chemistry (Winter 2011)
- Laboratory Instructor for Introductory Organic Chemistry (Fall 2008, Fall 2009)

Laboratory Analyst
Air Toxics Ltd., Folsom, CA 2007 – 2008

- Performed analyses of volatile organic or semi-volatile organic air samples using GC/MS instrumentation
- Generated data reports for clients
- Trained employees in standard preparation and instrumentation for GC/MS air analysis

Research Assistant
Pfizer Pharmaceuticals, La Jolla, CA 2006 – 2007

- Responsible for the synthesis, purification, and characterization of small molecules as part of a multidisciplinary project team in the antiviral department
- Working knowledge of proton and carbon NMR, TLC, FTIR, GC, LC/MS, UV/VIS, HPLC, rotovap, microwave, biotage, and chromatotron
- Performed research on new and competitive synthetic strategies

Publications

1. L. M. Randolph, C. L. M. LeGuyader, M. E. Hahn, C. M. Andolina, R. Mattrey, J. E. Millstone, M. Botta, M. Scadeng, and N. C. Gianneschi. *In Vivo* MRI reveals Morphology Dependent Biodistribution of Nanoparticles Versus Small Molecule Contrast Agents. *Submitted.* 2014
2. M. P. Thompson, L. M. Randolph, C. R. James, A. N. Davalos, M. E. Hahn, and N. C. Gianneschi. Labeling Polymers and Micellar Nanoparticles via Initiation, Propagation and Termination with ROMP. *Polym. Chem.,* **2014,** *5,* 1954.
3. M. E. Hahn, L. M. Randolph, L. Adamiak, M. P. Thompson, and N. C. Gianneschi. Polymerization of a peptide-based enzyme substrate. *Chem. Commun.* **2013**, *49*, 2873.
4. L. M. Randolph, M.-P. Chien and N. C. Gianneschi. Biological stimuli and biomolecules in the assembly and manipulation of nanoscale polymeric particles. *Chem. Sci.*, **2012**, *3*, 1363.

Conference Presentations

1. L. M. Randolph, C. L. M. LeGuyader, M. E. Hahn,* C. M. Andolina, R. F. Mattrey, J. E. Millstone, M. Botta, M. Scadeng, and N. C. Gianneschi*. Head-to-Head Comparison of Fibromicellar, Spherical micellar, Polymeric and Small Molecule MRI-Contrast Agents. Oral Presentation, TechConnect World Conference and Expo 2014, National Harbor, MD, June 16 - 18, 2014.
2. L. M. Randolph, M. P. Thompson, M. E. Hahn, C. M. LeGuyader, C. R. James, and N. C. Gianneschi*. MRI agent- and fluorophore-labeled

polymers and polymeric micellar nanoparticles. Oral Presentation, 245th ACS National Meeting, New Orleans, LA, April 7-11, 2013.

3. L. M. Randolph, M. P. Thompson, C. R. James, A. N. Davalos, M. E. Hahn, and N. C. Gianneschi*. Initiation, polymerization, and termination strategies in the formation of highly functionalized fluorescent polymers and polymeric nanoparticles. Poster Presentation, 245th ACS National Meeting, New Orleans, LA, April 7-11, 2013
4. L. M. Randolph, M. P. Thompson, M. E. Hahn, M. Botta, C. R. James, A. N. Davalos, N. C. Gianneschi*. Labeled Polymeric Micellar Nanoparticles. Poster presentation, Warwick 2012, "The Polymer Conference," Warwick, UK, July 9 – 12, 2012.
5. L. M. Randolph, M. E. Hahn, M. P. Thompson, N. C. Gianneschi*. Protease-Directed Manipulation of Micellar Architectures Using Peptide-Polymer Amphiphiles. Oral presentation, 243rd ACS National Meeting, San Diego, CA, March 25 – 29, 2012.
6. L. M. Randolph, M. P. Thompson, C. R. James, A. N. Davalos, N. C. Gianneschi*. Dye-Labeled Polymeric Micellar Nanoparticles. Poster Presentation, 243rd ACS National Meeting, San Diego, CA, March 25 – 29, 2012.
7. L. M. Randolph, M. E. Hahn, L. Adamiak, M. P. Thompson, N. C. Gianneschi*. Manipulation of Micellar Architectures Using Peptide-Polymer Amphiphiles. Poster Presentation, Gordon Research Conference: Colloidal, Macromolecular & Polyelectrolyte Solutions, Ventura, CA, Feb. 5 – 10, 2012.
8. L. M. Randolph, M.-P. Chien, M. P. Thompson, T.-H. Ku, N. C. Gianneschi*. Toward Nanoscale Supramolecular Switches for MRI Contrast Agents. Poster Presentation, 239th ACS National Meeting, San Francisco, CA, March 21 – 25, 2010.

Awards and Honors

1. Poster Award for Warwick 2012 "The Polymer Conference" 2012
2. Travel Award at the University of California, San Diego 2012
3. Travel Award at the University of California, San Diego 2010
4. Teaching Award at the University of California, San Diego 2008 - 2009
5. Provosts Honors at the University of California, San Diego 2006

Affiliations

Member of the American Chemical Society 2009 – present
UC San Diego Alumni Association 2006 - present

ABSTRACT OF THE DISSERTATION

Functionally Labeled Polymers And Nanoparticles: Synthetic Strategies And *In Vivo* Analysis

by

Lyndsay M. Randolph

Doctor of Philosophy in Chemistry

University of California, San Diego, 2014

Professor Nathan C. Gianneschi, Chair

In the development of labeled polymers and polymeric nanoparticles for biomedical applications, one desires synthetic approaches that allow the most direct route to incorporate functional moieties. We contend the most desirable route is *via* the direct incorporation of functional groups during the polymerization

process itself as monomers and/or chain transfer agents. In this work, we utilize ring-opening metathesis polymerization (ROMP) due to the high functional group tolerance of initiators and the ability to synthesize well-defined polymers of low dispersity and high molecular weight.

Our research group has had great success in developing peptide-polymeric nanomaterials with ROMP *via* a *graft-to* strategy for the incorporation of peptide substrates of matrix matalloproteinases (MMPs). However, this technique does not allow for complete conjugation of peptide substrates to the polymer backbone. For this reason we sought to develop peptidyl monomers that contain a MMP peptide substrate for *graft-through* polymerization. Amphiphilic block-copolymers were synthesized with the peptidyl-monomer as the hydrophilic block and slowly transitioned into water to form nanoparticles (NPs). A pilot study determined that if the peptide substrate is displayed on the shell of a polymeric nanoparticle, it no longer maintains bioactivity.

To further demonstrate the utility of labeling polymeric nanomaterials, a series of amphiphilic block copolymers end-labeled with dyes were synthesized and formulated into micellar nanoparticles. Dye monomer and chain transfer agent combinations were chosen that are known to operate either as a FRET acceptor (rhodamine) or as a quencher (DABCYL) of the donors, fluorescein and/or EDANS. Dye-labeled block copolymers were formulated into micellar nanoparticles, such that, the NP contained both a donor and acceptor. The FRET properties of mixed micellar nanoparticles were characterized by fluorescence spectroscopy and fluorescence lifetime.

Lastly, we endeavored to move toward more clinically relevant systems that utilize MRI as an imaging modality. For this reason, polymers were synthesized containing the FDA approved MRI-contrast agent gadolinium-1,4,7,10-tetraazacyclododecane-1,4,7,10-tetraacetic acid (Gd-DOTA). Gd-containing hydrophilic and amphiphilic block copolymers were synthesized that were capable of self-assembly into spherical and fibril-shaped morphologies. Utilizing a 7T MRI scanner, polymeric nanomaterials were injected into the peritoneal cavity (IP injection) of healthy C57Bl/6 mice to analyze the retention and biodistribution of these polymer materials.

1. Introduction

1.1 Background

Chemical biology involves the study of biological systems with the goal of understanding, perturbing, mimicking and interfacing with biological systems utilizing synthetic and/or semi-synthetic chemical tools. Advanced nanomaterials acting as the mediators of those types of interactions represents a new subfield within chemical biology. Indeed, living systems are replete with complex nanoscale materials and molecular self-assemblies. As such, there are a variety of natural materials that are routinely capable of programmed behavior including shape and size changes. However, in stark contrast to biological systems, programmable synthetic supramolecular and nanoscale assemblies are far behind in terms of function, structure and sophistication.[1-11] Characterizing and developing strategies for controlling structure at this challenging length scale has yielded important advances in nanoscale materials,[12-14] and yet the predictable bottom-up synthesis of soft nanomaterials remains a difficult problem. Inherently, this problem lends itself to approaches utilizing the supramolecular assembly of complex materials from simpler building blocks.

Amphiphilic systems are well suited for the development of functional supramolecular self-assemblies. A change in the chemical or physical nature of the hydrophilic portion of an amphiphile causes the formation, destruction, or morphology transition of the assemblies they form.[11,13-18] In this dissertation we describe such assemblies and our efforts to utilize complex amphiphiles to build up functional architectures for interacting with biological systems including *in vivo* imaging agents. The importance of imaging agents is to enable targeted,

selective labeling of diseased tissues, and satisfy the requirement of a visual interpretation of a disease state. Research in this field has helped us understand the behavior of synthetic nanoscale materials within biological organisms, utilizing a variety of probes such as fluorophores,[19-26] quantum dots,[21,23,24,27-32] positron emission tomography (PET) agents,[19,33,34] and/or magnetic resonance imaging (MRI) contrast agents.[19,35-37] Indeed, continuing research will also provide the optimal imaging tool to monitor such systems. The most effective approach is to covalently link an imaging agent to the self-assembled nanoscale object. In the introductory sections that follow, we describe responsive materials formed via the self-assembly of amphiphilic molecules, and their functionalization with a visual label with a focus on applications in biology and in medicine.

1.1.1 Types of Amphiphiles

Amphiphiles, molecules containing hydrophilic and hydrophobic portions, are ubiquitous in nature and include phospholipids, glycolipids, polysaccharides, and proteins. Their application in drug delivery systems is motivating research towards synthetic amphiphiles that can interface with biological molecules and tissues.[38-43] A variety of small molecules and polymeric amphiphilic structures can be synthesized with the ability to self-assemble into a variety of nanostructures.[11,13,14,38,44-48] The range of these structures vary from simple small molecule amphiphiles with one hydrophilic head and one or two hydrophobic tails[46,47] (Figure 1.1A), to more complicated systems like bolaamphiphiles[49] and gemini amphiphiles.[50,51] Bolaamphiphiles consist of two hydrophilic heads at

either end of an alkyl chain, where gemini amphiphiles consist of two polar and two apolar groups linked together by a spacer (Figure 1.1B-C).

The concept of amphiphiles also extends to polymeric systems, whereby an amphiphile can consist of multiple repeating units of a polar head group and hydrophobic moiety. Small molecule amphiphiles are limited by high critical micelle concentrations (CMCs) and rapid molecular exchange with a lower capacity for guest molecules.[46,47] In contrast, polymeric amphiphiles are capable of incorporating a wide variety of functional groups while larger polymeric chains prevent rapid molecular exchange, resulting in lower CMCs.[46] Another capability of polymeric amphiphiles is to form a linear amphiphilic system with repeating polar and apolar units (Figure 1.1D), or a brush copolymer amphiphile in which multiple repeating units contain either a polar or apolar polymer[39,47] (Figure 1.1E). Finally, hybrid polymeric amphiphiles allow for the conjugation of a synthetic polymer with biomolecules[10,11,40] and/or inorganic material.[52,53]

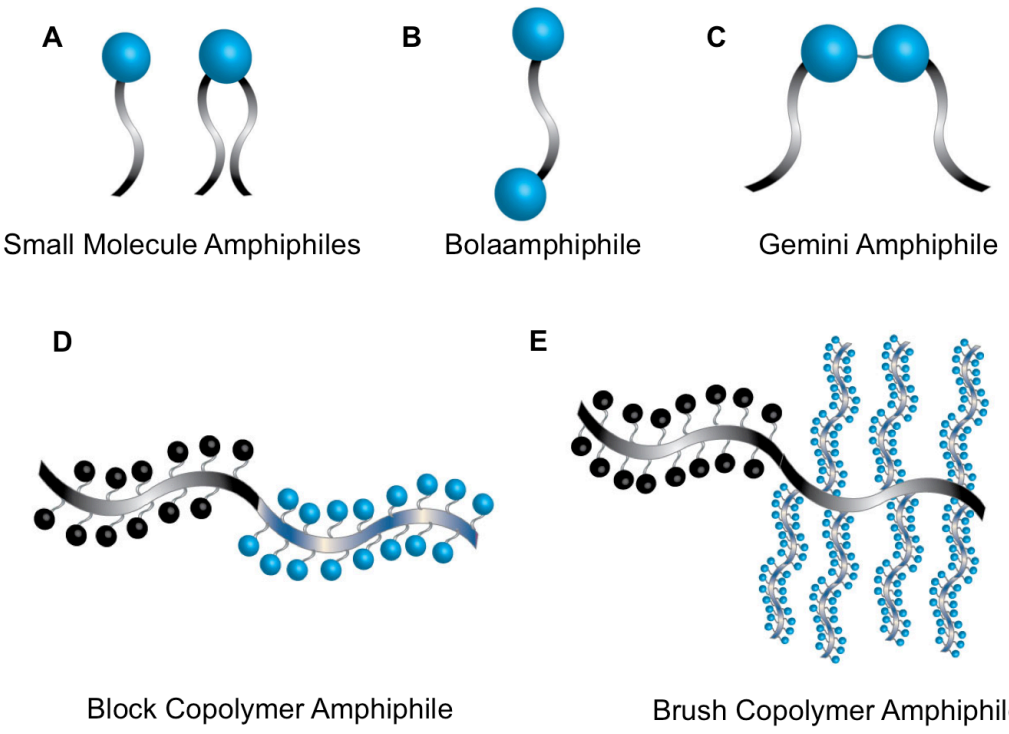

Figure 1.1 Structure of amphiphiles capable of self-assembly to generate nano- and microscale particles of various morphologies. A) Small molecule amphiphile with one polar head group (blue sphere) and a hydrophobic tail (gray ribbon) or two hydrophobic tails. B) Bolaamphiphile with two polar head groups connected by one hydrophobic linker. C) Gemini amphiphile with two polar head groups and two hydrophobic tails connected by a small linker. D) Block copolymer amphiphile with repeating units of a hydrophobic moiety (black spheres) and repeating units of a polar head group (blue spheres). E) Brush copolymer amphiphile with repeating units of a hydrophobic moiety and repeating units of another hydrophilic polymeric material.

1.1.2 Potential Roles of Morphologies from Self-Assembled Amphiphiles in Biomedical Applications

The controlled self-assembly of amphiphiles is well established in biological systems. However, the synthetic reproduction of this mechanism is a

task requiring some effort. Predictability over amphiphilic self-assembly in order to obtain an optimal morphology is integral to innovation in biological applications. One can obtain a variety of morphologies from the self-assembly of amphiphiles such as spherical micelles, vesicles, toroids, and cylindrical micelles (Figure 1.2).[13,54-56] The morphologies of polymeric amphiphiles is dependent on the ratio of hydrophobic to hydrophilic bulk in a single amphiphile.[13]

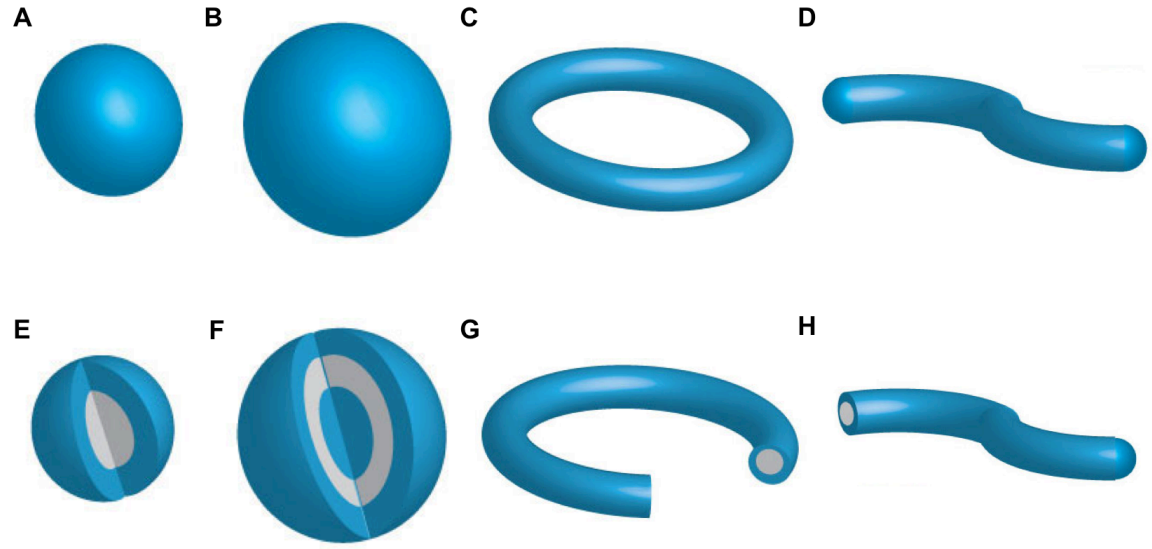

Figure 1.2 Types of three-dimensional architectures formed from the self-assembly of amphiphiles. A) Spherical micelle, B) spherical vesicle, C) toroidal micelle, D) cylindrical micelle, E) cross-section of spherical micelle F) cross-section of spherical vesicle, G) cross-section of toroidal micelle, H) cross-section of cylindrical micelle. Color code: blue represents hydrophilic corona, and grey represents hydrophobic core.

Well-defined nanomaterials are critical when moving towards biomedical applications, as is the generation of a label in order to track the materials. In terms of particle size effects, the enhanced permeability and retention (EPR) effect plays a role in the fate of nanoparticles once they have entered the blood

stream.[57-60] While this is a well-documented effect, other parameters are less well understood. This includes the role of morphology on blood circulation times, clearance mechanism, and cellular uptake rates. The seminal work of Discher and colleagues examined the effect of morphology on cellular uptake and pharmacokinetics.[61,62] An initial comparison of spherical micelles, cylindrical micelles and vesicles on circulation time led to the discovery that cylindrical shaped micelles have longer circulation times than spherical and vesicular shaped counterparts. The length of the cylinder accounts for the duration of circulation with shorter cylinders eluting faster than longer cylinders. In the case of spherical shaped nanoparticles, rapid cellular uptake was seen but this was not seen in the case of cylindrical shaped nanoparticles. The research of Mitragotri and colleagues explains that the physical orientation of cylindrical shaped particles when approaching a cell is critical in phagocytosis.[63] If the cylinder approaches from the side, it is more difficult for cells to endocytose the material. If the cylinder approaches head on, the cylindrical nanoparticle has a greater chance of endocytosis.

In combination, a picture develops illustrating the importance of controlling morphological parameters in the design of functional nanoscale and microscale materials designated for *in vivo* use. The following dissertation details our attempts to control these parameters and to test shape and size dependent properties of nanoscale imaging agents in animal models. Thus, the remainder of this chapter focuses on self-assembled polymeric nanomaterials for biological applications, and includes morphology effects, manipulation of materials with a

variety of biologically applicable stimuli, and labeling strategies to examine *in vitro* and *in vivo* assays for biologically relevant materials. The chapter is broken into two main sections 1) the use of biological stimuli in the assembly or manipulation of polymeric nanoparticles and 2) integration of visual labels into polymeric nanomaterials for *in vivo* applications. We shall provide a broad overview of research in the field of labeled polymeric nanoparticles assembled primarily of functionalized amphiphiles and well-defined nanomaterials designed with biologically relevant applications in mind.

1.2 Biological stimuli and biomolecules in the assembly and manipulation of nanoscale polymeric particles

Biomolecules are attractive as synthons in the preparation of complex synthetic materials. The advantage of such an approach is that with the incorporation of biomolecules, one can impose evolutionarily derived properties on artificial structures. Therefore, biohybrid materials possess the potential to respond to natural biochemical signals, including those associated with certain disease states via dramatic switches in their physical morphology and/or chemical structure.[10] In a biological context, morphology transitions are common responses to patterns of specific stimuli enabling many of the processes necessary for life. The expectations for the synthetic mimicking and understanding of nanomaterials that can undergo changes in morphology in response to stimuli reach far and wide. Hence, the preparation of nanostructured, semi-synthetic and biohybrid materials may have future utility in applications not

traditionally accessible to biological systems. Inherent to biological molecules are desirable properties, such as order at the nanometer length scale and well-defined patterns of selective recognition elements.

Polymeric amphiphiles are well suited for the development of functional supramolecular systems, as changes in the chemical or physical nature of the hydrophilic portion of an amphiphile lead to formation, destruction, or morphology transition of the assemblies.[11,13-18] A significant body of research have described efforts to trigger and manipulate the morphology of discrete assemblies of amphiphiles[15] utilizing stimuli such as pH,[64,65] temperature,[66] small molecules or ions,[67,68] enzymes,[6,69,70] and light.[71,72] In turn, the focus has grown on systems capable of responding to stimuli inherent to biological systems such as enzymatic reactions[6,69,70,73,74], protein expression patterns,[75-77] DNA sequences,[78-80] and cell-surface receptor recognition.[81,82] Biochemical stimuli constitute programmed, specific interactions of great efficiency, and, in general, are under utilized within chemical and/or biochemical applications. Future designs taking these properties into account reveals an increased utility for synthetic, stimuli-responsive nanomaterials in a multitude of arenas, including *in vivo* applications.

The use biological molecule together with synthetic polymers unites the programmability of biomolecules with the chemical diversity inherent to and enabled by synthetic organic chemistry. Biological molecules are programmed by evolution to respond to, and interact with, specific stimuli and thus their desired use in nanostructures. We now focus on biomolecules as programming tools in the assembly and manipulation of nanoscale polymeric nanoparticles and

micelles. The goal is to introduce the field through several highlighted examples for different types of materials and stimuli. We will also describe systems intended for biological applications, which utilize polymeric structures that are not biological, but are responsive to biologically relevant stimuli. Although there are a variety of stimuli-responsive nanomaterials that contain DNA,[7,79,80,83-91] peptides,[92-98] or proteins,[99-101] and are responsive to a an assortment of stimuli, these sections focus solely on amino acid containing polymers or non-biological systems that respond to enzymes. This section is split into two main portions: 1) polymeric nanoscale particles made from a combination of synthetic and amino acid moieties capable of responding to stimuli, and 2) polymeric nanoscale particles that are entirely synthetic but respond to an enzymatic stimuli. The use of biomolecular interactions to increase complexity is the main focus. Also covered are systems in which degradation mediates selective processes, for perspective. Inorganic particles programmed with biomolecules are excluded, as it is beyond the scope of this work, although comprehensive reviews are available.[102-104]

1.2.1 Enzyme Responsive Peptide-Based Polymeric Nanoparticles

Natural and non-natural amino acids offer greater chemical diversity than nucleic acids, but exhibit less predictable binding and recognition. At the same time they are susceptible to optimization via molecular evolution strategies,[105,106] and are capable of selective targeting,[107] signaling,[108-110] receptor binding,[81,82] and behaving as substrates for specific enzymes.[111,112] The incorporation of

amino acids and peptides into polymeric materials, as functional and structural building blocks, is of great interest due to the tremendous potential of making synthetic particles susceptible to the inherent biological characteristics of the peptide sequence.[113,114] Our focus shifts now to peptide-polymeric materials that take advantage of the solution properties of biohybrid architectures. Of particular interest is the process peptides undergo for coupling nanostructures to enzymatic reactions. Peptide polymeric systems that are responsive to temperature, light, pH, or dual responsive systems are excluded, as they are not relevant to this work.

Enzyme-responsive systems. Enzymes play a critical role in biology through a myriad of natural processes involving the manipulation of nanoscale self-assemblies, including the replication of nucleic acids,[115] decomposition of biomaterials which includes extracellular matrices,[116] and the assembly of viruses.[117,118] This has been the inspiration for efforts to create materials that respond to specific enzymatic triggers by building them from peptide substrates, or incorporating peptide substrates into the material. To date, the majority of research into organic enzyme-responsive systems focuses on phosphorylation, de-phosphorylation, and other enzymatic reactions of peptide-only nanostructures to control their formation.[6,119-121] We highlight the research into the utility of enzymatic reactions to control the structural characteristics of peptide–polymer conjugates.

α-Chymotrypsin is a serine protease responsible for cleavage on the C-terminal side of tyrosine, phenylalanine and tryptophan.[122] With this in mind,

Cenker and colleagues designed a peptide–polymer conjugate capable of hydrolysis upon treatment with α-chymotrypsin.[123] Conjugation of PEG_{3000} to the peptide sequence βAβAKLVFF led to the formation of spherical micelles approximately 10 nm in diameter where the peptide is contained in the hydrophobic core and PEG is located on the hydrophilic shell. After treatment with α-chymotrypsin, the enzyme cleaves between the F–F residues on the peptide leaving an F–PEG_{3000} and βAβAKLVF behind as determined by mass spectrometry. The released peptide fragment and F–PEG shows no noticeable secondary nanostructures. This example highlights the potential for delivery of therapeutic peptide fragments in response to specific enzymes.

Another enzyme with utility in stimuli responsive systems is phosphatases. Phosphatases are a class of enzyme that remove phosphoryl groups attached to serine, threonine or tyrosine residues.[122] These enzymes play a vital role in turning off signaling pathways that are activated by kinases. Borner and colleagues utilized an acid phosphatase to manipulate peptide–polymer conjugates (Figure 1.3).[124] The polymer consists of a PEO block linking to a repeating peptide segment of threonine and valine diads $(TV)_5$. This repeating segment of TV is known to form β-sheet aggregates in water.[125] The introduction of three phosphothreonine units into the $(TV)_5$ peptide aggregator results in a double hydrophilic block copolymer. Only upon dephosphorylation with an acid phosphatase is it possible to form nanofibrils.

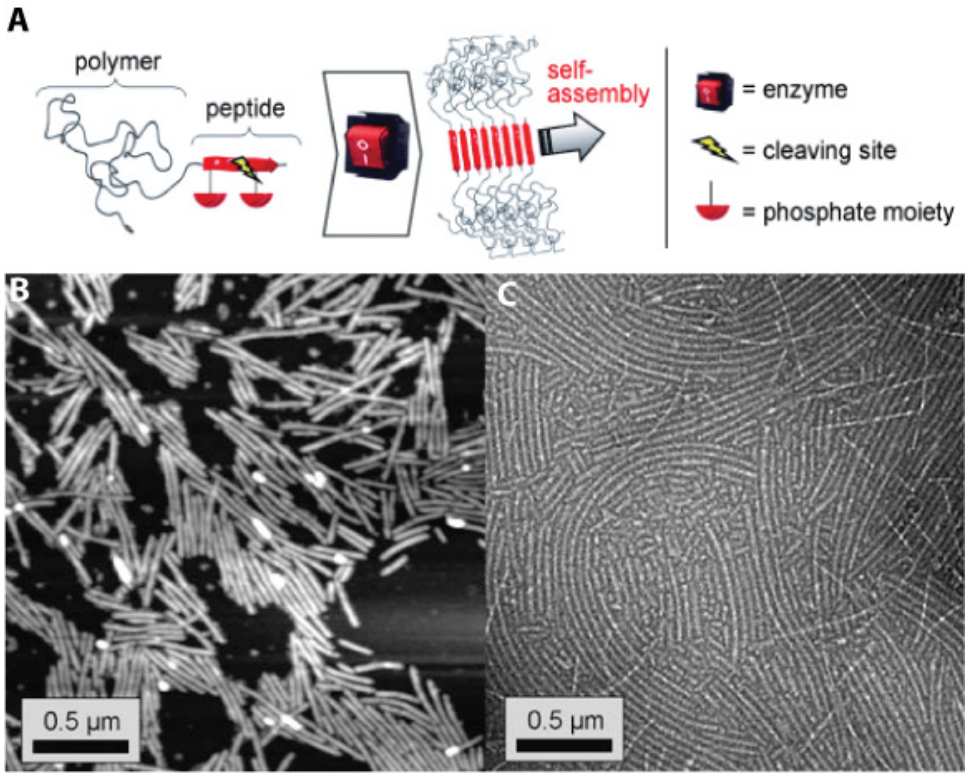

Figure 1.3 (A) Schematic representation of enzyme-switchable PEO–peptide conjugates. Microstructures formed by enzyme triggered self-assembly of PEO–peptide conjugates: (B) visualized by AFM 7 days after enzyme treatment and (C) TEM micrograph of structures stained with uranyl acetate, after 10 days. Adapted from ref. 124. Copyright 2009 Wiley- VCH Verlag GmbH & Co.

Inspired by the utility of enzymes as catalytic amplification tools and selective protagonists in natural systems, our group developed peptide–polymer amphiphiles (PPAs) capable of forming well-defined enzyme-responsive spherical micelles.[69] These micelles undergo responses to several enzymes demonstrating *in situ*, selective, reversible and user-defined shifts in micellar nanoparticle morphology. Utilizing the recognition properties of a substrate for selective enzymatic cleavage, and/or phosphorylation/dephosphorylation, one can read and manipulate information stored in the micelle shell, causing dramatic, and occasionally reversible changes in morphology and particle size.

Figure 1.4 illustrates the reversible morphological change observed for the peptide material in response to sequential phosphorylation/dephosphorylation cycles that occur in remarkably high yield.

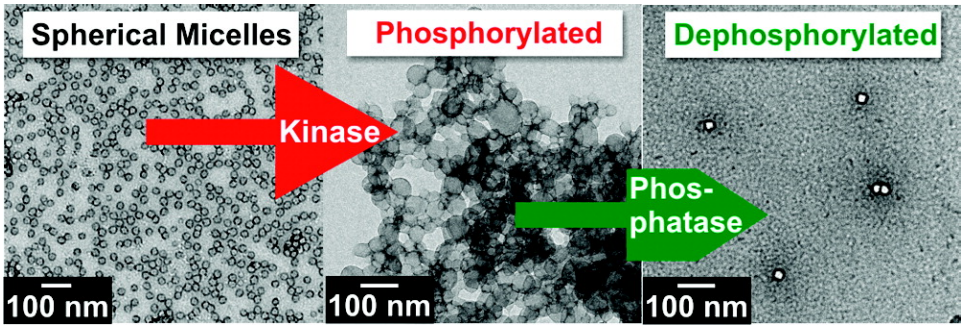

Figure 1.4 Response of peptide polymer particles to sequential additions of protein kinase A and protein phosphatase 1. Reprinted with permission from T. H. Ku, M. P. Chien, M. P. Thompson, R. S. Sinkovits, N. H. Olson, T. S. Baker and N. C. Gianneschi, J. Am. Chem. Soc., 2011, 133, 8392–8395. Copyright 2011 American Chemical Society.

1.2.2 Enzyme Responsive Nanoparticles

Stimuli-responsive polymeric nanomaterials have attracted increasing attention for biomedical applications because of the potential to switch function and release components of the material upon interaction with disease-associated signals. This section discusses fully abiotic structures that form only from synthetic polymers, and are not themselves biohybrid polymeric materials, but are nevertheless, designed to recognize biologically relevant stimuli. Included is a discussion of specific nanoscale materials and their response to enzymes. Chemical or physical stimuli endogenous to biological systems are a topic of exploration for interacting with nanoscale materials intended for biomedical applications. Such stimuli include low pH environments (as found within late

endosomes), overexpressed cell-surface receptors, excreted disease-associated enzymes, and oxidative microenvironments. We focus predominantly on systems where the enzymes induce a morphology change and/or cause an increase in complexity rather than degradation processes. Systems such as these offer several potential benefits, as opposed to degradable particles, and are described below.

The response of a material to a given stimulus constitutes a detection event. In the case of enzymatically responsive materials, these detection events are catalytic, selective, and in some cases, specific to a particular state of disease in a given tissue or cell.[116,126-131] Therefore, materials capable of responding in a dramatic fashion to enzymes may be applicable in catalytically amplified *in vitro* schemes for enzyme detection, or in selective therapeutic and/or diagnostic delivery *in vivo*. Enzymes, such as proteases, kinases, phosphatases, and oxidases, recognize proteins or peptides as substrates to catalyze various reactions. Enzymatic reactions on abiotic substrates, which result in morphology changes and catalyzed degradation of micelles and/or nanoparticles, are highlighted.

Enzymes as stimuli resulting in structural destabilization. Encapsulation of enzymes for the purpose of *in vivo* delivery within vesicles provides protection from proteases present in biological fluids and prolongs the lifetime of an enzyme by slowing the denaturation process. Incorporation of an enzyme such as glucose oxidase (GOx) may provide controlled access to the substrate and the release of payload via disruption of the barrier function within the membrane.

Hubbell, et al. described a unique system in which GOx encapsulated within PEG–PPS–PEG ((poly(ethylene glycol))–(poly(propylene sulfide))–PEG) polymersome.[132] This enzyme-loaded polymersome is permeable to glucose resulting in intravesicular formation of H_2O_2 upon generation of gluconic acid. Peroxide generation causes polymersome destabilization (Figure 1.5) and particle destruction. This enzyme-amplified approach to particle degradation has potential utility in drug delivery and the detection of biological analytes.

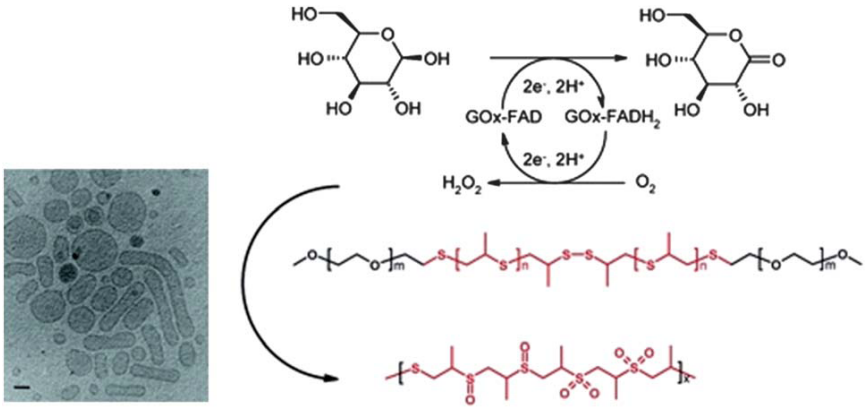

Figure 1.5 GOx-catalyzed oxidation of D-glucose to gluconolactone (gluconic acid). This results in the production of H_2O_2 in the presence of oxygen, causing an inside-out disruption in the membrane. Cryo-TEM micrograph shows the unilamellar structure of enzyme-loaded polymersomes. Scale bar = 100 nm. Adapted with permission from Langmuir, 2004, 20, 3487–3491. Copyright 2004 American Chemical Society.

Enzyme-driven assembly of nanoparticles. A range of materials, including hydrogels, have been demonstrated to undergo enzyme-driven assembly processes.[6] However, to our knowledge, there is only one example of the direct assembly of a polymeric nanoparticle or micelle in response to an enzymatic stimulus. Hawker and colleagues developed an enzyme-responsive system whereby self-assembly of purely abiotic block copolymers are triggered in the

presence of a phosphatase under physiological conditions.[70] This approach utilizes a water-soluble block copolymer consisting of monomers containing phosphate moieties and a PEG polymer. The phosphate moieties are cleaved upon addition of acid phosphatase (APase) generating an amphiphilic block copolymer *in situ* (Figure 1.6). Subsequently, the polymers aggregate to generate well-defined polymeric micelles.

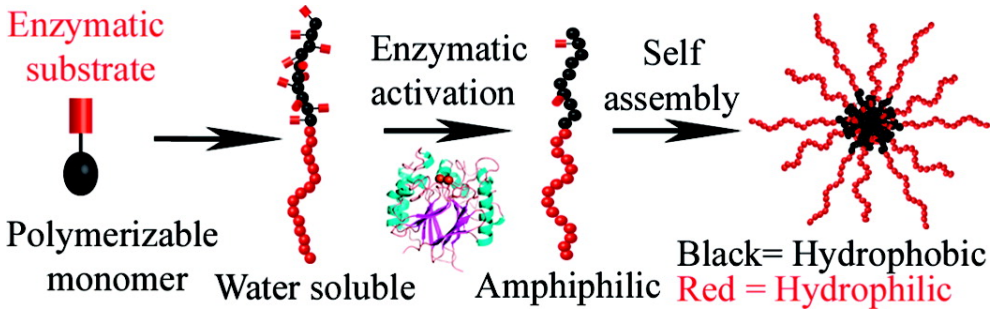

Figure 1.6 Schematic representation of enzymatic activation of a water-soluble block copolymer, resulting in an amphiphilic polymer and subsequent self-assembly into colloidal nanostructures. Reprinted with permission from *J. Am. Chem. Soc.*, 2009, **131**, 13949–13951. Copyright 2009 American Chemical Society.

1.3 Incorporation of Visual Labels

Developing analytical strategies to track, in real time, various nanomaterials is necessary to progress towards applications in complex biological milieu. It is critical to confirm the location and/or a specific chemical events such as those described in the previous section and this requires a visual label to track specific processes. Examples of strategies that have been employed include labeling nanomaterials with fluorophores,[19-21,133] radionucletides,[19,134,135] paramagnetic ions,[19,35,37,136] or other

nanoparticles.[133,137,138] It is necessary to determine an appropriate label depending on whether the material will be applied *in vitro* or *in vivo*. For example, when choosing a label for *in vivo* use, one should consider adopting a labeling strategy involving the least invasive strategy (i.e. MRI). This requirement is not crucial when experimenting with labeled nanoparticles *in vitro*.

The remainder of this chapter focuses on strategies for labeling polymeric nanomaterials. This is an introduction into two separate strategies for labeling nanoparticles with visual tags. The focus of this section is broken into two parts: 1) the incorporation of fluorescent labels into nanoparticles and 2) strategies to tag nanoparticles with MRI contrast agents. This discussion does not include quantum dots, radionucleotides, or inorganic nanoparticles incorporated into nanoparticles. Reviews do exist for the interested reader.[31,135,138-141]

1.3.1 Fluorescent Labeled Nanoparticles

Fluorescent molecules are often put to use in biomedical research. Fluorescence is an ideal tool used in chemosensors,[142-144] biological imaging,[145-147] diagnostics,[148,149] and therapy.[146,150] One of the limiting factors of fluorescent molecules is tissue-induced light absorption and reflection. These factors decrease the signal-to-noise ratios, making the detection of fluorescent signals difficult. Many researchers prefer agents in fluorescent imaging, such as quantum dots and organic fluorophores, over genetically engineered molecules such as fluorescent proteins and bioluminescence.[151,152] Their resistance to photobleaching and long fluorescent lifetime give quantum dots an advantage

over organic fluorophores, however studies question the potential health risks such as cytotoxicity and induced apoptosis.[153] Small molecule organic fluorophores, of course, also pose drawbacks in their usage. Despite being less cytotoxic, problems include photostability and stability under physiological conditions.

Scientists have employed the grafting of these small molecules onto polymeric systems in order to improve organic based fluorophores. This technique offers the ability to incorporate multiple fluorophores in one macromolecule, improving stability and allowing for a greater signal to noise ratio. In the event that these polymeric systems are capable of forming stable nanoparticles, they provide extra shielding for the fluorescent molecule against photobleaching and degradation at physiological conditions.[23,154-156]

The next section focuses on recent strategies for incorporating metal-free fluorescent molecules into polymeric nanoparticles. While many research groups have had success encapsulating fluorescent dyes into polymeric nanomaterials, the problem of leakage is inherent.[157-163] The use of well-defined materials is critical when analyzing complex biological reactions on the nanoscale. Only a brief review of the covalent incorporation of fluorescent molecules is included. The most robust labeling strategy is, arguably, chemical conjugation of fluorescent molecules to polymeric nanoparticles. This is achieved at two variations: 1) Post polymer and/or post-particle conjugation or 2) direct incorporation of the fluorophores during the polymerization procedure. The

following examples examine the success of covalent incorporation of fluorophores.

The technique of emulsion polymerization has been applied for the incorporation of fluorophores into polymeric nanoparticles.[164-169] This technique involves a monomer, initiator, and dispersion medium and in some cases a colloidal stabilizer placed in an inhomogeneous mixture, resulting in a colloidal suspension containing the newly formed polymer.[170] Peng and colleagues availed this polymerization technique to incorporate a polymerizable anthrapyridone dye.[165] In this work, they chose anthrapyridone because long wavelength dyes, such as Cy5, are known to degrade in the presence of radicals. Anthrapyridone can survive radical polymerization techniques and co-polymerization with methyl methacrylate and 4-chloromethyl styrene results in a fluorescent nanoparticle. They assembled a polymeric nanoparticle with anthrapyridone, not containing a polymerizable moiety, in order to make a direct comparison regarding leakage of a non-covalent dye versus covalent incorporation into a polymeric nanoparticle. They found that the leakage of dye from the covalent fluorescent nanoparticle is one-tenth the amount when compared to the doped fluorescent nanoparticle (i.e. non-covalent encapsulation). Surface functionalization of the fluorescent nanoparticle with folic acid further illustrates the utility of this labeling strategy. When Peng and colleagues incubate these fluorescent nanoparticles with HeLa cells, which are over-expressed with folate receptors, the fluorescent nanoparticles undergo endocytosis.

Ring-opening-methathesis polymerization (ROMP) is another technique to covalently incorporate fluorophores.[171] In our laboratory, we developed a fluorogenic peptide polymer amphiphile capable of producing an “on” signal in response to enzymatic activity.[74] In this research, we synthesized a block copolymer consisting of a hydrophobic phenyl monomer (Figure 1.7), and a conjugatable *N*-hydroxysuccinimide (NHS) monomer, split into two equal portions and terminated with either rhodamine or fluorescein. We chose this particular dye pair because of their ability to produce a FRET signal when within the Förster radius. To further alter the fluorogenic polymers we adapted a post-polymerization modification with an MMP-2/9 peptide substrate. MMP-2/9 is known to be over-expressed in many cancerous cell lines and is, therefore, a relevant biomarker to detect *in vivo*.[127,130,172] Next, we carefully transitioned these fluorogenic amphiphilic polymers from organic solvent into water to form fluorescein, rhodamine, or a FRET labeled polymeric nanoparticle (containing known amounts of fluorescein and rhodamine labeled polymers). When performing an *in vitro* experiment to test the enzymatic response of these systems, we observed a dramatic morphology change from spherical micelles to aggregated structures, as evidenced by transmission electron microscopy (TEM). More importantly, when fluorescein and rhodamine labeled particles are incubated with MMP, a unique FRET signal appears, indicating an enzymatically-triggered rearrangement of the nanoparticles to aggregates. *In vivo* experimentation using nude mice containing an HT-1080 xenograft, a human cancer model known to overexpress MMPs, provided further confirmation.[172]

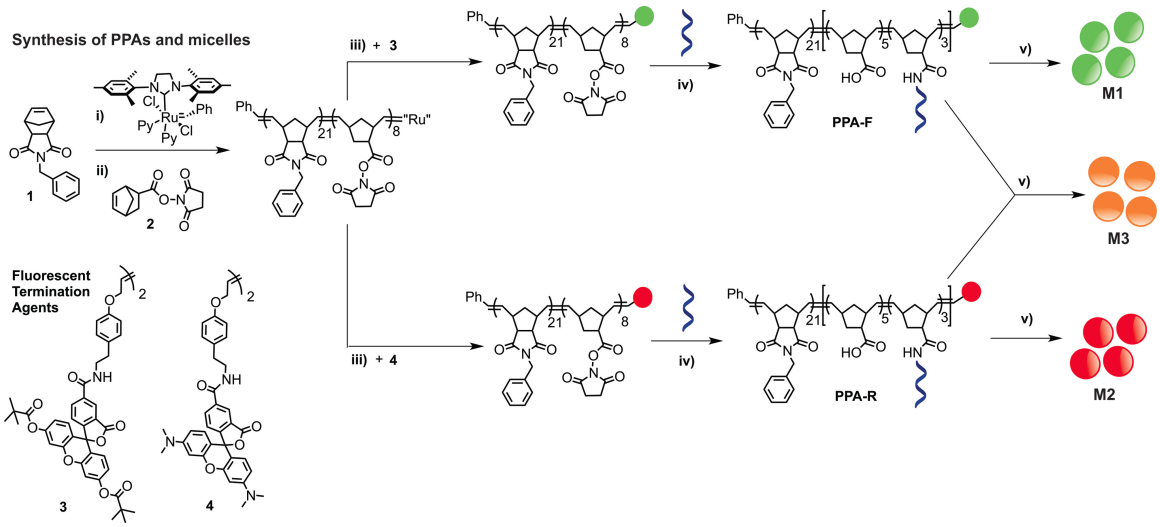

Figure 1.7 Preparation of enzyme-responsive fluorescent polymeric nanoparticles with ROMP. Synthesis: i) **1** was mixed with a modified Grubbs' 2nd generation initiator and an aliquot was analyzed by SEC-MALS to confirm the degree of polymerization. ii) **2** was added and an aliquot was analyzed to confirm the 21:8 block copolymer ratio. iii) The resulting polymer was split into two pots and mixed with a fluorescein (**3**) or rhodamine (**4**) chain transfer agent represented by either the green sphere for fluorescein or red sphere for rhodamine. iv) MMP peptide substrates were added to the block copolymers to form PPA-F and PPA-R. v) Dialysis of PPAs from DMSO to PBS (pH 7.4) over 24 h generated micellar nanoparticles. **M1** contains PPA-F, **M2** contains PPA-R, and **M3** contains PPA-F and PPA-R. Adapted from ref. 74. Copyright 2013 WILEY-VCH Verlag GmbH & Co. KGaA, Weinheim.

An emerging class of fluorescent materials, containing π-conjugated polymer nanoparticles allow for high extinction coefficient polymeric nanoparticles and ease of functionalization with targeting ligands.[25,173-175] Swager and colleagues synthesized a fluorescent multi-block conjugated polymer nanoparticle for *in vivo* tumor targeting.[176] In this report, they synthesized an ABCBA block copolymer that consists of poly-(p-phenyleneethylene) (PPE) doped with 0.5 and 5 mol% perylene monoidimide (PMI), making up the C block. A post-polymerization modification allowed addition of an oligoethylene glycol (OEG) block (A-block) and a folic acid block (B-block), flanking the PPE/PMI

block. These well-defined polymeric materials were then transitioned into water through solvent exchange to form well-defined fluorescent nanoparticles. The study found that the injection of nude mice bearing KB tumors (known to overexpress folate receptors[177]) with fluorescent nanoparticles led to the accumulation of only polymeric materials containing folic acid at the tumor site, as determined by fluorescent imaging. With the fluorescently labeled NP, they uncovered no apparent cytotoxicity or undesired accumulation. These results further prove the utility of *in vivo* imaging with fluorescent labeled nanoparticles.

1.3.2 Polymeric Nanoparticles Labeled with MRI-Contrast Agents

Whilst labeling polymeric nanoparticles with fluorescent tags has proven to be useful *in vitro* and *in vivo* for small animal imaging, the utility has not made its way into real-world clinical applications. The exigent dilemma being that non-invasive deep tissue imaging is not possible using fluorescence imaging techniques. By contrast, a variety of other imaging modalities are commonly utilized for clinical applications such as single-photon emission computed tomography (SPECT), positron emission tomography (PET), and magnetic resonance imaging (MRI). While all of these imaging modalities have proven vital for diagnostics, we focus on MRI, as SPECT and PET are beyond the scope of the research presented in the following chapters.

MRI is a noninvasive imaging modality that examines the relaxation of water protons of various tissues in the body. The goal of incorporating contrast agents is to affect the T_1 (spin-spin) relaxation or T_2 (spin-lattice) relaxation of the

surrounding water molecules. T_1 contrast agents are typically based on paramagnetic gadolinium chelates, which enhance the relaxation rate of surrounding water protons resulting in a bright signal in MRI. T_2 contrast agents are composed of superparamagnetic iron oxide nanoparticles and result in negative contrast in MRI scans.[37,137] Though there has been much research in the field of T_2 contrast agents,[137,178,179] it is beyond the scope of the research discussed here. The remaining section describes several examples of synthetic routes to label polymeric nanoparticles with gadolinium based contrast agents.

Many of the current FDA approved MRI contrast agents contain stable small molecule Gd-poly(aminocarboxylate) complexes such as Gd-diethylenetriaminepentaacetic (Gd-DTPA, Magnevist®) and Gd-1,4,7,10-tetraazacyclododecane-1,4,7,10-tetraacetic acid (Gd-DOTA, Dotarem®).[37] Gadolinium (Gd^{3+}) chelates decrease any unwanted toxicity induced by free Gd^{3+} ions. However, these chelates have low molecular weights and therefore rapid renal clearance. For this reason, many research groups focus on appending Gd-chelates to nanoparticles in an effort to increase circulation times with increased molecular weight.[37] These systems are characterized by the inclusion of Gd-chelates by encapsulation into nanoparticles[180,181] or covalent incorporation into nanoparticles containing dendrimers,[37,182,183] proteins,[184,185] and polymeric nanoparticles,[35,37,186-190] our focus is now solely on the covalent incorporation of Gd-chelates into polymeric nanoparticles.

Post-Particle-Formation Chelation. Conjugation of Gd-chelates to the surface of nanoparticles is a facile route to chemically modify nanoparticles to act as functional MRI-contrast agents. A typical route to incorporate these contrast agents is surface modification with chemical linkers capable of simple conjugation reactions with Gd^{3+} chelates. Non-toxic and biodegradble poly($_{D,L}$-lactide-co-glycolide) (PLGA) is a polymer scaffold that facilitates functionalization either before of after particle formation.[191] Gabor and colleagues performed tests on a series of spacers for conjugation of DTPA bisanhydride or DOTA-NHS followed by Gd^{3+} complexation.[189] They determine that a branched polyethyleneimine (PEI) is optimal in achieving the highest loading of Gd^{3+} and therefore is used for further analysis. They remove excess Gd^{3+} through extensive dialysis, however trace amounts are still detected. Further characterization of the material determines its potential as a biodegradable contrast agent. A maximum relaxivity (r_1) of 17.5 $mM^{-1}sec^{-1}$ per Gd^{3+} is achieved at 1.5 T, which approximates to four times that of the small molecule analogues.

Shell crosslinking is another reliable tactic to increase r_1 and stability of micellar nanoparticles for *in vivo* applications. The increase of water hydration in the shell of micellar nanoparticles and the addition of enhanced stability, make it an excellent candidate as a T_1 contrast agent. Wooley and colleagues synthesized an amphiphilic block copolymer consisting of poly-(acrylic acid) (PAA) as the hydrophilic shell and poly-(methyl acrylate) (PMA) as the hydrophobic core (see Figure 1.8).[187] The block copolymer is then transitioned into water to form polymeric micelles which is subsequently crosslinked with 2,2'-

(ethylenedioxy)bis(ethylamine), consuming approximately 40% of acrylic acid residues. This allows for the remaining available acrylic acid units to be functionalized with an amino modified Gd-DTPA complex (Figure 1.8) resulting in 21% loading as determined by ICP-OES. Conjugation of pre-complexed contrast agent to the PAA-*b*-PMA nanoparticle reduced the probability of having excess Gd^{3+} present. Additional relaxivity measurements determined excellent per Gd^{3+} relaxivity of 22.6 $mM^{-1}sec^{-1}$ at 37 ºC and a magnetic field strength of 7 T and 39.0 $mM^{-1}sec^{-1}$ at 40 ºC and 0.5 T. The superiority of contrast enhancement over the small molecule analogue of 4.0 $mM^{-1}sec^{-1}$ at 0.5 T is evident.

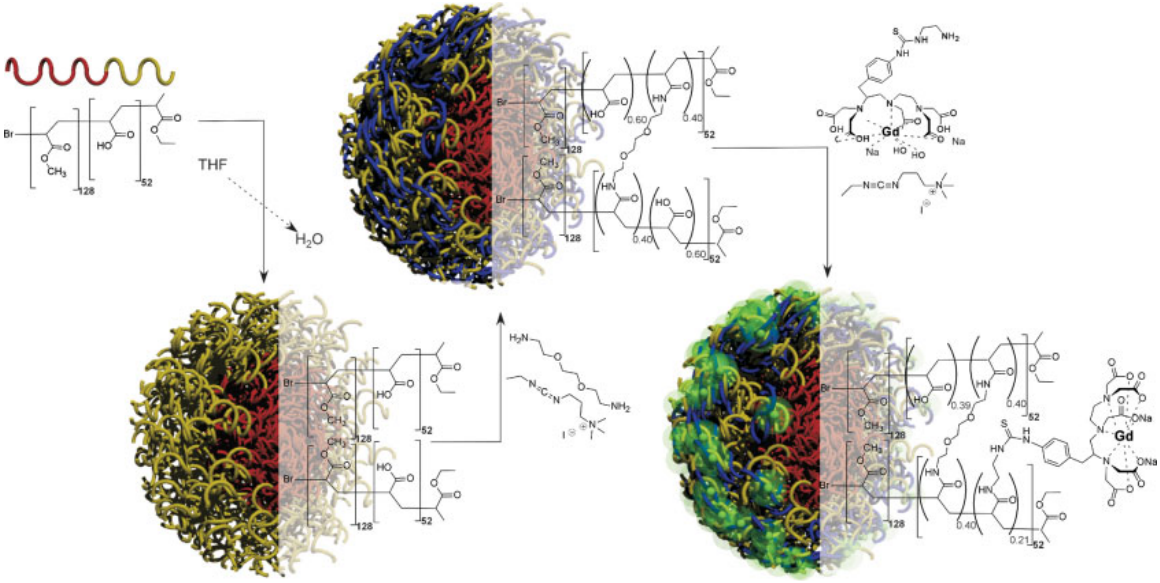

Figure 1.8 Schematic representation of the synthesis of Gd^{3+}-labeled polymeric micelles. Transition from a THF solution of the amphiphilic block copolymer PAA-*b*-PMA into water results in a polymeric micellar structure. Subsequent crosslinking of the shell with a diamine moiety produces a stabilized polymeric micelle which is amenable to functionalization with an amine modified Gd-DTPA onto the hydrophilic shell. Reprinted with permission from reference 187. Copyright © 2005 WILEY-VCH Verlag GmbH & Co. KGaA, Weinheim.

A desirable trait of polymeric nanomaterials for *in vivo* use is extended blood circulation half-lives, which typical small molecule analogues do not possess. A common method for increasing the stealth of materials is to add a polyethylene oxide (PEO) component into polymeric materials.[192] With this in mind, Detrembleur and colleagues synthesized an amphiphilic block copolymer micelle that contains a PEO shell and a poly-(ε-caprolactone) (PCL) block as the hydrophobic core.[190] After transition into water to form spherical nanoparticles, a protecting group is removed leading to an aldehyde-functionalized shell. This allows for conjugation of an amine-modified Gd-DTPA onto the shell of the nanoparticle, with a conjugation efficiency of 60%, as determined by ICP-MS analysis. Further study shows that enhanced Gd^{3+} relaxivity at 20 MHz (0.5 T) (12 $mM^{-1}sec^{-1}$) was achieved. The results of this method show improvement over small molecule analogues and have the additional benefit of increased stealth and size for *in vivo* applications.

Post-Polymerization Conjugation. A drawback to post particle conjugation of chelates is poor loading efficiency. Another commonly used technique to covalently incorporate contrast agents is to initially incorporating them into the polymer itself, followed by nanoparticle formation. In this fashion, Zhang and colleagues directly incorporated a modified DTPA chelate into the polymeric backbone.[186] First, a poly-(L-glutamic acid)-*b*-polylactide (PLG-*b*-PLA) is synthesized and then modified with an amine functionalized DTPA chelate. The post-polymerization strategy results in a 40% loading efficiency. The amphiphilic copolymer PLG(DTPA)-*b*-PLA was then transitioned into water through dialysis

and chelated with Gd^{3+}. After extensive dialysis, excess Gd^{3+} is removed and relaxivity measurements at 4.7 T concluded that a two-fold enhancement of per Gd^{3+} relaxivity is achieved (r_1 = 7.90 $mM^{-1}sec^{-1}$). To examine if this type of Gd-loaded micelle could be viable for *in vivo* applications, they performed an MTT assay. This assay determined that no observable cytotoxicity is found at concentrations up to 100 μg/mL of Gd-loaded micelles.

A goal of many research groups is to integrate a therapeutic agent and a diagnostic tool in order to image the successful targeting of a therapeutic agent. This field is often termed theranostics. Many researchers incorporate the targeting moieties, drug molecules, and/or contrast agents onto polymeric nanomaterials in an effort to develop the ultimate delivery vehicle. To reach this goal, Liu and colleagues synthesized a pH-disintegradable micellar nanoparticle containing, Gd-DOTA as a contrast agent, folic acid (FA) as a targeting moiety, and doxorubicin (DOX) as a cancer therapeutic drug.[193] The nanoparticle is synthesized from an azide funtionalized β-cylodextran (CD) group with poly-(methacrylamide) (PHPMA). FA and DOX are conjugated post-polymerization to afford a 2% labeling with folic acid and 8% with DOX. Lastly, an alkynyl-DOTA-Gd is "clicked" onto the azide functionalized CD to achieve the final product of $(DOTA\text{-}Gd)_7$-CD-$(PHPMA\text{-}\textit{FA}\text{-}\textit{DOX})_{14}$. The amphiphilic polymer was then self-assembled in aqueous solutions to form ~20-30 nm spherical particles. They determined that, without addition of DOX, particles are completely water soluble and non-toxic. However, with the addition of DOX, spherical nanoparticles formed, and only 15% of HeLa cells are viable at concentrations greater than 80

mg/L. *In vitro* MRI at 1.5 T determined that nanoparticle solutions have a per Gd^{3+} relaxivity of 11.4 $mM^{-1}sec^{-1}$, higher than that of the alkynyl-DOTA-Gd complex by three-fold. *In vivo* analysis in healthy rats showed renal clearance through the bladder of $(DOTA\text{-}Gd)_7$-CD-$(PHPMA\text{-}FA\text{-}DOX)_{14}$ nanoparticles immediately following intravenous injection and continued clearance up to one hour.

The generation of a mixed micellar system is another approach to enhance contrast in MRI. Mixed micellar systems allow the incorporation of two different polymers, containing a desired functionality, that can self-assemble into the same micellar nanoparticle. Liu and colleagues present an example of this strategy. Two amphiphilic polymers were synthesized, both containing a hydrophobic poly-(ε-caprolactone) (PCL) block and a hydrophilic poly-(oligo(ethylene glycol) monomethyl ether methacrylate) (POEGMA) block.[188] The POEGMA block is functionalized with an azide during the polymerization procedure in order to easily "click" on an alkynyl modified folic acid or Gd-DOTA. The newly formed PCL-*b*-P(OEGMA-FA) and PCL-*b*-P(OEGMA-Gd) are then transitioned simultaneously into water in a 1:1 ratio (w/w) to form a mixed micelle containing targeting moieties (FA) and a diagnostic imaging agent (Gd-DOTA). This mixed micellar nanoparticle forms spherical structures of approximately 30 nm as determined by DLS, TEM, and AFM. These were subsequently injected into healthy rabbits and monitored for any contrast enhancement in the liver. They found that if the folic acid targeting moeity is not present, a decreased contrast enhancement is seen in the liver. This is in stark contrast to when folic

acid is present. However, both systems at 1.5 T see upwards of twice the enhancement than the small molecule analogue. The folic acid modified mixed micelle circulates up to 120 minutes post injection, where the small molecule clears within 30 minutes.

1.4 Summary and Thesis Overview

1.4.1 Summary

A growing body of work describes materials capable of interfacing with biological systems by responding to relevant biochemical signals. The development of nanomaterials capable of responding in a predictable fashion in biological organisms is certainly of increasing interest for a range of *in vivo* biomedical applications. This approach is complementary to many research efforts to develop visual probes to indicate a particular biological function. Researchers face tremendous challenges when aiming to utilize nanoparticles for *in vivo* applications, the most important of which is the development of materials capable of selective targeting as well as possessing the required stability and degradability in complex biological milieu.

The field of functionally labeled nanomaterials is still in its infancy and many factors still require exploration such as the synthesis of well-defined nanomaterials with predictable morphology, and loading of the label itself. In order to enhance retention and blood circulation, many researchers are moving toward polymeric nanoparticle systems capable of forming spherical, cylindrical, vesicular, and toroidal morphologies. The ideal outcome is to create a vessel to

release desired cargo only in response to specific stimuli such as pH, enzymes, or other exogenous stimuli. In order to visualize particular reactions at the nanoscale, one needs an appropriate label to interpret accurate conclusions. The need for covalent linkages of fluorophores helps researchers study stimuli induced reactions *in vitro* and is invaluable for creating well-defined materials. However, the ability to probe fluorescence non-invasively is an arduous process, which creates a need for clinically relevant labels to be appended onto nanoparticles. The non-invasive imaging of MRI offers an ideal platform to visualize biological functions. Many researchers are exploring appending T_1 contrast agents onto nanoparticle systems. Designing a material that one can track once *in vivo* and which contains all of the desired functions such as targeting moieties, long circulation, and visualization is an important goal for this research. Herein, a detailed study of various techniques to label polymeric nanoparticles and study their behavior *in vivo* will be described.

1.4.2 Thesis Overview

Chapter 2. In this chapter, we describe initial synthetic efforts to develop well-defined peptide-programmed amphiphiles capable of detecting and responding to inflammation- and cancer-associated enzymes. Polymers of norbornenyl-modified peptide-based enzyme substrates are prepared via ring-opening metathesis polymerization (ROMP). Peptides co-polymerized with a hydrophobic phenyl monomer are able to form well-defined spherical nanoparticles. Peptides displayed on water-soluble homopolymers retain the

ability to be enzymatically processed by a disease-associated enzyme when synthesized by post-polymerized modification. In contrast, when the peptides are densely arrayed on a nanoparticle derived from a self-assembled amphiphilic block copolymer, they function with reduced activity as enzymatic substrates.

Chapter 3. In this chapter we compare and contrast two approaches for labeling polymers with functional groups via ROMP. We explore the incorporation of functionality via covalently modified chain transfer agents and monomers. The goal is to allow the generation of selectively labeled and well-defined polymers that can in turn lead to the formation of labeled nanomaterials. Norbornene analogues, prepared as functionalized monomers for ROMP, include fluorescent dyes (EDANS) and quenchers (DABCYL). In addition, we describe a set of symmetrical olefins for terminally labeling polymers, and for the generation of FRET labeled nanoparticles.

Chapter 4. The multistep synthesis and polymerization of a DTPA chelate is described. Additionally, a norbornene-based analogue of the FDA approved small molecule MRI contrast agent Gd-DOTA (Norb-Gd-DOTA-MA) is polymerized via ROMP as a hydrophilic component in water-soluble or amphiphilic block copolymers. The amphiphiles assemble in aqueous solution to form micellar nanoparticles of spherical or fibril-shaped morphology. These two types of particles have water-soluble shells containing a polymerized block of Gd-DOTA-MA, while the analogous hydrophilic polymeric species is completely dispersed in aqueous solution. The relaxation parameters of these Gd^{3+} containing materials are assessed by ^{1}H NMRD.

Chapter 5. This study directly compares a solvated Gd^{3+} containing polymer and Gd^{3+} nanoparticles of spherical and fibril morphology to each other and to the small molecule Gd-DOTA contrast agent when introduced via intraperitoneal (IP) injection into mice. Clearance from the bladder is observed in anatomical scans via MRI, and through a decrease in T_1 over time. Clearance is rapid for Gd-DOTA with minimum T_1 times observed in the bladder at 2 hours. Similarly, clearance through the bladder is observable for the dispersed, hydrophilic Gd-labeled polymer. This behavior is in contrast to that observed for the nanoparticle formulations, whereby little clearance through the bladder is observed, and considerable retention within the IP space is seen for the first few hours. After one week, clearance is equivalent for all materials as determined by ICP-MS. These *in vivo* studies are the culmination of an effort to control the labeling and the morphology of amphiphile self-assemblies. In addition, they have set the stage for the development of drug and diagnostic carrying particles for IP treatment of diseases associated within that space, including ovarian cancer.

1.5 Acknowledgments

Chapter 1, in part, is a reprint of Randolph, Lyndsay M., Chien, Miao-Ping, and Gianneschi, Nathan C. “Biological stimuli and biomolecules in the assembly and manipulation of nanoscale polymeric particles.” *Chem. Sci.* ***3,*** 1363-1380 (2012). The dissertation author was the primary author of this paper.

1.6 References

(1) Winfree, E.; Liu, F.; Wenzler, L. A.; Seeman, N. C. *Nature* **1998**, *394*, 539.

(2) Gothelf, K. V.; LaBean, T. H. *Org. Biomol. Chem.* **2005**, *3*, 4023.

(3) Seeman, N. C. *Mol. Biotechnol.* **2007**, *37*, 246.

(4) Aldaye, F. A.; Palmer, A. L.; Sleiman, H. F. *Science* **2008**, *321*, 1795.

(5) Kato, T.; Goodman, R. P.; Erben, C. M.; Turberfield, A. J.; Namba, K. *Nano Lett.* **2009**, *9*, 2747.

(6) Hahn, M. E.; Gianneschi, N. C. *Chem. Commun.* **2012**, *47*, 11814.

(7) Alemdaroglu, F. E.; Herrmann, A. *Org. Biomol. Chem.* **2007**, *5*, 1311.

(8) Frezza, B. M.; Cockroft, S. L.; Ghadiri, M. R. *J. Amer. Chem. Soc.* **2007**, *129*, 14875.

(9) Ashkenasy, G.; Ghadiri, M. R. *J. Amer. Chem. Soc.* **2004**, *126*, 11140.

(10) Randolph, L. M.; Chien, M.-P.; Gianneschi, N. C. *Chem. Sci.* **2012**, *3*, 1363.

(11) Fuks, G.; Mayap Talom, R.; Gauffre, F. *Chem. Soc. Rev.* **2011**, *40*, 2475.

(12) Blanazs, A.; Madsen, J.; Battaglia, G.; Ryan, A. J.; Armes, S. P. *J. Amer. Chem. Soc.* **2011**, *133*, 16581.

(13) Jain, S.; Bates, F. S. *Science* **2003**, *300*, 460.

(14) Smart, T.; Lomas, H.; Massignani, M.; Flores-Merino, M. V.; Perez, L. R.; Battaglia, G. *Nano Today* **2008**, *3*, 38.

(15) Wang, Y.; Xu, H.; Zhang, X. *Adv. Mater.* **2009**, *21*, 2849.

(16) Bütün, V.; Liu, S.; Weaver, J. V. M.; Bories-Azeau, X.; Cai, Y.; Armes, S. P. *React. Funct. Polym.* **2006**, *66*, 157.

(17) Discher, D. E.; Eisenberg, A. *Science* **2002**, *297*, 967.

(18) Hawker, C. J.; Wooley, K. L. *Science* **2005**, *309*, 1200.

(19) Liu, A.; Zhai, S.; Zhang, B.; Yan, B. *TrAC-Trend. Anal. Chem.* **2013**, *48*, 1.

(20) Wang, G.; Peng, Q.; Li, Y. *Acc. Chem. Res.* **2011**, *44*, 322.

(21) Wang, F.; Tan, W. B.; Zhang, Y.; Fan, X.; Wang, M. *Nanotechnology* **2006**, *17*, R1.

(22) Tian, Z.; Wu, W.; Li, A. D. *ChemPhysChem* **2009**, *10*, 2577.

(23) Jiang, S.; Gnanasammandhan, M. K.; Zhang, Y. *J. R. Soc. Interface* **2010**, *7*, 3.

(24) Liu, J.; Yang, X.; He, X.; Wang, K.; Wang, Q.; Guo, Q.; Shi, H.; Huang, J.; Huo, X. *Sci. China Chem.* **2011**, *54*, 1157.

(25) Li, K.; Liu, B. *J. Mater. Chem.* **2012**, *22*, 1257.

(26) Vollrath, A.; Schubert, S.; Schubert, U. S. *J. Mater. Chem. B* **2013**, *1*, 1994.

(27) Chan, W. C. W.; Maxwell, D. J.; Gao, X.; Bailey, R. E.; Han, M.; Nie, S. *Curr. Opin. Biotechnol.* **2002**, *13*, 40.

(28) Drbohlavova, J.; Adam, V.; Kizek, R.; Hubalek, J. *Int. J. Mol. Sci.* **2009**, *10*, 656.

(29) Bau, L.; Tecilla, P.; Mancin, F. *Nanoscale* **2011**, *3*, 121.

(30) Shang, L.; Nienhaus, G. U. *Mater. Today* **2013**, *16*, 58.

(31) Zhong, W. *Anal. Bioanal. Chem.* **2009**, *394*, 47.

(32) Coto-Garcia, A. M.; Sotelo-Gonzalez, E.; Fernandez-Arguelles, M. T.; Pereiro, R.; Costa-Fernandez, J. M.; Sanz-Medel, A. *Anal Bioanal Chem* **2011**, *399*, 29.

(33) Dunphy, M. P. S.; Lewis, J. S. *J. Nucl. Med.* **2009**, *50*, 106S.

(34) Mankoff, D. A.; Eary, J. F.; Link, J. M.; Muzi, M.; Rajendran, J. G.; Spence, A. M.; Krohn, K. A. *Clin. Cancer Res.* **2007**, *13*, 3460.

(35) Liu, Y.; Zhang, N. *Biomaterials* **2012**, *33*, 5363.

(36) Gianolio, E.; Stefania, R.; Di Gregorio, E.; Aime, S. *Eur. J. Inorg. Chem.* **2012**, *2012*, 1934.

(37) Villaraza, A. J.; Bumb, A.; Brechbiel, M. W. *Chem. Rev.* **2010**, *110*, 2921.

(38) Hamley, I. W. *Soft Matter* **2011**, *7*, 4122.

(39) Jain, J. P.; Ayen, W. Y.; Kumar, N. *Curr Pharm Des* **2011**, *17*, 65.

(40) Brinkhuis, R. P.; Rutjes, F. P. J. T.; van Hest, J. C. M. *Polym. Chem.* **2011**, *2*, 1449.

(41) Luk, Y.-Y.; Abbott, N. L. *Curr. Opin. Colloid Interface Sci.* **2002**, *7*, 267.

(42) Rösler, A.; Vandermeulen, G. W. M.; Klok, H.-A. *Adv. Drug Deliv. Rev.* **2001**, *53*, 95.

(43) Chakraborty, C.; Pal, S.; Doss, G. P.; Wen, Z. H.; Lin, C. S. *Front. Biosci.* **2013**, *18*, 1030.

(44) Pietsch, T.; Gindy, N.; Fahmi, A. *Polymer* **2008**, *49*, 914.

(45) Ringsdorf, H.; Schmidt, G.; Schneider, J. *Thin Solid Films* **1987**, *152*, 207.

(46) Wang, C.; Wang, Z.; Zhang, X. *Acc. Chem. Res.* **2012**, *45*, 608.

(47) Halperin, A. *J. Macromol. Sci., Polym. Rev.* **2006**, *46*, 173.

(48) Opsteen, J. A.; Cornelissen, J. J. L. M.; van Hest, J. C. M. *Pure Appl. Chem.* **2004**, *76*, 1309.

(49) Nuraje, N.; Bai, H.; Su, K. *Prog. Polym. Sci.* **2013**, *38*, 302.

(50) Rubio-Magnieto, J.; Luis, S. V.; Orlof, M.; Korchowiec, B.; Sautrey, G.; Rogalska, E. *Colloids Surf., B* **2013**, *102*, 659.

(51) Shrestha, R. G.; Nomura, K.; Yamamoto, M.; Yamawaki, Y.; Tamura, Y.; Sakai, K.; Sakamoto, K.; Sakai, H.; Abe, M. *Langmuir* **2012**, *28*, 15472.

(52) Moffitt, M. G. *J. Phys. Chem. Lett.* **2013**, *4*, 3654.

(53) Zhang, M.; Müller, A. H. E. *J. Polym. Sci., Part A: Polym. Chem.* **2005**, *43*, 3461.

(54) Sorrenti, A.; Illa, O.; Ortuno, R. M. *Chem. Soc. Rev.* **2013**, *42*, 8200.

(55) Zhang, W.; Müller, A. H. E. *Prog. Polym. Sci.* **2013**, *38*, 1121.

(56) Holder, S. J.; Sommerdijk, N. A. J. M. *Polym. Chem.* **2011**, *2*, 1018.

(57) Taurin, S.; Nehoff, H.; Greish, K. *J. Controlled Release* **2012**, *164*, 265.

(58) Maeda, H.; Matsumura, Y. *Crit Rev Ther Drug Carrier Syst* **1989**, *6*, 193.

(59) Maeda, H. *Adv. Drug Deliv. Rev.* **2001**, *46*, 169.

(60) Muggia, F. M. *Clin. Cancer Res.* **1999**, *5*, 7.

(61) Geng, Y.; Dalhaimer, P.; Cai, S.; Tsai, R.; Tewari, M.; Minko, T.; Discher, D. *Nat. Nanotechnol.* **2007**, *2*, 249.

(62) Christian, D. A.; Cai, S.; Garbuzenko, O. B.; Harada, T.; Zajac, A. L.; Minko, T.; Discher, D. E. *Mol. Pharm.* **2009**, *6*, 1343.

(63) Champion, J. A.; Mitragotri, S. *Proc. Natl. Acad. Sci. U.S.A.* **2006**, *103*, 4930.

(64) Lee, N. S.; Lin, L. Y.; Neumann, W. L.; Freskos, J. N.; Karwa, A.; Shieh, J. J.; Dorshow, R. B.; Wooley, K. L. *Small* **2011**, *7*, 1998.

(65) Versluis, F.; Tomatsu, I.; Kehr, S.; Fregonese, C.; Tepper, A. W. J. W.; Stuart, M. C. A.; Ravoo, B. J.; Koning, R. I.; Kros, A. *J. Amer. Chem. Soc.* **2009**, *131*, 13186.

(66) Moughton, A. O.; O'Reilly, R. K. *Chem. Commun.* **2010**, *46*, 1091.

(67) Zhang, L.; Yu, K.; Eisenberg, A. *Science* **1996**, *272*, 1777.

(68) Ishihara, Y.; Bazzi, H.; Toader, V.; Godin, F.; Sleiman, H. *Chem. Eur. J.* **2007**, *13*, 4560.

(69) Ku, T.-H.; Chien, M.-P.; Thompson, M. P.; Sinkovits, R. S.; Olson, N. H.; Baker, T. S.; Gianneschi, N. C. *J. Amer. Chem. Soc.* **2011**, *133*, 8392.

(70) Amir, R. J.; Zhong, S.; Pochan, D. J.; Hawker, C. J. *J. Amer. Chem. Soc.* **2009**, *131*, 13949.

(71) Zou, J.; Tao, F.; Jiang, M. *Langmuir* **2007**, *23*, 12791.

(72) Fomina, N.; McFearin, C.; Sermsakdi, M.; Edigin, O.; Almutairi, A. *J. Amer. Chem. Soc.* **2010**, *132*, 9540.

(73) Chien, M.-P.; Thompson, M. P.; Lin, E. C.; Gianneschi, N. C. *Chem. Sci.* **2012**, *3*, 2690.

(74) Chien, M.-P.; Thompson, M. P.; Barback, C. V.; Ku, T.-H.; Hall, D. J.; Gianneschi, N. C. *Adv. Mater.* **2013**, *25*, 3599.

(75) Shi, H.; Tsai, W.-B.; Garrison, M. D.; Ferrari, S.; Ratner, B. D. *Nature* **1999**, *398*, 593.

(76) van Tilborg, G. A.; Strijkers, G. J.; Pouget, E. M.; Reutelingsperger, C. P.; Sommerdijk, N. A.; Nicolay, K.; Mulder, W. J. *Magnet. Reson. Med.* **2008**, *60*, 1444.

(77) Savariar, E. N.; Ghosh, S.; González, D. C.; Thayumanavan, S. *J. Amer. Chem. Soc.* **2008**, *130*, 5416.

(78) Mao, Y.; Luo, C.; Deng, W.; Jin, G.; Yu, X.; Zhang, Z.; Ouyang, Q.; Chen, R.; Yu, D. *Nucleic Acids Res.* **2004**, *32*, e144/1.

(79) Chien, M. P.; Rush, A.; Thompson, M.; Gianneschi, N. *Angew. Chem. Int. Ed.* **2010**, *49*, 5076.

(80) Ding, K.; Alemdaroglu, F.; Börsch, M.; Berger, R.; Herrmann, A. *Angew. Chem. Int. Ed.* **2007**, *46*, 1172.

(81) Huang, J.; Ding, J. *Soft Matter* **2010**, *6*, 3395.

(82) Ruoslahti, E. *Annu. Rev. Cell Dev. Biol.* **1996**, *12*, 697.

(83) Rush, A. M.; Thompson, M. P.; Tatro, E. T.; Gianneschi, N. C. *ACS Nano* **2013**, *7*, 1379.

(84) Aldaye, F. A.; Sleiman, H. F. *J. Amer. Chem. Soc.* **2007**, *129*, 13376.

(85) Li, Z.; Zhang, Y.; Fullhart, P.; Mirkin, C. A. *Nano Lett.* **2004**, *4*, 1055.

(86) Chen, X.-J.; Sanchez-Gaytan, B. L.; Hayik, S. E. N.; Fryd, M.; Wayland, B. B.; Park, S.-J. *Small* **2010**, *6*, 2256.

(87) Alemdaroglu, F. E.; Alemdaroglu, N. C.; Langguth, P.; Herrmann, A. *Macromol. Rapid Commun.* **2008**, *29*, 326.

(88) Johnston, A.; Caruso, F. *Angew. Chem. Int. Ed.* **2007**, *46*, 2677.

(89) Johnston, A. P. R.; Lee, L.; Wang, Y.; Caruso, F. *Small* **2009**, *5*, 1418.

(90) Wang, J.; Alemdaroglu, F. E.; Prusty, D. K.; Herrmann, A.; Berger, R. *Macromolecules* **2008**, *41*, 2914.

(91) Chien, M.-P.; Thompson, M. P.; Gianneschi, N. C. *Chem. Commun.* **2011**, *47*, 167.

(92) Checot, F.; Brulet, A.; Oberdisse, J.; Gnanou, Y.; Mondain-Monval, O.; Lecommandoux, S. *Langmuir* **2005**, *21*, 4308.

(93) Agut, W.; Brulet, A.; Taton, D.; Lecommandoux, S. *Langmuir* **2007**, *23*, 11526.

(94) Dreher, M. R.; Simnick, A. J.; Fischer, K.; Smith, R. J.; Patel, A.; Schmidt, M.; Chilkoti, A. *J. Amer. Chem. Soc.* **2007**, *130*, 687.

(95) Kim, W.; Thévenot, J.; Ibarboure, E.; Lecommandoux, S.; Chaikof, E. *Angew. Chem. Int. Ed.* **2010**, *49*, 4257.

(96) Zhao, C.; Zhuang, X.; He, C.; Chen, X.; Jing, X. *Macromol. Rapid Commun.* **2008**, *29*, 1810.

(97) Agut, W.; Brulet, A.; Schatz, C.; Taton, D.; Lecommandoux, S. *Langmuir* **2010**, *26*, 10546.

(98) Zhang, X.; Li, J.; Li, W.; Zhang, A. *Biomacromolecules* **2007**, *8*, 3557.

(99) Wang, R.-M.; Li, G.; Zhang, H.-F.; He, Y.-F.; He, N.-P.; Lei, Z. *Polym. Adv. Technol.* **2010**, *21*, 685.

(100) Boyer, C.; Bulmus, V.; Liu, J.; Davis, T. P.; Stenzel, M. H.; Barner-Kowollik, C. *J. Amer. Chem. Soc.* **2007**, *129*, 7145.

(101) Huang, X.; Yin, Y.; Jiang, X.; Tang, Y.; Xu, J.; Liu, J.; Shen, J. *Macromol. Biosci.* **2009**, *9*, 1202.

(102) Gomez-Romero, P. *Adv. Mater.* **2001**, *13*, 163.

(103) Storhoff, J. J.; Mirkin, C. A. *Chem. Rev.* **1999**, *99*, 1849.

(104) Ofir, Y.; Samanta, B.; Rotello, V. M. *Chem. Soc. Rev.* **2008**, *37*, 1814.

(105) Azzazy, H. M. E.; Highsmith, W. E. *Clin. Biochem.* **2002**, *35*, 425.

(106) Bratkovic, T. *Cell. Mol. Life Sci.* **2010**, *67*, 749.

(107) Duvshani-Eshet, M.; Keren, H.; Oz, S.; Radzishevsky, I. S.; Mor, A.; Machluf, M. *J. Gene Med.* **2008**, *10*, 1150.

(108) Boonen, K.; Creemers, J. W.; Schoofs, L. *BioEssays* **2009**, *31*, 300.

(109) Molkentin, J. D. *J. Clin. Invest.* **2003**, *111*, 1275.

(110) Kawamura, K.; Oishi, J.; Kang, J.-H.; Kodama, K.; Sonoda, T.; Murata, M.; Niidome, T.; Katayama, Y. *Biomacromolecules* **2004**, *6*, 908.

(111) Jiang, T.; Olson, E. S.; Nguyen, Q. T.; Roy, M.; Jennings, P. A.; Tsien, R. Y. *Proc. Natl. Acad. Sci. U.S.A.* **2004**, *101*, 17867.

(112) von Maltzahn, G.; Harris, T. J.; Park, J.-H.; Min, D.-H.; Schmidt, A. J.; Sailor, M. J.; Bhatia, S. N. *J. Amer. Chem. Soc.* **2007**, *129*, 6064.

(113) Bull, S. R.; Guler, M. O.; Bras, R. E.; Meade, T. J.; Stupp, S. I. *Nano Lett.* **2005**, *5*, 1.

(114) Cui, H.; Webber, M. J.; Stupp, S. I. *J. Pept. Sci.* **2010**, *94*, 1.

(115) Lehman, I. R.; Bessman, M. J.; Simms, E. S.; Kornberg, A. *J. Biol. Chem.* **1958**, *233*, 163.

(116) Kessenbrock, K.; Plaks, V.; Werb, Z. *Cell* **2010**, *141*, 52.

(117) von Schwedler, U. K.; Stemmler, T. L.; Klishko, V. Y.; Li, S.; Albertine, K. H.; Davis, D. R.; Sundquist, W. I. *EMBO J.* **1998**, *17*, 1555.

(118) Kang, H.; Yu, J.; Jung, G. *Biochem J* **2008**, *416*, 47.

(119) Signarvic, R. S.; DeGrado, W. F. *J. Mol. Biol.* **2003**, *334*, 1.

(120) Yang, Z.; Liang, G.; Wang, L.; Xu, B. *J. Amer. Chem. Soc.* **2006**, *128*, 3038.

(121) Lowik, D. W. P. M.; Leunissen, E. H. P.; van den Heuvel, M.; Hansen, M. B.; van Hest, J. C. M. *Chem. Soc. Rev.* **2010**, *39*, 3394.

(122) Berg, J. M.; L. Tymoczko, J.; Stryer, L. *Biochemistry*; Sixth ed.; W.H. Freeman and Company: New York, 2007.

(123) Castelletto, V.; McKendrick, J. E.; Hamley, I. W.; Olsson, U.; Cenker, C. *Langmuir* **2010**, *26*, 11624.

(124) Kühnle, H.; Börner, H. *Angew. Chem. Int. Ed.* **2009**, *48*, 6431.

(125) Janek, K.; Behlke, J.; Zipper, J.; Fabian, H.; Georgalis, Y.; Beyermann, M.; Bienert, M.; Krause, E. *Biochemistry* **1999**, *38*, 8246.

(126) Sawyers, C. L. *Nature* **2008**, *452*, 548.

(127) Davies, B.; Waxman, J.; Wasan, H.; Abel, P.; Williams, G.; Krausz, T.; Neal, D.; Thomas, D.; Hanby, A.; Balkwill, F. *Cancer Res.* **1993**, *53*, 5365.

(128) MacDougall, J. R.; Bani, M. R.; Lin, Y.; Muschel, R. J.; Kerbel, R. S. *Br. J. Cancer* **1999**, *80*, 504.

(129) MacDougall, J. R.; Bani, M. R.; Lin, Y.; Rak, J.; Kerbel, R. S. *Cancer Res.* **1995**, *55*, 4174.

(130) Jinga, D. C.; Blidaru, A.; Condrea, I.; Ardeleanu, C.; Dragomir, C.; Szegli, G.; Stefanescu, M.; Matache, C. *J. Cell. Mol. Med.* **2006**, *10*, 499.

(131) Maatta, M.; Santala, M.; Soini, Y.; Turpeenniemi-Hujanen, T.; Talvensaari-Mattila, A. *Acta Obstet. Gynecol. Scand.*, *89*, 380.

(132) Napoli, A.; Boerakker, M. J.; Tirelli, N.; Nolte, R. J. M.; Sommerdijk, N. A. J. M.; Hubbell, J. A. *Langmuir* **2004**, *20*, 3487.

(133) Liang, S.; Pierce, D. T.; Amiot, C.; Zhao, X. *Synth. React. Inorg. Me.* **2005**, *35*, 661.

(134) Mume, E.; Asad, A.; Di Bartolo, N. M.; Kong, L.; Smith, C.; Sargeson, A. M.; Price, R.; Smith, S. V. *Dalton Trans.* **2013**, *42*, 14402.

(135) Rossin, R. In *Nanoplatform-Based Molecular Imaging*; John Wiley & Sons, Inc.: 2011, p 399.

(136) Cittadino, E.; Botta, M.; Tei, L.; Kielar, F.; Stefania, R.; Chiavazza, E.; Aime, S.; Terreno, E. *ChemPlusChem* **2013**, *78*, 712.

(137) Bin Na, H.; Hyeon, T. In *Nanoplatform-Based Molecular Imaging*; John Wiley & Sons, Inc.: 2011, p 279.

(138) Coto-García, A.; Sotelo-González, E.; Fernández-Argüelles, M.; Pereiro, R.; Costa-Fernández, J.; Sanz-Medel, A. *Anal. Bioanal. Chem.* **2011**, *399*, 29.

(139) Welch, M. J.; Hawker, C. J.; Wooley, K. L. *J. Nucl. Med.* **2009**, *50*, 1743.

(140) Chen, N.-T.; Cheng, S.-H.; Souris, J. S.; Chen, C.-T.; Mou, C.-Y.; Lo, L.-W. *J. Mater. Chem. B* **2013**, *1*, 3128.

(141) Faramarzi, M. A.; Sadighi, A. *Adv. Colloid Interface Sci.* **2013**, *189–190*, 1.

(142) Das, S.; Dutta, M.; Das, D. *Anal. Methods* **2013**, *5*, 6262.

(143) Hu, B.; Lu, P.; Wang, Y. *New J. Chem.* **2013**, *37*, 1645.

(144) Singh, K.; Sareen, D.; Kaur, P.; Miyake, H.; Tsukube, H. *Chem. Eur. J.* **2013**, *19*, 6914.

(145) Huang, J.; Yang, X.; He, X.; Wang, K.; Liu, J.; Shi, H.; Wang, Q.; Guo, Q.; He, D. *TrAC-Trend. Anal. Chem.* **2014**, *53*, 11.

(146) Yang, Y. *Microchim. Acta* **2014**, *181*, 263.

(147) Tyrakowski, C. M.; Snee, P. T. *Phys. Chem. Chem. Phys.* **2014**, *16*, 837.

(148) Geißler, D.; Linden, S.; Liermann, K.; Wegner, K. D.; Charbonnière, L. J.; Hildebrandt, N. *Inorg. Chem.* **2013**.

(149) Canfarotta, F.; Whitcombe, M. J.; Piletsky, S. A. *Biotech. Adv.* **2013**, *31*, 1585.

(150) Na, Z.; Jian, N.; Rong, H. *Nano Biomed. Eng.* **2013**, *5*, 131.

(151) Badr, C. E.; Tannous, B. A. *Trends Biotechnol.* **2011**, *29*, 624.

(152) Xie, B.-W.; Mol, I. M.; Keereweer, S.; van Beek, E. R.; Que, I.; Snoeks, T. J. A.; Chan, A.; Kaijzel, E. L.; Löwik, C. W. G. M. *PLoS ONE* **2012**, *7*, e31875.

(153) Tsoi, K. M.; Dai, Q.; Alman, B. A.; Chan, W. C. W. *Acc. Chem. Res.* **2012**, *46*, 662.

(154) He, X.; Wang, K.; Cheng, Z. *Wiley Interdiscip. Rev. Nanomed. Nanobiotechnol.* **2010**, *2*, 349.

(155) Wagh, A.; Qian, S. Y.; Law, B. *Bioconjugate Chem.* **2012**, *23*, 981.

(156) Napp, J.; Behnke, T.; Fischer, L.; Würth, C.; Wottawa, M.; Katschinski, D. M.; Alves, F.; Resch-Genger, U.; Schäferling, M. *Anal. Chem.* **2011**, *83*, 9039.

(157) Saxena, V.; Sadoqi, M.; Shao, J. *Int. J. Pharm.* **2004**, *278*, 293.

(158) Ma, Y.; Sadoqi, M.; Shao, J. *Int. J. Pharm.* **2012**, *436*, 25.

(159) Zheng, C.; Zheng, M.; Gong, P.; Jia, D.; Zhang, P.; Shi, B.; Sheng, Z.; Ma, Y.; Cai, L. *Biomaterials* **2012**, *33*, 5603.

(160) Schadlich, A.; Rose, C.; Kuntsche, J.; Caysa, H.; Mueller, T.; Gopferich, A.; Mader, K. *Pharm Res* **2011**, *28*, 1995.

(161) Deniz, E.; Kandoth, N.; Fraix, A.; Cardile, V.; Graziano, A. C.; Lo Furno, D.; Gref, R.; Raymo, F. M.; Sortino, S. *Chemistry* **2012**, *18*, 15782.

(162) Sarkar, D. *J. Photochem. Photobiol., A* **2013**, *252*, 194.

(163) Chang, S.; Wu, X.; Li, Y.; Niu, D.; Gao, Y.; Ma, Z.; Gu, J.; Zhao, W.; Zhu, W.; Tian, H.; Shi, J. *Biomaterials* **2013**, *34*, 10182.

(164) Sauer, R.; Turshatov, A.; Baluschev, S.; Landfester, K. *Macromolecules* **2012**, *45*, 3787.

(165) Qiang, X.; Wu, T.; Fan, J.; Wang, J.; Song, F.; Sun, S.; Jiang, J.; Peng, X. *J. Mater. Chem.* **2012**, *22*, 16078.

(166) Dossi, M.; Ferrari, R.; Dragoni, L.; Martignoni, C.; Gaetani, P.; D'Incalci, M.; Morbidelli, M.; Moscatelli, D. *Macromol. Mater. Eng.* **2013**, *298*, 771.

(167) Zandanel, C.; Vauthier, C. *Eur J Pharm Biopharm* **2012**, *82*, 66.

(168) Chen, J.; Zhang, P.; Fang, G.; Weng, C.; Hu, J.; Yi, P.; Yu, X.; Li, X. *Polym. Chem.* **2012**, *3*, 685.

(169) Chen, J.; Zhang, P.; Fang, G.; Yi, P.; Yu, X.; Li, X.; Zeng, F.; Wu, S. *J. Phys. Chem. B* **2011**, *115*, 3354.

(170) Slomkowski, S.; Alemán, J. V.; Gilbert, R. G.; Hess, M.; Horie, K.; Jones, R. G.; Kubisa, P.; Meisel, I.; Mormann, W.; Penczek, S.; Stepto, R. F. T. *Pure Appl. Chem.* **2011**, *83*, 2229.

(171) Thompson, M. P.; Randolph, L. M.; James, C. R.; Davalos, A. N.; Hahn, M. E.; Gianneschi, N. C. *Polym. Chem.* **2014**.

(172) Bremer, C.; Bredow, S.; Mahmood, U.; Weissleder, R.; Tung, C.-H. *Radiology* **2001**, *221*, 523.

(173) Thomas, S. W.; Joly, G. D.; Swager, T. M. *Chem. Rev.* **2007**, *107*, 1339.

(174) Tuncel, D.; Demir, H. V. *Nanoscale* **2010**, *2*, 484.

(175) Baier, M. C.; Huber, J.; Mecking, S. *J. Amer. Chem. Soc.* **2009**, *131*, 14267.

(176) Ahmed, E.; Morton, S. W.; Hammond, P. T.; Swager, T. M. *Adv. Mater.* **2013**, *25*, 4504.

(177) Lee, R. J.; Low, P. S. *J. Biol. Chem.* **1994**, *269*, 3198.

(178) Gu, L.; Fang, R. H.; Sailor, M. J.; Park, J.-H. *ACS Nano* **2012**, *6*, 4947.

(179) Na, H. B.; Song, I. C.; Hyeon, T. *Adv. Mater.* **2009**, *21*, 2133.

(180) Courant, T.; Roullin, V. G.; Cadiou, C.; Callewaert, M.; Andry, M. C.; Portefaix, C.; Hoeffel, C.; de Goltstein, M. C.; Port, M.; Laurent, S.; Elst, L. V.; Muller, R.; Molinari, M.; Chuburu, F. *Angew. Chem. Int. Ed.* **2012**, *51*, 9119.

(181) Chen, K.-J.; Wolahan, S. M.; Wang, H.; Hsu, C.-H.; Chang, H.-W.; Durazo, A.; Hwang, L.-P.; Garcia, M. A.; Jiang, Z. K.; Wu, L.; Lin, Y.-Y.; Tseng, H.-R. *Biomaterials* **2011**, *32*, 2160.

(182) Jaspers, K.; Versluis, B.; Leiner, T.; Dijkstra, P.; Oostendorp, M.; van Golde, J. M.; Post, M. J.; Backes, W. H. *PLoS One* **2011**, *6*, e16159.

(183) Langereis, S.; Dirksen, A.; Hackeng, T. M.; van Genderen, M. H. P.; Meijer, E. W. *New J. Chem.* **2007**, *31*, 1152.

(184) Dumas, S.; Jacques, V.; Sun, W. C.; Troughton, J. S.; Welch, J. T.; Chasse, J. M.; Schmitt-Willich, H.; Caravan, P. *Invest. Radiol.* **2010**, *45*, 600.

(185) Li, S.; Jiang, J.; Zou, J.; Qiao, J.; Xue, S.; Wei, L.; Long, R.; Wang, L.; Castiblanco, A.; White, N.; Ngo, J.; Mao, H.; Liu, Z.-R.; Yang, J. J. *J. Inorg. Biochem.* **2012**, *107*, 111.

(186) Guodong Zhang, R. Z., Xiaoxia Wen, Li Li, Chun Li *Biomacromolecules* **2008**, *9*, 36.

(187) Turner, J. L.; Pan, D.; Plummer, R.; Chen, Z.; Whittaker, A. K.; Wooley, K. L. *Adv. Funct. Mater.* **2005**, *15*, 1248.

(188) Liu, T.; Qian, Y.; Hu, X.; Ge, Z.; Liu, S. *J. Mater. Chem.* **2012**, *22*, 5020.

(189) Ratzinger, G.; Agrawal, P.; Korner, W.; Lonkai, J.; Sanders, H. M.; Terreno, E.; Wirth, M.; Strijkers, G. J.; Nicolay, K.; Gabor, F. *Biomaterials* **2010**, *31*, 8716.

(190) Grogna, M.; Cloots, R.; Luxen, A.; Jerome, C.; Passirani, C.; Lautram, N.; Desreux, J.-F.; Detrembleur, C. *Polym. Chem.* **2010**, *1*, 1485.

(191) Ratzinger, G.; Fillafer, C.; Kerleta, V.; Wirth, M.; Gabor, F. **2010**, *27*, 1.

(192) Ayyagari, A. L.; Zhang, X.; Ghaghada, K. B.; Annapragada, A.; Hu, X.; Bellamkonda, R. V. *Magnet. Reson. Med.* **2006**, *55*, 1023.

(193) Liu, T.; Li, X.; Qian, Y.; Hu, X.; Liu, S. *Biomaterials* **2012**, *33*, 2521.

2. Labeling Polymers With Complex Peptides Via Graft-To and Graft-Through Polymerization

2.1 Introduction

The sophistication of functional biohybrid polymers and soft organic nanoparticles (NPs), which display biomolecules on a synthetic skeleton, is of increasing interest.[1-3] These polymer bioconjugates contain biomolecules, such as peptides or nucleic acids, for the purpose of facilitating recognition events and other processes specific to their sequence. Furthermore, current research tasks these polymers with programming dynamic nanomaterial morphology in response to enzyme-catalyzed reactions.[4-11] Our aim in this study is to establish a new approach towards the display of peptides as brush copolymers and within polymeric NPs via their direct incorporation into polymers via graft-through polymerization reactions.

We strive for a well-controlled method for the incorporation of arraying peptides as brushes conjugated to polymeric backbones or polymeric NPs. Our inspiration comes from previous work employing living polymerization methods for the preparation of peptide-bearing polymers synthesized either from conjugation after polymerization[5,12] (graft-to) or directly from monomers (graft-through), which contain polymerizable peptide units.[13-19] In this work, we chose to optimize ring-opening metathesis polymerization (ROMP) for the purpose of allowing the preparation of well-defined peptide substrate-containing polymers and polymeric NPs. We reasoned an initial study of such systems would have broad implications for the design of future polymeric materials displaying peptides for reaction with enzymes, or for resistance to their environment. Therefore, we sought to answer the following key questions regarding polymeric

peptide-based synthetic materials synthesized by graft-through polymerization with ROMP: (1) Can well defined enzymatically active peptide-containing polymers be synthesized utilizing graft-to conjugation techniques; (2) Can graft-through peptide polymers be generated with relatively high degrees of polymerization and with low dispersity and (3) Can well-defined peptide-brush copolymers generated via graft-through polymerization techniques be formulated into NPs of low polydispersity?

2.2 Post-Polymerization Modification

One of the only examples of the enzyme-driven assembly of a polymer into a nanoparticle comes from Hawker and coleagues.[10] Inspired by this approach, we designed a polymer capable of assembling into nanoscale architectures upon enzymatic activation with matrix metalloproteinases (MMPs) (Figure 2.1). To create an enzyme responsive peptide-polymer we synthesized a block copolymer using ROMP, containing different ratios of a water solubilizing oligoethylene glycol (OEG) block together with a *N*-hydroxysuccinimide (NHS) block that is amenable to conjugation with the N-terminus of a peptide. The peptide sequence used in these studies were designed as substrates for the cancer-associated enzymes, matrix-metalloproteinase 2 and 9 (MMP-2/9).[20] In the presence of MMP-2/9, the peptide sequence is cleaved between the Gly-Leu residues, leaving a truncated peptide sequence of Gly-Pro-Leu-Gly. We hypothesized that this sequence would provide enough build up of hydrophobicity to cause an aggregation event (Figure 2.1). This section discusses the synthetic

strategy and preliminary enzyme responsiveness of these peptide-containing block-copolymers.

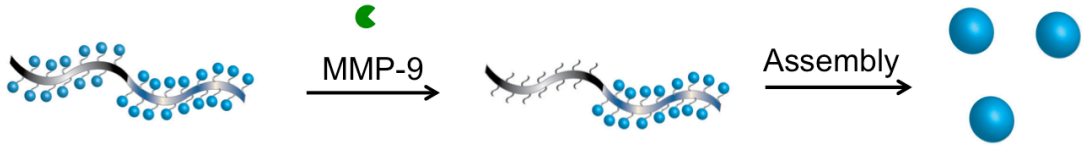

Figure 2.1 Schematic representation of the enzyme activation of a solvated polymer resulting in an amphiphilic block copolymer and subsequent self-assembly.

2.2.1 Synthesis of Peptide Brush Copolymers

Block copolymers were synthesized using ROMP to create a hydrophilic polymer that is capable of conjugation with the N-terminus of the MMP peptide substrate (GPLGLAG) and/or the cleavage fragment (GPLG). For this reason, two different block copolymers containing an NHS block of monomer **1** and an OEG block of monomer **2** were synthesized (Figure 2.2). A known amount of NHS monomer **1** ("m" equivalents) was polymerized and a small portion was quenched with ethyl vinyl ether (EVE). The homopolymer of **1** was analyzed by size exclusion chromatography coupled with multi-angle light scattering (SEC-MALS) allowing the determination of the degree of polymerization (DP) of the first block. Next, "n" equivalents of OEG monomer **2** was added to the living polymer and quenched with EVE to give the final block copolymers **3** and **4** (Table 2.1). Polymers **3** and **4** have the composition of $\mathbf{1}_{24}$-*b*-$\mathbf{2}_{40}$ and $\mathbf{1}_{15}$-*b*-$\mathbf{2}_{42}$ with an excellent dispersity of 1.06 and 1.09 respectively (Table 2.1).

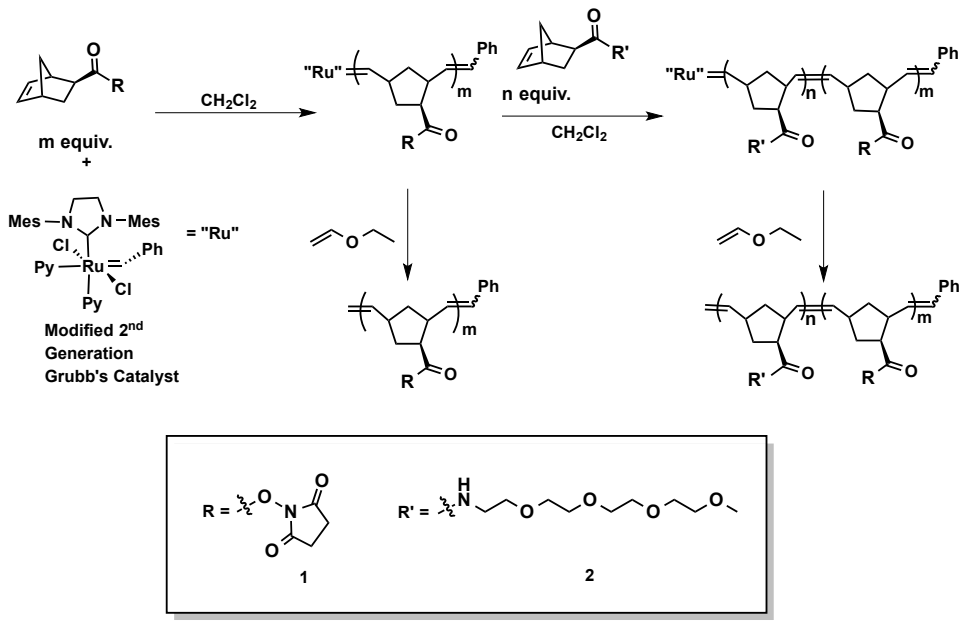

Figure 2.2 General synthetic scheme for the preparation of hydrophilic block copolymers.

Table 2.1 Characterization of Block Copolymers **3** and **4**. [a] Degree of polymerization of monomer **1**. [b] Degree of polymerization of monomer **2**. [c] Number average molecular weight as determined by SEC-MALS. [d] Dispersity as determined by SEC-MALS.

Polymer	DP_m (**1**)[a]	DP_n (**2**)[b]	M_n[c]	M_w/M_n[d]
3	24	40	18,700	1.063
4	15	42	17,300	1.089

Polymers **3** and **4** were further modified by chemical conjugation of the MMP-2/9 peptide substrate of the sequence GPLGLAG (Figure 2.3). Each of the polymers contains an NHS activated ester block, allowing for conjugation of the N-terminus of the peptide to the polymer backbone. To add further water-solubility to the peptide block, an additional post-polymerization modification was implemented by adding OEG onto the C-terminus of the peptide in the presence of HBTU to afford water-soluble polymers **5** and **6** (Table 2.2). Following each

post-polymerization modification, the polymers are analyzed by SEC-MALS, however in both cases inconclusive data was obtained. After addition of the peptide substrate and OEG to polymers **3** and **4**, the molecular weight decreased as determined by SEC-MALS of the peptide-polymers **5** and **6** (Table 2.1 and Table 2.2). Reasons for this may include problems with aggregation leading to inaccuracies in correctly interpreting the refractive index and hence preventing accurate characterization of the polymer conjugates. Regardless, we decided to continue with polymers **5** and **6** and run a pilot enzymatic study to test our initial hypothesis (Section 2.2.2).

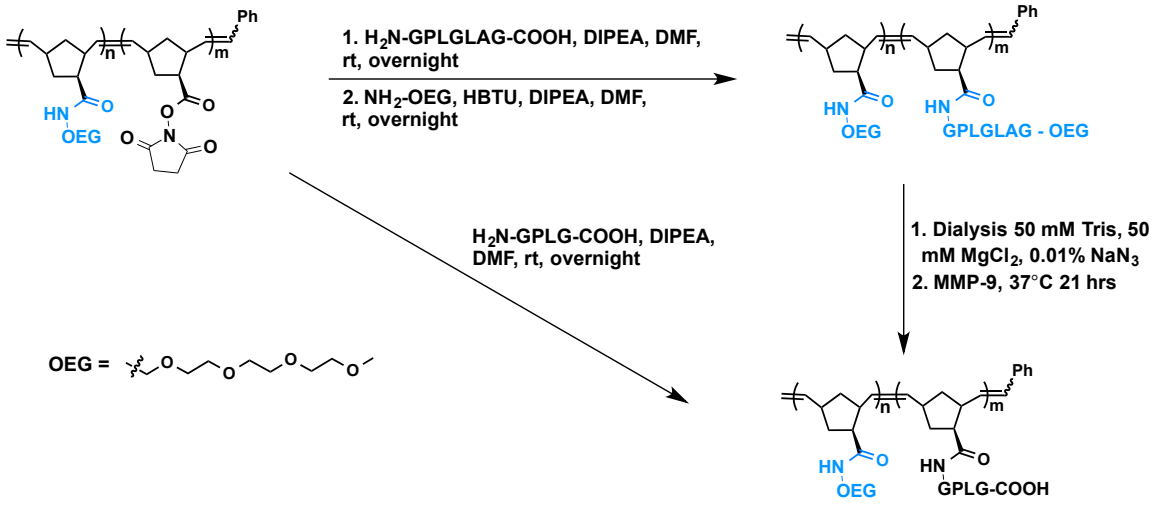

Figure 2.3 Synthetic approaches for the enzymatic or chemical formation of peptide polymer amphiphiles (PPAs). Blue indicates the hydrophilic component of each polymer.

Table 2.2 Peptide Block Copolymer Characterization. [a] Characterization by SEC-MALS after addition of GPLGLAG was unsuccessful. [b] Characterization after addition of OEG was unsuccessful. [c] Addition of GPLG as determined by SEC-MALS. [d] Not applicable. [e] Characterization by SEC-MALS was unsuccessful. [f] Characterization by SEC-MALS was unsuccessful.

Polymer	Post-Polymerization Addition of Peptide	Post Polymerization Addition of OEG	M_n	M_w/M_n
5	-[a]	-[b]	56,340	1.205
6	-[a]	-[b]	13,380	1.089
7	8[c]	na[d]	18,860	1.243
8	-[e]	na[d]	-[f]	-[f]

In addition to polymers **5** and **6**, polymers containing the peptide sequence after enzymatic cleavage (i.e. GPLG) were synthesized. Using the same polymers **3** and **4**, conjugation of GPLG to the NHS block afforded peptide polymer amphiphiles (PPAs) **7** and **8**. After addition of GPLG to polymer **3**, the polymer was characterized by SEC-MALS to determine the number of peptides successfully conjugated to the polymer backbone. As shown in Table 2.2, polymer **7** affords the successful conjugation of 8 peptides however the dispersity increased from 1.09 to 1.24. It is assumed that the increase in dispersity is a result of different distribution of successful peptide conjugations to polymer **3**. Similar to polymers **5** and **6**, characterization by SEC-MALS led to inconclusive results in the case of polymer **8.** Even though the exact composition and molecular weight of polymers **5**, **6**, and **8** are unknown, we conducted a preliminary experiment to compare the enzymatic and synthetic routes to forming PPAs. Indeed, we highlight this attempt at generating peptide-brush polymers via

graft-to conjugation in part because the failure of this strategy lead directly to our efforts to achieve graft-through polymerization of peptides as will be discussed later in this chapter.

2.2.2 Enzymatic vs. Chemical Formation of PPAs

The enzymatic response of polymers **5** and **6** was examined by addition of MMP-9 to aqueous solutions of each of the polymers. Separately, each polymer was transitioned from DMF to a 50 mM Tris, 50 mM $MgCl_2$ buffer. Analysis by dynamic light scattering (DLS) and transmission electron microscopy (TEM) confirms the absence of aggregates (data not shown). Next, polymers **5** and **6** are incubated with MMP-9 at 37 ºC for 24 hours. Additionally, polymers **5** and **6** are incubated in buffer at 37 ºC for 24 hours to confirm that heat does not cause an aggregation event (data not shown). Polymer **5**, containing a theoretical maximum of 24 MMP peptide substrates, displayed a tri-modal distribution by DLS of 75, 350, and 1120 nm aggregates (Figure 2.4B). TEM revealed a large distribution of sheet-like aggregates upon activation with MMP-9 (Figure 2.4C), but in the absence of MMP-9, polymer **5** showed no NP formation as determined by DLS or TEM. Polymer **6**, with a theoretical maximum of 15 peptides, showed smaller aggregate formation by DLS after incubation with MMP-9 (Figure 2.4E), however TEM showed larger aggregates. This discrepancy in aggregation could be the result of drying the sample onto a carbon/formvar grid, where in solution, the nanoparticles stay dispersed.

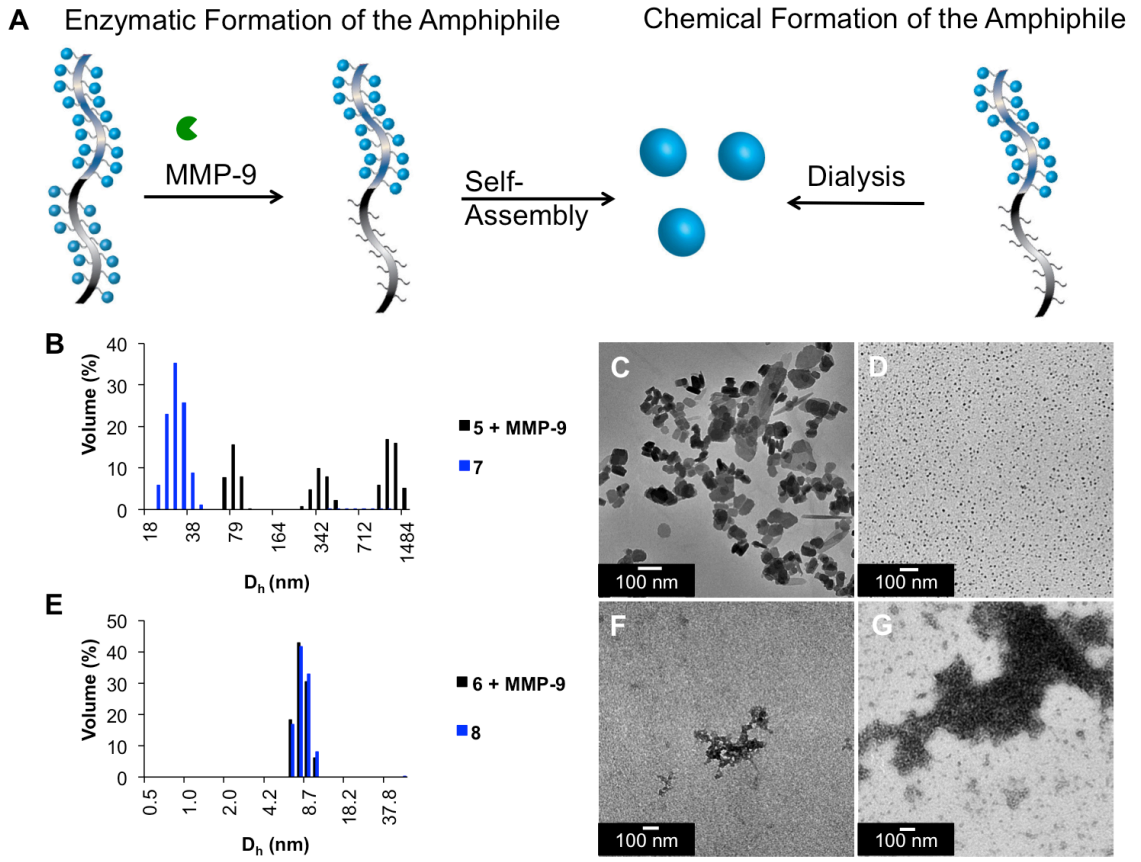

Figure 2.4 Comparison of enzymatic and synthetic routes to PPA and NP formation. A) Schematic representation of enzymatic activation and self-assembly of a solvated peptide polymer and the self-assembly of a synthetic PPA. B) DLS of polymer **5** after activation with MMP-9 and polymer **7** after transition into an aqueous environment. C) TEM, stained with 1% uranyl acetate, of polymer **5** after treatment with MMP-9. D) TEM, stained with 1% uranyl acetate, of polymer **7** after transition into an aqueous solution. E) DLS of polymer **6** after activation with MMP-9 and polymer **8** after transition into water. F) TEM, stained with 1% uranyl acetate, of polymer **6** after treatment with MMP-9. G) TEM, stained with 1% uranyl acetate, of polymer **8** after transition into 50 mM Tris, 50 mM $MgCl_2$.

We hypothesized that a synthetic polymer containing the cleavage sequence of GPLG would self-assemble into similar structures as the enzymatic product of solvated polymers **5** and **6**. For this reason, we transitioned polymers **7** and **8** separately from methanol into a 50 mM Tris, 50 mM $MgCl_2$ solution. Both

samples were analyzed by DLS and TEM (Figure 2.4) and compared to their enzymatically generated counterparts. Polymer **7** theoretically should form the same nanostructures as polymer **5** after treatment with MMP-9. However, by DLS and TEM we saw a significantly different pattern of nanostructures. Analysis by DLS reveals smaller aggregates with a hydrodynamic diameter of 20 nm, which is in contrast to the tri-modal distribution visualized for the enzymatically-driven formation of the same PPA (Figure 2.4B). TEM additionally shows small nanoparticles scattered throughout the grid (Figure 2.4D). However, the enzymatically formed PPA shows a larger size distribution of thin sheet-like aggregates (Figure 2.4C). In the case of polymer **8**, comparison of the synthetic and enzymatic formulation of a PPA results in an identical DLS trace and very similar TEM images (Figure 2.4E-G). However, it is difficult to draw a clear conclusion from these results, as the polymers themselves are not fully characterized by standard methods. Again, these were initial attempts used to generate this class of copolymer, that lead directly to our concerted effort to develop and optimize the graft-through polymerization of complex peptide polymers. The initial efforts will be described in the following section.

2.3 Graft-Through Polymerization to Generate Peptide Brush Copolymers

The results we obtained from post-polymerization formation of PPAs led us to attempt the preparation of PPAs utilizing a graft-through approach. One must note that polymers prepared with a graft-through approach can be chemically homogenous in nature, due to the propagation step of polymerization.

Indeed, the fidelity of that step is responsible for the polymer quality as it is responsible for incorporating functionality. This is in contrast to post-polymerization modification strategies in which less than quantitative modification of the polymer backbone is naturally expected[5,12] and often difficult to characterize, as shown above. This is inherently the case because standard conjugation reactions are usually not as efficient as any of the polymerization reactions used to generate low dispersity polymers. When these studies were initiated ROMP was known to have the ability to enable polymerization of short norbornyl-modified oligopeptides (1-3 amino acids) with aliphatic sequences to varying degrees. However, this often came with high dispersity and a low complexity of peptide side chains.[14,18,19,21] Moreover, we found no studies examining the graft-through incorporation of specific peptide-based enzyme substrates into polymeric materials. It is necessary that more complex peptides be incorporated if this strategy is to be useful for developing functional materials.

2.3.1 Synthesis of a Polymerizable Peptide Substrate

We began the process by preparing amphiphilic block copolymers, utilizing norbornenyl-peptide monomers, capable of formulating into nanoparticles (*vide infra*) shown in Figure 2.5. Each contains a polymerizable norbornenyl group conjugated to the N-terminus of a peptide sequence. Monomers **9** and **10** contain an amino acid sequences that are known substrates of (MMP-2/9),[20] with a water-solubilizing group, 4-((2-(2-(2-

aminoethoxy)ethoxy)ethyl)amino)-4-oxobutanoic acid (Ebes), included in the structures to promote micelle formation.

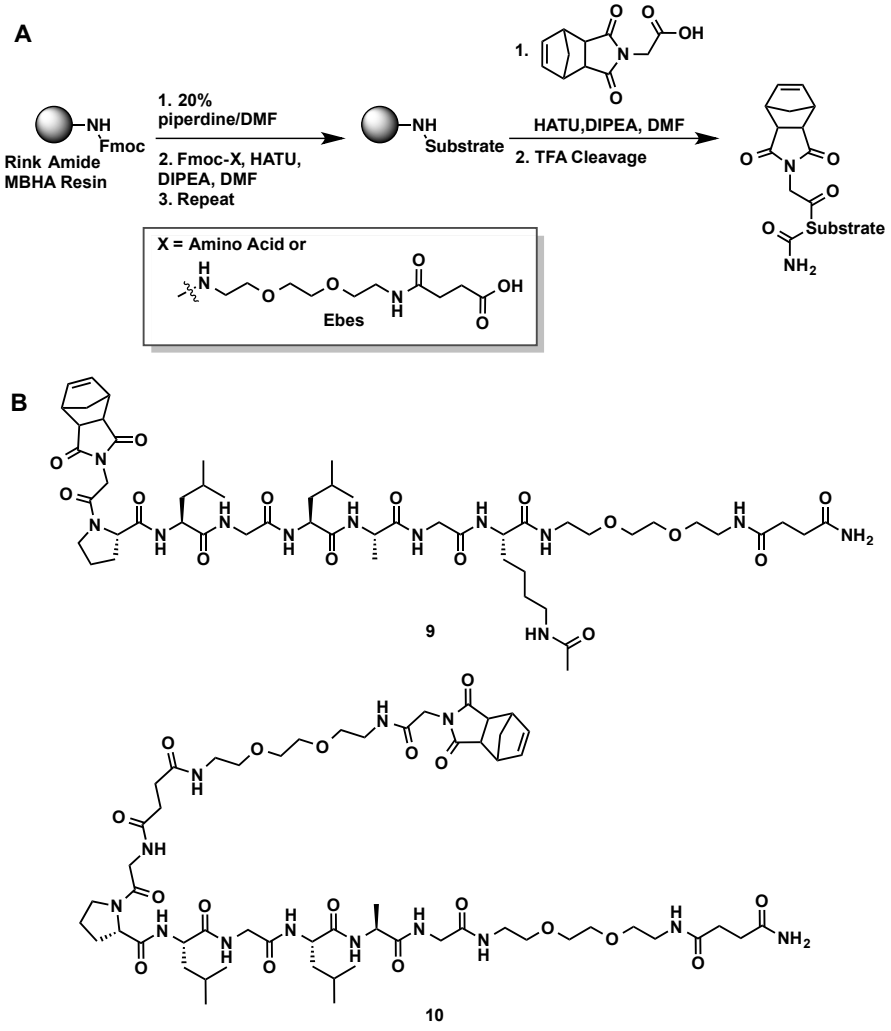

Figure 2.5 General synthetic scheme for the preparation of polymerizable peptide monomers **9** and **10**. A) General solid phase synthetic scheme. B) Structure of peptide monomers.

Monomers **9** and **10** were synthesized using standard solid phase peptide coupling. The resin is first treated with 20% piperidine in DMF, utilizing an Fmoc-protected rink amide MBHA resin (Figure 2.5A). HATU coupling with amino acids and/or Ebes is repeated until the final sequence is achieved. Before cleavage from the resin, a norbornenyl-functionalized glycine was coupled onto the final peptide sequence and cleaved from the resin with TFA to produce the final peptide monomer. It should be noted that polymerization was optimal when a

norbornenyl-pyrrolidine-2,5-dione was conjugated to the peptide sequence rather than a norbornene with a single exo-carboxamide moiety, as used in the post-polymerization strategy described above. The sequence is Norb-GPLGLAGK(Ac)-Ebes-NH_2 (Monomer **9**) or Norb-G-Ebes-GPLGLAG-Ebes-NH_2 (Monomer **10**). Monomer **9** and **10** are purified by reverse phase HPLC (RP-HPLC) and analysis by ESI-MS confirms the correct molecular weight (Figure 2.6 and Figure 2.7).

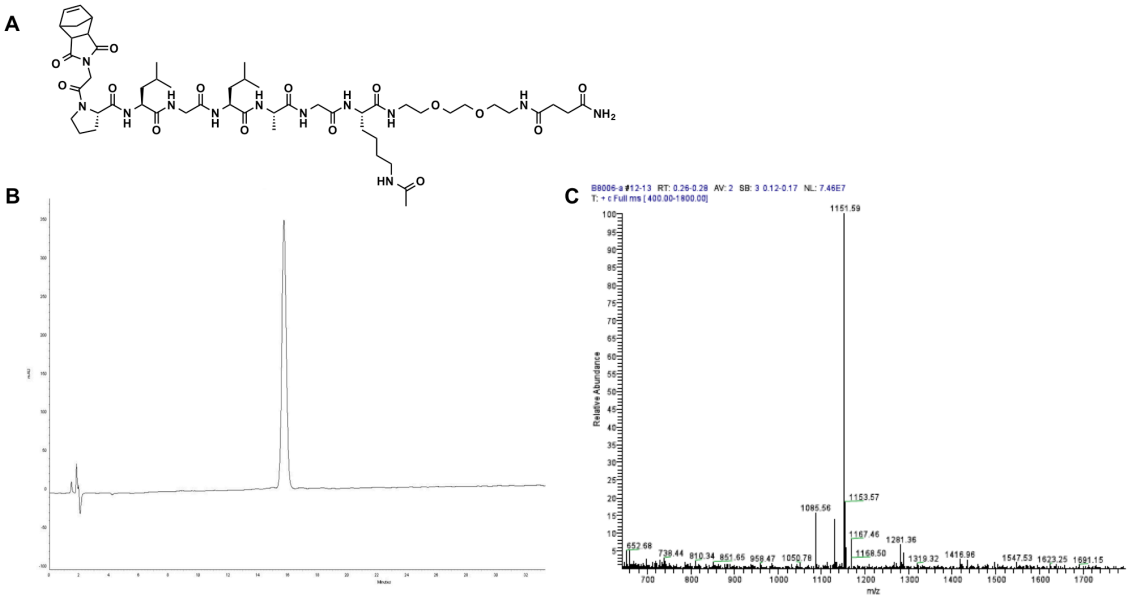

Figure 2.6 Characterization of monomer **9**. A) Structure of monomer **9**. B) Analytical RP-HPLC of purified monomer **9** on a 25 – 35% ACN in H_2O with 0.1% TFA gradient. C) ESI-MS of monomer **9**; found *m/z* 1129.43, expected 1129.62 $M+H^+$; found *m/z* 1151.59, expected 1151.61 $M+Na^+$.

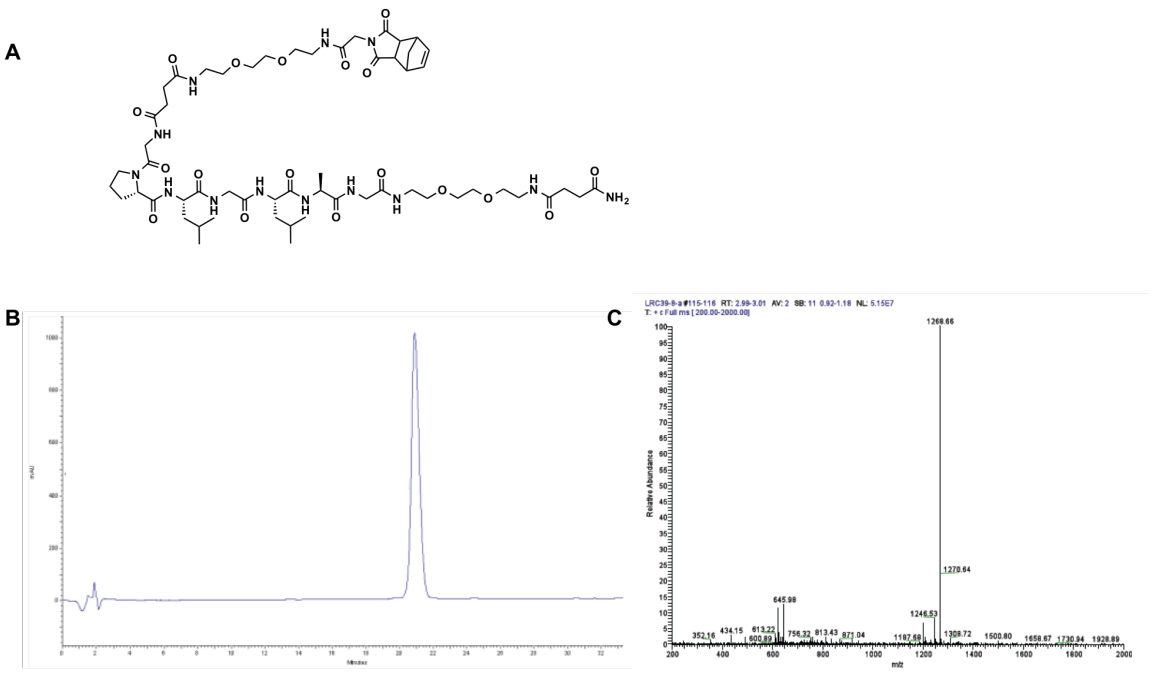

Figure 2.7 Characterization of monomer **10**. A) Structure of monomer **10**. B) Analytical RP-HPLC of pure monomer **10** over a 22 – 29% ACN in H_2O with 0.1% TFA. C) ESI-MS of monomer **10**. Found *m/z* 1246.53, expected 1246.67 $M+H^+$; found *m/z* 1268.66, expected 1268.65 $M+Na^+$; found *m/z* 645.98, expected 645.82 $M+2Na^+$.

2.3.2 Polymerization of Peptide Monomers

We set out to determine if peptides of this class were efficiently polymerized via ROMP in order to prepare homopolymers with a high degree of polymerization and simultaneous low dispersity. Monomer **9** was polymerized using a modified 2nd generation Grubbs' catalyst at room temperature.[16] NMR spectroscopy demonstrated that the polymerization reaction was complete, as evidenced by the conversion of norbornenyl olefinic protons to polynorbornene olefinic protons (Figure 2.8B). SEC-MALS revealed the achievement of both a high degree of polymerization (DP > 100) and a favorable low dispersity (M_w/M_n = 1.01, Figure 2.8A, Table 2.3). It is important to note that optimal conditions,

including the use of anhydrous dinitrogen atmospheres, were required for ideal results using either dimethylformamide (DMF) or dichloromethane–methanol mixtures as effective solvents. If polymerizations were exposed to ambient air, reaction times were significantly increased and in many cases, NMR would reveal incomplete conversion of monomer to polymer.

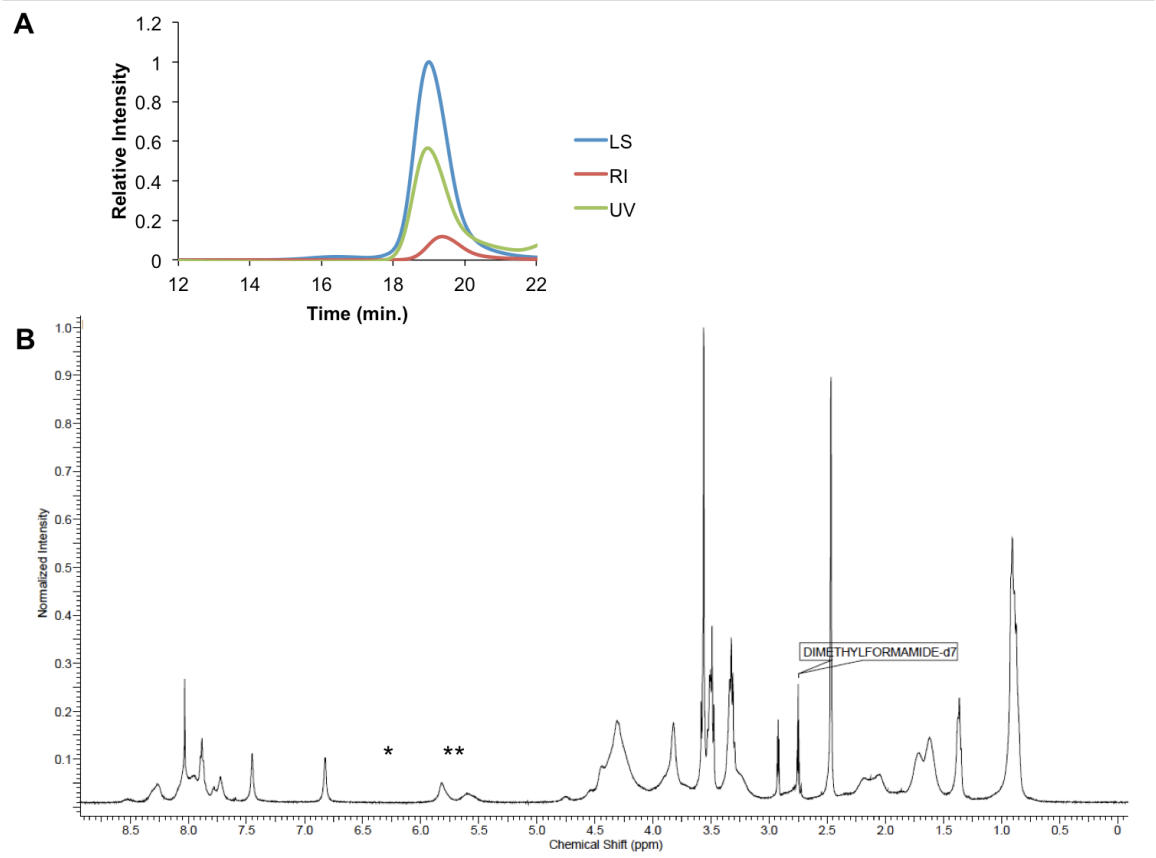

Figure 2.8 Characterization for the polymerization of monomer **9**. A) SEC-MALS of a homopolymer of monomer **9**. B) NMR of a homopolymer of monomer **9** showing complete consumption of norbornene olefin protons (annotated by *) and appearance of polymer backbone peaks (annotated by **).

Table 2.3 Characterization of Graft-Through PPAs. [a] Monomer displayed in bold with subsequent degree of polymerization (DP of block m or n) in parentheses. [b] Only a homopolymer is synthesized.

Entry	Polymer	Monomer (DP_m)[a]	Monomer (DP_n)[a]	M_n	M_w/M_n
1	**12**	**9** (131)	-[b]	125,300	1.012
2	**13**	**9** (13)	**11** (116)	44,630	1.200
3	**14**	**11** (74)	**10** (5)	23,570	1.056

Next, we set out to determine if graft-through peptide ROMP could be used in the preparation of peptide-containing amphiphilic block copolymers (PPAs) of low dispersity, which could then be formulated into NPs. We accomplished the one-pot synthesis of PPA **13** with the addition of a modified 2nd generation Grubbs' catalyst (Figure 2.9) to a solution of hydrophilic peptidyl monomer **9**, followed by the addition of hydrophobic monomer **11**, as previously prepared in our laboratory.[4] Polymerization of the hydrophobic monomer **11**, followed by the hydrophilic norbornenyl peptide monomer **10** (PPA **14**), was prepared by reversing the order of monomer addition. This allowed us to demonstrate generality in the polymerization process with respect to order of addition (Figure 2.9). We utilized SEC-MALS to determine the absolute number-average molecular weight (M_n), weight-average molecular weight (M_w), degree of polymerization (DP), and dispersity of PPAs **13** and **14** prior to generation of NPs (Table 2.3).

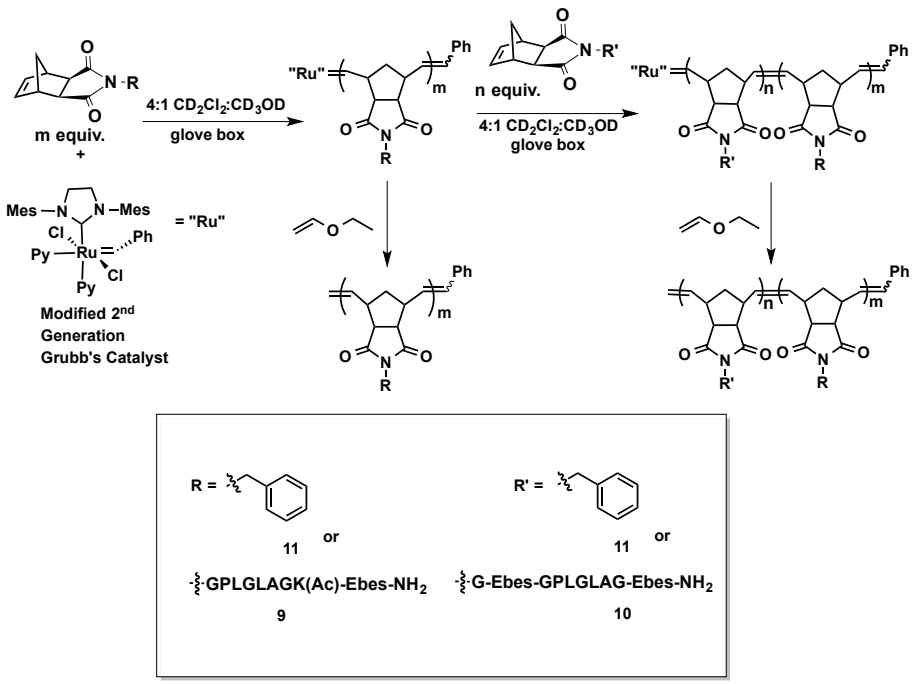

Figure 2.9 General synthetic scheme for the preparation of PPAs **13** and **14**.

2.3.3 Nanoparticle formation of PPAs

Each polymer was dissolved separately in DMF to begin the formulation of PPAs into NPs. We follow this by gradually adding water to a final concentration of 50% by volume.[22] Then, we dialyzed incipient NP suspensions against water to remove any excess DMF. We employed DLS in water to determine the hydrodynamic diameter of the NPs derived from PPAs **13** and **14** (Figure 2.10). This resulted in a hydrodynamic diameter of 28 nm for PPA **13** and 124 nm for PPA **14**. Statistical analysis of the DLS data informed us that the size distribution of the nanoparticles is narrow with correspondingly low polydispersities (0.062 for PPA **13** and 0.020 for PPA **14**). TEM of the NPs validated the DLS data, which shows the presence of spherical particles (Figure 2.10). We note that the

resulting micelles are observed to be stable, without change in DLS or TEM, for at least 6 months at 4 ºC.

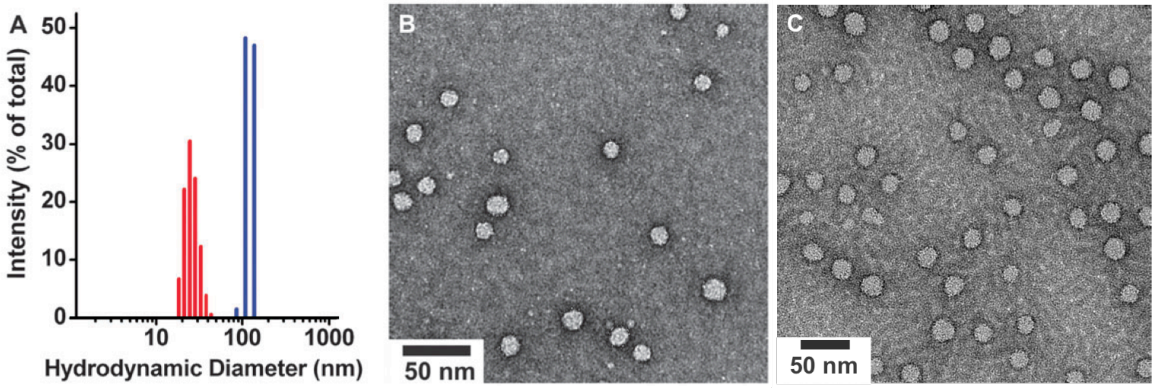

Figure 2.10 NP characterization of PPA **13** and PPA **14**. A) DLS of PPA **13** (red) and PPA **14** (blue), B) TEM of PPA **13**, C) TEM of PPA **14**.

2.3.4 Enzymatic Response of Graft-Through Peptide Polymers

NPs derived from PPA **13** were incubated with active MMP-2 and no proteolysis product could be identified by RP-HPLC under the same conditions used for processing water-soluble peptide polymers prepared by the graft-to technique described above.[23] This implies that the peptide substrates arrayed on the particle are protected from protease-mediated cleavage. We hypothesize that this is due to steric crowding of the displayed peptides on the NP scaffold that forbids the enzyme from accessing the scissile peptide bond within the displayed peptides. This is in contrast to the high activity we have observed for related systems that are responsive to MMP catalyzed cleavage when prepared via post-polymerization modification of polymers with peptides.[5,12] Notably, these related systems are characterized by a lower density of peptides displayed, due to low conjugation efficiency inherent to such reactions. These results hint at the possibility of arranging peptides to capitalize on resistance to proteolytic

degradation versus optimizing for activity and responsiveness. Extensive studies focusing on the relationships between substrate spatial density, polymer structure,[24] particle morphology, reaction conditions, sequence identity and enzymatic activity are currently underway in our laboratories.[25]

2.4 Conclusions

Our work demonstrates several important principles crucial to the future use of peptide containing polymers and NPs prepared by graft-to and graft-through polymerization procedures. We have demonstrated the difficulty in characterizing peptide polymers prepared by a graft-to technique. NPs can be prepared from water-soluble peptide polymers by the enzymatic activation with over expressed enzyme MMP-9. Synthetic formulation of the enzyme cleavage product to a PPA results are inconsistent with the enzymatic product. This led us to directly polymerize peptide substrates for the synthesis of peptide polymer amphiphiles.

We have utilized graft-through polymerization for the preparation of peptide containing homopolymers and block copolymers, which possess a high degree of polymerization and simultaneous low dispersity. The resulting NPs, formulated via self-assembly of two different peptide-containing amphiphilic block copolymers, are also of low dispersity. Blocks of peptides, when chosen appropriately, can function as the hydrophilic block of a block-copolymer PPA while the order of polymerization is not crucial. These peptide substrates of MMPs, displayed on a water-soluble polymer, are able to be enzymatically

processed, as shown by our group.[23] In contrast, when displayed on the NP scaffold, the same peptide is less susceptible to proteolysis.[23]

2.5 Experimental

2.5.1 General Methods

All reagents were purchased from commercial sources and used without further purification unless otherwise indicated below. CD_2Cl_2, CH_2Cl_2, CH_3OH, and CD_3OD used in polymerization reactions were dried over CaH_2 and 5 Å molecular sieves. These were then degassed with 3 freeze-pump-thaw cycles. Sealed ampules of DMF-d_7 (Cambridge Isotopes) were used without modification. Monomer **1** was prepared as previously described.[26] Modified 2nd Generation Grubbs' Ruthenium initiator, $(IMesH_2)(C_5H_5N)_2(Cl)_2Ru{=}CHPh$, was prepared as previously described.[27] 2,5,8,11-tetraoxatridecan-13-amine (NH_2-OEG) was prepared as described previously.[28] Norbornenyl-glycine was prepared as previously described.[16] Monomer **11** was prepared as previously described.[4] Polymerizations were performed under dry dinitrogen atmospheres. Polymer dispersity and molecular weight were determined by size-exclusion chromatography (Phenomenex Phenogel 5u **10**, 1K-75K, 300 x 7.80 mm in series with a Phenomex Phenogel 5u **10**, 10K-1000K, 300 x 7.80 mm (0.05 M LiBr in DMF)) using a Shimadzu LC-10ATVP pump equipped with a multi-angle light scattering detector (DAWN-HELIOS, Wyatt Technology), a refractive index detector (Hitachi L-2490) and a UV-Vis detector (SPD-10AVP) normalized to a polystyrene standard. The *dn/dc* values used were 0.179 for all polymers. The ^1H

NMR spectra were recorded on a Varian Mercury Plus spectrometer. Chemical shifts (^{1}H) are reported in δ (ppm) relative to the residual solvent peak. Mass spectra were obtained at the UCSD Chemistry and Biochemistry Molecular Mass Spectrometry Facility. D_h was determined by DLS on a Nano-ZS90- (Malvern) or DynaPro NanoStar (Wyatt). TEM images were acquired on a carbon Forvar grid (Ted Pella, Inc.) with 1% uranyl acetate stain on a FEI Tecnai G2 Sphera at 200 kV.

2.5.2 General Synthetic Procedures

Synthesis of OEG Monomer **2**. NH_2-OEG (483 mg, 2.33mmol) and DIPEA (739 mL, 4.24 mmol) were added to a solution of the NHS monomer (500 mg, 2.12 mmol) in dry DCM (12 mL). The reaction was stirred at room temperature under a nitrogen atmosphere overnight. The reaction mixture was concentrated to dryness and purified by flash chromatography, 10% MeOH in DCM to give a clear oil.

Peptide sequences used in graft-to polymerization were synthesized manually using standard Fmoc solid phase peptide synthesis on Wang Resin. Peptide monomers **9** and **10** were synthesized manually using standard Fmoc solid phase peptide synthesis on Rink amide resin (H-Rink Amide-ChemMatrix®, PCAS BioMatrix, Inc., Saint-Jean-sur-Richelieu, Quebec, Canada). Chain assembly was carried out with HBTU activation using a 5-fold excess of amino acid over the resin in DMF with DIPEA as the base. A stream of dry N_2 was used to agitate the reaction mixture. Fmoc removal was carried out with 20%

piperidine in DMF (1 x 3 minutes, followed by 1 x 10 minutes). Cleavage of peptides from the resin was achieved with 95% TFA, 2.5% triisopropylsilane (TIS), and 2.5% H_2O (cleavage cocktail). Crude peptide products of GPLGLAG and GPLG were precipitated and washed with cold Et_2O and used without further purification. Correct molecular weight was determined by ESI-MS. Peptide monomers **9** and **10** were dissolved in 0.1% TFA in water (solvent A). A minimal amount of 0.1% TFA in acetonitrile (solvent B) was added to aid dissolution of any non-dissolved material. RP-HPLC analysis of peptide monomers were performed on a Hitachi-Elite LaChrom L-2130 pump with a binary gradient. Detection was at 214 nm using an in-line UV-Vis detector (Hitachi-Elite LaChrom L-2420). For analysis, an analytical scale Phenomenex Jupiter 4u Proteo 90A column (150 x 4.60 mm) was utilized. For purification, a semi-preparative Phenomenex Jupiter 4u Proteo 90A column (250 x 10.0 mm) was utilized.

Identities and purities of the norbornenyl-peptide monomers were confirmed by RP-HPLC and ESI-MS with detection at 214 nm.

2.5.3 Polymerization Procedures

Synthesis of Polymer **3.** $(IMesH_2)(C_5H_5N)_2(Cl)_2Ru{=}CHPh$ (4.5 mg, 6 μmole) was added to a stirred 2.4 mL solution containing monomer **1** (50 mg, 213 μmole) in CH_2Cl_2 cooled to -78 ºC. The solution was allowed to warm to room temperature and after 1 hour, 5% of the solution was removed and quenched with ethyl vinyl ether (0.05 mL). **2** (28.7 mg, 88 μmole) pre dissolved in 0.1 mL of CH_2Cl_2 was added to the remaining solution. After 1 hour, 0.1 mL of

ethyl vinyl ether was added to the reaction mixture and stirred for 20 minutes. The polymer was then precipitated with an excess of ice-cold diethyl ether and collected by centrifugation. SEC-MALS (Polymer **3**): Homopolymer of **1**: M_n = 5,674; M_w/M_n = 1.08; DP = 24. Copolymer of **1**-*b*-**2**: M_n = 18,700; M_w/M_n = 1.06; DP = 40.

Synthesis of Polymer **4**. $(IMesH_2)(C_5H_5N)_2(Cl)_2Ru{=}CHPh$ (3.5 mg, 5 μmole) was added to a stirred 2.2 mL solution containing monomer **1** (27 mg, 116 μmole) in CH_2Cl_2 cooled to -78 ºC. The solution was allowed to warm to room temperature and after 1 hour, 2% of the solution was removed and quenched with ethyl vinyl ether (0.04 mL). **2** (38 mg, 116 μmole) was added to the remaining solution. After 1.5 hours, 0.05 mL of ethyl vinyl ether was added to the reaction mixture and stirred for 20 minutes. The polymer was then precipitated with an excess of ice-cold diethyl ether and collected by centrifugation. SEC-MALS (Polymer **4**): Homopolymer of **1**: M_n = 3,505; M_w/M_n = 1.03; DP = 15. Copolymer of **1**-*b*-**2**: M_n = 17,340; M_w/M_n = 1.09; DP = 42.

Synthesis of Polymer **5**. DIPEA (0.008 mL, 43 μmol) was added to a stirred solution of polymer **3** (16.7 mg, 0.892 μmol) and MMP-substrate (NH_2-GPLGLAG-COOH, 25 mg, 43 μmol) in DMF (2.3 mL). After 24 hours, the reaction was concentrated under reduced pressure (55 mg) and analyzed by SEC-MALS (no usable data was obtained). Then, DIPEA (0.014 mL, 79.6 μmol) was added to a stirred solution of the peptide-polymer (25 mg, 0.8 μmol), HBTU (30 mg, 79.6 μmol), and 2,5,8,11-tetraoxatridecan-13-amine (NH_2-OEG)[28] (8.25 mg, 39.8 μmol) in DMF (2.0 mL). After 15 hours, the reaction was concentrated

under reduced pressure resulting in 90 mg of a brown oil. SEC-MALS (Polymer **5**): M_n = 56,340, M_w/M_n = 1.205.

Synthesis of Polymer **6**. DIPEA (0.008 mL, 43 μmol) was added to a stirred solution of polymer **4** (25 mg, 1.43 μmol) and MMP-peptide substrate (NH_2-GPLGLAG-COOH, 25 mg, 43 μmol) in DMF (2.3 mL). After 24 hours, the reaction was concentrated under reduced pressure (60 mg) and analyzed by SEC-MALS (no usable data was obtained). Then, DIPEA (0.012 mL, 72 μmol) was added to a stirred solution of the peptide-polymer (30 mg, 1.2 μmol), HBTU (27 mg, 72 μmol), and 2,5,8,11-tetraoxatridecan-13-amine (NH_2-OEG)[28] (7.5 mg, 36 μmol) in DMF (1.8 mL). After 15 hours, the reaction was concentrated under reduced pressure resulting in 77 mg of a brown oil. SEC-MALS (Polymer **6**): M_n = 13,380, M_w/M_n = 1.089.

Synthesis of Polymer **7**. Polymer **3** (28.5 mg, 2 μmol) was added to a stirred solution of the peptide NH_2-GPLG-COOH (25 mg, 73 μmol) in DMF (0.38 mL). The solution was further diluted with DMF (3.4 mL) and DIPEA (0.013 mL, 73 μmol) was added. After 15 hours, the reaction mixture was concentrated under reduced pressure resulting in 49 mg of a brown oil. SEC-MALS (Polymer **7**): M_n = 18,860, M_w/M_n = 1.243, number of peptides conjugated = 8.

Synthesis of Polymer **8**. Polymer **4** (10 mg, 0.6 μmol) in DMF (0.35mL) was added to a stirred solution of the peptide NH_2-GPLG-COOH (6 mg, 17 μmol) in DMF (0.89 mL). DIPEA (0.003 mL, 17 μmol) was added to the reaction mixture and stirred at room temperature under an argon atmosphere. After 15 hours, the reaction mixture was concentrated under reduced pressure resulting in 23 mg of

a brown oil. SEC-MALS (Polymer **8**): No usable data was obtained.

Synthesis of Polymer **12**. $(IMesH_2)(C_5H_5N)_2(Cl)_2Ru{=}CHPh$ (0.136 mg, 0.188 μmole) pre-dissolved in 0.02 mL of DMF-d_7 was added to a stirred 0.43 mL solution containing monomer **9** (18 mg, 18.8 μmole) in DMF-d_7. After 48 hours, the solution was quenched with 0.01 mL of ethyl vinyl ether. The resulting solution was used directly for analysis and without further purification. SEC-MALS: M_n = 125,300, M_w/M_n = 1.012, DP = 131.

Synthesis of PPA **13**. $(IMesH_2)(C_5H_5N)_2(Cl)_2Ru{=}CHPh$ (0.17 mg, 0.23 μmole) pre-dissolved in 0.04 mL of a dry/degassed mixture CH_2Cl_2:CH_3OH (4:1) was added to a stirred 0.4 mL solution containing **9** (3.95 mg, 3.5 μmole) in CH_2Cl_2:CH_3OH (4:1). After 1 hour, 10% of the solution was removed and quenched with ethyl vinyl ether. **11** (2.92 mg, 11.54 μmole) pre dissolved in 0.1 mL of the same solvent mixture was added to the remaining solution. After 1 hour, 0.1 mL of ethyl vinyl ether was added to the reaction mixture and stirred for 20 minutes. The polymer was then precipitated with 12 mL of ice-cold diethyl ether and collected by centrifugation. SEC-MALS (PPA **13**): Homopolymer of **9**: M_n = 15,240; M_w/M_n = 1.07; DP = 13. Copolymer of **9**-*b*-**11**: M_n = 44,630; M_w/M_n = 1.20; DP = 116.

Synthesis of PPA **14**. $(IMesH_2)(C_5H_5N)_2(Cl)_2$-$Ru{=}CHPh$ (0.218 mg, 0.3 μmole) pre-dissolved in 0.1 mL of dry/degassed CD_2Cl_2:CD_3OD (4:1) was added to a stirred 0.4 mL solution containing the hydrophobic monomer **11** (5.3 mg, 22.5 μmole) in CD_2Cl_2:CD_3OD (4:1). After 0.5 hour, 10% of the solution was removed and quenched with ethyl vinyl ether and saved for later analysis.

norbornenyl-peptide monomer **10** (1.89 mg, 1.5 μmole) pre-dissolved in 0.15 mL of the same solvent mixture was added to the remaining solution. After 1 hour, 0.1 mL of ethyl vinyl ether was added to the reaction mixture, which was stirred for 20 minutes. The resulting solution was used directly for analysis and micelle formation without further purification. SEC-MALS (PPA **14**): Homopolymer of **11:** M_n = 17,010; M_w/M_n = 1.025; DP = 74. Copolymer of **11**-*b*-**10**: M_n = 23,570; M_w/M_n = 1.056; DP = 5.

2.5.4 Micelle Formation

Micelle Formation of Polymers **7** and **8**. Separate solutions of PPAs **7** and **8**, dissolved in CH_3OH to a final concentration of ~5 mg/mL, were prepared. The resulting mixture was dialyzed against 50 mM Tris, 50 mM $MgCl_2$, 0.1% NaN_3 in water for a minimum of 24 hours x 3 using Pierce Snakesin dialysis tubing (MWCO = 10 kDa).

Micelle Formation of Polymers **13** and **14**. Separate solutions of PPAs **13** and **14**, dissolved in DMF to a final concentration of ~1 mg/mL, were prepared. Then, an equivalent volume of water was added drop wise over approximately 10 minutes. The resulting mixture was dialyzed against water for a minimum of 8 hours x 3 using Pierce Snakesin dialysis tubing (MWCO = 10 kDa).

2.5.5 Enzymatic Reactions

Enzyme Activation. 4-Aminophenylmercuric acetate (APMA) (8.6 mg, 24 μmol) was dissolved in a freshly prepared 0.1 M NaOH solution (1.0 mL). MMP-9

(0.2 μg) in 50 mM Tris, 150 mM NaCl, 5 mM $CaCl_2$, 1 mM $ZnCl_2$, pH 7.4 (2 μL) was added to the AMPA (0.4 μL) solution. The temperature was increased to 37 ºC for 2 hours and the mixture was centrifuged every 20 minutes to ensure the enzyme remained hydrated.

Enzymatic Activation of Polymers **5** and **6**. Separate solutions of polymers **5** and **6**, dissolved in DMF to a final concentration of ~5 mg/mL, were prepared. The resulting mixture was dialyzed against 50 mM Tris, 50 mM $MgCl_2$, 0.1% NaN_3 in water for 24 hours using Pierce Snakesin dialysis tubing (MWCO = 3.5 kDa). The activated MMP-9 (2 μL) was added to the aqueous polymer solutions (100 μL) and heated to 37 ºC for 24 hours. A solution of the aqueous polymer (100 μL) without addition of enzyme was also heated to 37 ºC for 24 hours. Samples were then analyzed by DLS and TEM as shown in Figure 2.4.

2.6 Acknowledgements

The material in chapter 2, in part, is a reprint of Hahn, Michael E., Randolph, Lyndsay M., Adamiak, Lisa, Thompson, Matthew P. and Gianneschi, Nathan C. “Polymerization of a peptide-based enzyme substrate.” *Chem. Commun.* **49**, 2873-2875 (2013). The dissertation author was the secondary author of this paper.

2.7 References

(1) Gauthier, M. A.; Klok, H.-A. *Chem. Commun.* **2008**, 2591.

(2) Lutz, J.-F.; Börner, H. G. *Prog. Polym. Sci.* **2008**, *33*, 1.

(3) Gauthier, M. A.; Gibson, M. I.; Klok, H.-A. *Angew. Chem. Int. Ed.* **2009**, *48*, 48.

(4) Chien, M. P.; Rush, A.; Thompson, M.; Gianneschi, N. *Angew. Chem. Int. Ed.* **2010**, *49*, 5076.

(5) Ku, T.-H.; Chien, M.-P.; Thompson, M. P.; Sinkovits, R. S.; Olson, N. H.; Baker, T. S.; Gianneschi, N. C. *J. Amer. Chem. Soc.* **2011**, *133*, 8392.

(6) Randolph, L. M.; Chien, M.-P.; Gianneschi, N. C. *Chem. Sci.* **2012**, *3*, 1363.

(7) Hahn, M. E.; Gianneschi, N. C. *Chem. Commun.* **2012**, *47*, 11814.

(8) Börner, H. G. *Macromol. Rapid Commun.* **2011**, *32*, 115.

(9) Hughes, M.; Birchall, L. S.; Zuberi, K.; Aitken, L. A.; Debnath, S.; Javid, N.; Ulijn, R. V. *Soft Matter* **2012**, *8*, 11565.

(10) Amir, R. J.; Zhong, S.; Pochan, D. J.; Hawker, C. J. *J. Amer. Chem. Soc.* **2009**, *131*, 13949.

(11) Wang, C.; Chen, Q.; Wang, Z.; Zhang, X. *Angew. Chem. Int. Ed.* **2010**, *49*, 8612.

(12) Chien, M.-P.; Thompson, M. P.; Lin, E. C.; Gianneschi, N. C. *Chem. Sci.* **2012**, *3*, 2690.

(13) Ayres, L.; Koch, K.; van Hest, J. C. M. *Macromolecules* **2005**, *38*, 1699.

(14) Biagini, S. C. G.; Parry, A. L. *J. Polym. Sci., Part A: Polym. Chem.* **2007**, *45*, 3178.

(15) Breitenkamp, R. B.; Ou, Z.; Breitenkamp, K.; Muthukumar, M.; Emrick, T. *Macromolecules* **2007**, *40*, 7617.

(16) Conrad, R. M.; Grubbs, R. H. *Angew. Chem. Int. Ed.* **2009**, *48*, 8328.

(17) Fernández-Trillo, F.; Duréault, A.; Bayley, J. P. M.; van Hest, J. C. M.; Thies, J. C.; Michon, T.; Weberskirch, R.; Cameron, N. R. *Macromolecules* **2007**, *40*, 6094.

(18) Maynard, H. D.; Okada, S. Y.; Grubbs, R. H. *Macromolecules* **2000**, *33*, 6239.

(19) Roberts, K. S.; Sampson, N. S. *J. Org. Chem.* **2003**, *68*, 2020.

(20) Kessenbrock, K.; Plaks, V.; Werb, Z. *Cell* **2010**, *141*, 52.

(21) Parry, A. L.; Bomans, P. H. H.; Holder, S. J.; Sommerdijk, N. A. J. M.; Biagini, S. C. G. *Angew. Chem. Int. Ed.* **2008**, *47*, 8859.

(22) Riess, G. *Prog. Polym. Sci.* **2003**, *28*, 1107.

(23) Hahn, M. E.; Randolph, L. M.; Adamiak, L.; Thompson, M. P.; Gianneschi, N. C. *Chem. Commun.* **2013**, *49*, 2873.

(24) Becker, M. L.; Liu, J.; Wooley, K. L. *Chem. Commun.* **2003**, 180.

(25) Kammeyer, J. K.; Blum, A. P.; Adamiak, L.; Hahn, M. E.; Gianneschi, N. C. *Polym. Chem.* **2013**, *4*, 3929.

(26) Pontrello, J. K.; Allen, M. J.; Underbakke, E. S.; Kiessling, L. L. *J. Amer. Chem. Soc.* **2005**, *127*, 14536.

(27) Sanford, M. S.; Love, J. A.; Grubbs, R. H. *Organometallics* **2001**, *20*, 5314.

(28) Infante, M. R.; Seguer, J.; Pinazo, A.; Vinardell, M. P. *J. Dispersion Sci. Technol.* **1999**, *20*, 621.

3. Labeling Polymers And Micellar Nanoparticles *Via* Propagation And Termination With ROMP

3.1 Introduction

In the development of labeled polymers, and polymeric nanoparticles, one desires synthetic approaches that allow the most direct route to the incorporation of functional moieties with minimal post-polymerization modifications, and/or post-particle conjugations.[1-17] The most desirable route is via the direct incorporation of functional groups during the polymerization process itself (i.e. as monomers, initiators or termination agents), preventing the need for subsequent low yielding and difficult to characterize graft-to reactions on macromolecules or at particle surfaces. Moreover, post-polymerization modifications and reactions on particle surfaces are difficult to control and yield unpredictably labeled materials. The problem is compounded for particles where chemical functionalities can be difficult to elucidate on nano- and micro-scale surfaces, and/or exceptionally difficult to reproduce. In this work, we have chosen to focus on a functional group tolerant living polymerization method precisely because of the multiple options available for directly incorporating complex functional groups.[18-21] The goal is to avoid the need for post-polymerization modifications given the substrate scope of the chosen initiator. This is a common goal for those interested in functional nanoparticles capable of expressing some functionality on their shell and/or their core. Therefore, our aim in this paper is to elucidate the capability of ring opening metathesis polymerization (ROMP) with respect to the incorporation of dye labels. ROMP was chosen as it is an important and useful polymerization method for the generation of well-defined polymers of low dispersity and highly functionalized architecture.[3,16,17,22] Multiple initiators are

commercially available[23-26] and exhibit good stability in ambient conditions making them generally accessible.[25-29] These properties make ROMP particularly amenable to producing specialized functional polymers for synthetic, biomedical and nanomaterials applications, especially where complex copolymers generated via direct polymerization of functional groups are desirable.[3,16,17,20,21,30-33] There are three opportunities to introduce functionality into polymers via ROMP, (1) the use of an initiator containing a functional alkylidene (Figure 3.1 – (ii)), (2) the use of strained olefin-based monomers containing various functionalities (Figure 3.1 – (i), (iii)), and (3) the use of functionalized termination (or chain transfer) agents (Figure 3.1 – (iv)).[34] The most popular and easily deployed method for preparing functional polymers is through the use of monomers that either contain the desired functionality or allow for its incorporation via a post-polymerization modification.[16,17] In addition, the use of functionalized termination agents that allow end-labeling of polymers has garnered increasing attention.[30,35-42] Herein, the incorporation of monomers and chain transfer agents are assessed and utilized for the preparation of micellar nanoparticles assembling from fluorescently labeled amphiphilic block copolymers.

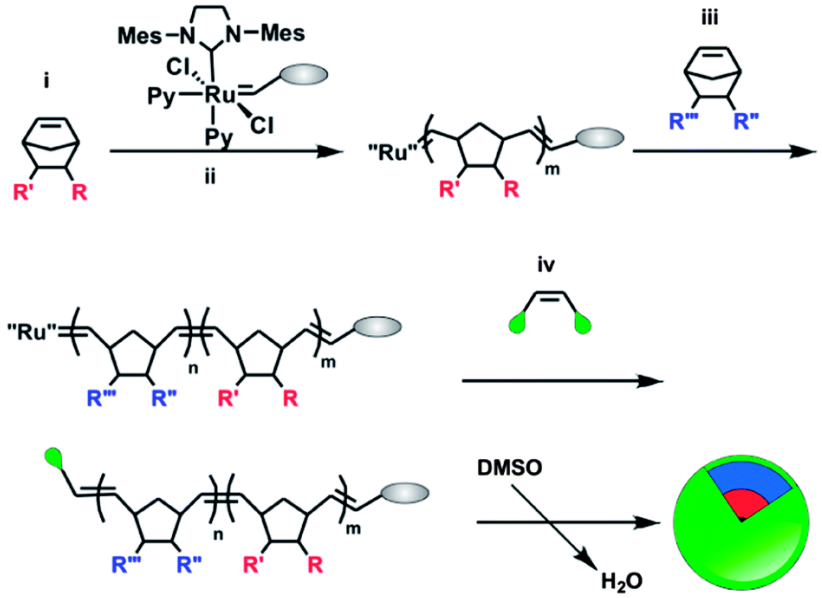

Figure 3.1 General scheme for the synthesis of functionalized polymers via ROMP. Monomers ((i) and (iii)), initiators (ii) and termination agents (iv) containing functional groups can be used to synthesize labeled amphiphilic polymers that assemble into labeled micelles.

3.2 Incorporation of Dye Monomers into Polymeric Nanomaterials

3.2.1 Monomer Synthesis

Labeling studies were conducted by employing the most convenient approach; namely, the incorporation of dye modified monomers by doping them in small quantities together with non-functional monomers. This procedure has been used via ROMP, for introducing small quantities of functional groups into polymers as tags, without dominating polymer structure.[43] For this reason, we synthesized two novel monomers containing either an EDANS dye or a DABCYL quencher. This dye pair was chosen so that for later analysis we could determine if this is a viable label to incorporate into polymeric materials and see an “off” signal of fluorescence if DABCYL and EDANS are within the Förster radius (see below).

EDANS and DABCYL monomers **1** and **2** (Figure 3.2) were synthesized by direct conjugation of the dye to a polymerizable norbornene moiety. EDANS monomer **1** was synthesized by amide coupling of the primary amine on EDANS in the presence of triethylamine (TEA) to a norbornene anhydride. This reaction was complete in 12 hours in DMF at 130 ºC with an excellent yield of 97% (Figure 3.2A). In the case of DABCYL monomer **2**, an amine modified norbornene was synthesized as previously described,[44] and coupled to DABCYL acid in the presence of HATU and *N,N*-Diisopropylethylamine (DIPEA). The reaction is carried out in DMF over 48 hours and results in a 72% yield of monomer **2**.

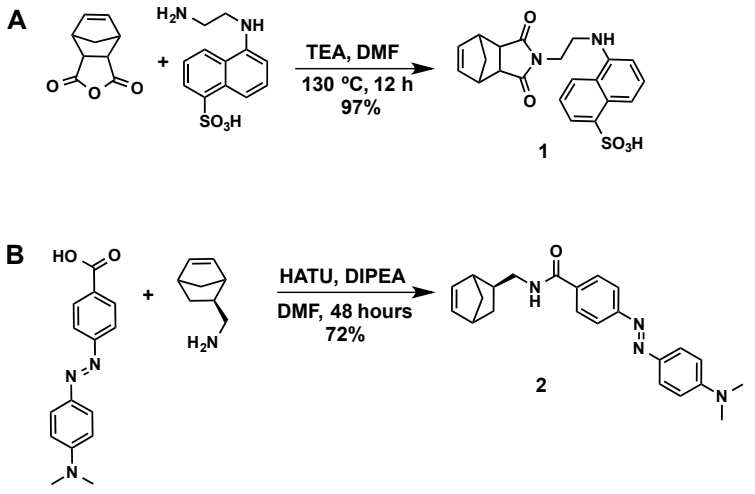

Figure 3.2 Synthetic schemes of dye labeled monomers. A) Synthesis of EDANS monomer **1**. B) Synthesis of DABCYL monomer **2**.

3.2.2 Polymer Design and Synthesis

To produce end-functionalized polymers, with incorporation of minimal quantities of dye label, we sought to end polymerization reactions with a 1:1 ratio

of monomer to initiator (M:I) on the living polymer, in appropriate stoichiometric excess with respect to initiator (Figure 3.3). Therefore, we aim to prepare two polymers that are identical except for the dye used as the end-label. Specifically, the objective is to determine if amphiphilic block copolymers can be synthesized in this fashion to form labeled micelles incorporating different dyes, but with equivalent morphologies in their final state. This implies that one could use this tagging strategy to routinely label polymers and particles with different groups, without greatly influencing their overall properties with respect to particle formation. To examine this, we prepared a set of amphiphilic polymers containing either a tag of EDANS or DABCYL (Table 3.1). A block copolymer containing a hydrophobic phenyl monomer (**3**) and a hydrophilic oligoethylene glycol monomer (**4**) was synthesized and then split into two equal parts while the polymer was still living. One equivalent of **1** or **2** was added to these two solutions, giving two labeled amphiphilic polymers with either EDANS or DABCYL.

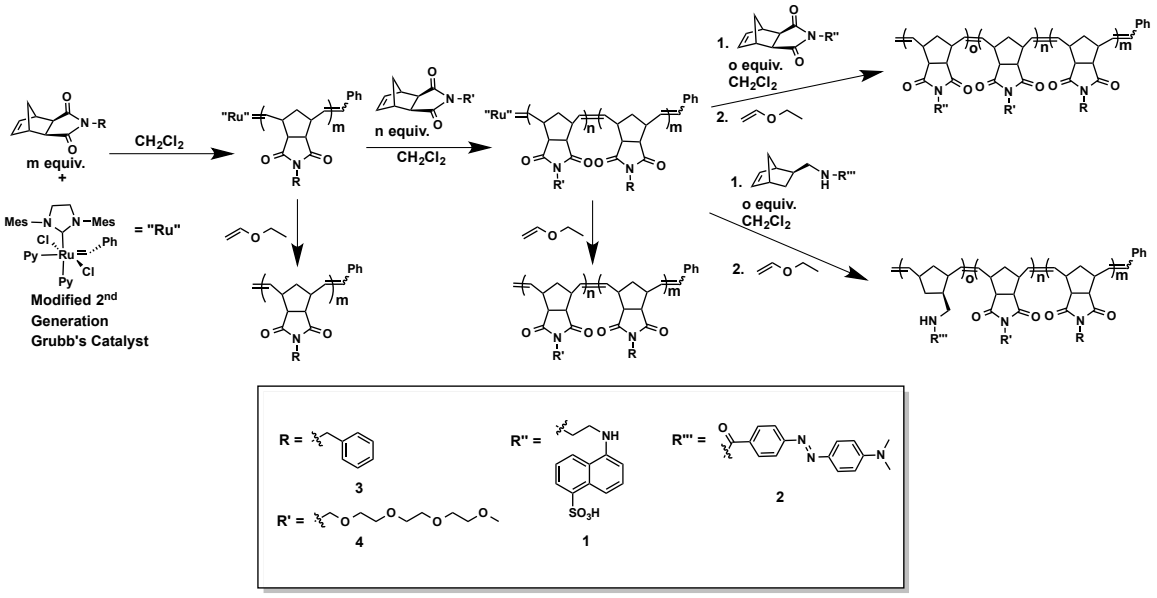

Figure 3.3 General synthetic scheme for the production of labeled polymers. Hydrophobic monomer **3** (*m* equivalents) is reacted with a modified 2nd generation Grubb's catalyst followed by addition of *n* equivalents of hydrophilic monomer **4**. This amphiphilic block copolymer is then split into two equal portions and *o* equivalents of monomer **1** or **2** is added to produce an EDANS or DABCYL labeled polymer. After complete polymerization of each block, an analytical sample is removed and quenched with ethyl vinyl ether (EVE) for analysis by SEC-MALS (see Table 3.1).

Before the addition of a second and third monomer, a small sample is removed from the polymerization mixture and quenched with ethyl vinyl ether (EVE). This was then analyzed by size-exclusion chromatography coupled with multi-angle light scattering (SEC-MALS) to determine the degree of polymerization (DP), number average molecular weight (M_n) and dispersity (M_w/M_n) of each of the polymers (see Table 3.1). Through this analysis it was determined that we were able to synthesize polymers of the composition $\mathbf{3}_{91}$-*b*-$\mathbf{4}_6$-*b*-$\mathbf{1}_2$ (polymer **5**) containing an EDANS label with an excellent dispersity of 1.04 and a DABCYL labeled polymer of composition $\mathbf{3}_{91}$-*b*-$\mathbf{4}_6$-*b*-$\mathbf{2}_4$ (polymer **6**) with a dispersity of 1.10.

Table 3.1 Polymer characterization of EDANS and DABCYL labeled polymers. [a] Polymer resulting from the polymerization of monomers **1 – 4**. [b] Degree of polymerization of block *m* (see figure 3.3). [c] Degree of polymerization of block *n*. [d] Degree of polymerization of block *o*. [e] No polymer number assigned. [f] No monomer was polymerized to complete this block.

Entry	Polymer of Monomer #[a]	Polymer	DP_m[b]	DP_n[c]	DP_o[d]	M_n	M_w/M_n
1	**3**	-[e]	91	-[f]	-[f]	8,074	1.018
2	**3**-*b*-**4**	-[e]	91	6	-[f]	9,991	1.062
3	**3**-*b*-**4**-*b*-**1**	**5**	91	6	2	10,540	1.038
4	**3**-*b*-**4**-*b*-**2**	**6**	91	6	4	10,480	1.103

3.2.3 Particle Formation and Characterization

The resulting EDANS and DABCYL labeled polymers **5** and **6** were formulated separately into two particles, **P1** and **P2** via dialysis from DMSO into water.[45] Additionally, they were mixed together in a 1:1 ratio in DMSO and slowly transitioned from organic solvent into water to form a fluorescently quenched particle (**P3**). The newly formed micellar aggregates were characterized by dynamic light scattering (DLS) and determined to each have a similar hydrodynamic diameter of roughly 150 - 300 nm and relatively low polydispersities (Table 3.2). As revealed by transmission electron microscopy (TEM), **P1**, **P2**, and **P3** each exhibit a mixed phase of spherical and cylindrical micelles, but are dominated by cylindrical micelles of similar dimensions (Figure 3.4). It should be noted that a pure cylindrical phase has been proven difficult to achieve.[46] Most notably, the consistency in overall morphology is extremely

promising with respect to deploying this tagging approach without subsequently perturbing the formation of polymeric nanoparticles.

Table 3.2 Characterization of EDANS and DABCYL labeled nanomaterials by DLS. [a] hydrodynamic diameter as determined by DLS. [b] Polydispersity index as determined by DLS. [c] EDANS and DABCYL labeled polymers present in a 1:1 ratio.

Particle	Polymer Composition	D_h[a]	PDI[b]
P1	**5**	255	0.308
P2	**6**	164	0.265
P3	**5** + **6**[c]	295	0.285

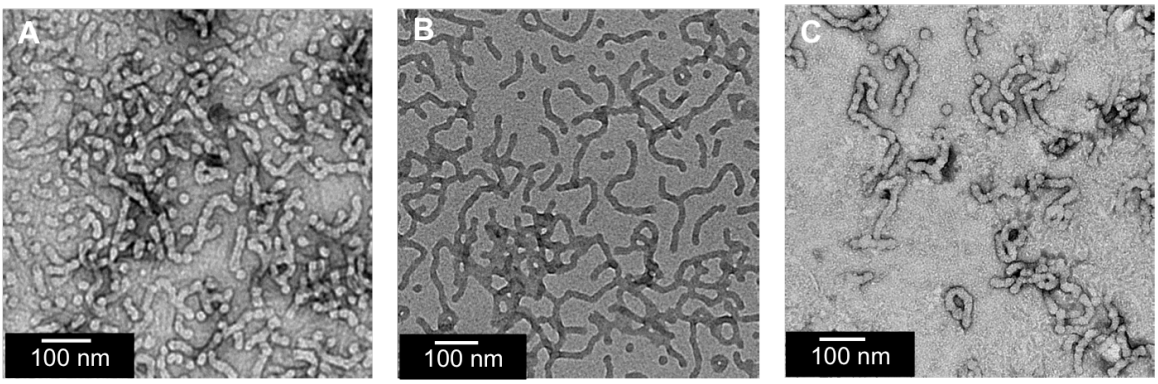

Figure 3.4 TEM of particles **P1** – **P3**. A) TEM of EDANS labeled particle **P1**. B) TEM of DABCYL labeled particle **P2**. C) TEM of mixed particle **P3**.

3.2.4 Fluorescence of EDANS and DABCYL Labeled Particles.

The spectral properties of fluorescently labeled aggregates **P1**–**P3** were analyzed by exciting each of the structures at 335 nm. As shown in Figure 3.5, the characteristic EDANS emission maximum is observed at 450 nm for **P1** (55 μM EDANS). When **P2** (12 μM) is excited at 335 nm, there is no observable emission, which is expected for DABCYL. However **P3**, containing both donor (EDANS, 55 μM) and quencher (DABCYL, 12 μM) shows a significant decrease

in fluorescence consistent with these dyes now interacting within the Förster radius.[47] Indeed, it can be concluded that the EDANS and DABCYL in **P3** must be within 33 Å of one another.[48]

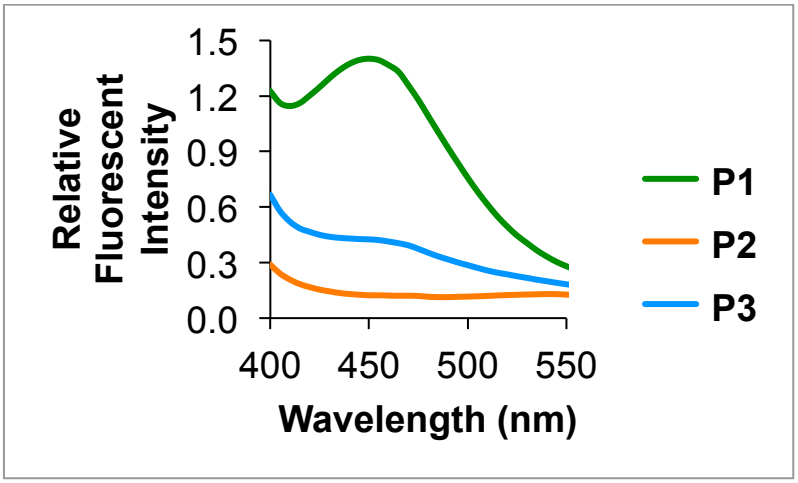

Figure 3.5 Fluorescence emission spectra of **P1** – **P3** excited at 335 nm. Concentration of **P1**: 55 μM with respect to EDANS; Concentration of **P2**: 12 μM with respect to DABCYL; Concentration of **P3**: 55 μM EDANS and 12 μM DABCYL.

3.3 Incorporation of Dye Termination Agents into Polymeric Nanomaterials

3.3.1 Synthesis of Dye Termination Agents and Termination Efficiency

While we have successfully shown in the previous section that a small incorporation of monomer is effective for incorporating tags onto the ends of polymers, it is desirable to have a more robust approach where one can reliably incorporate a single functional unit onto each polymer. To facilitate this, we synthesized three termination agents (**7**–**9**) that incorporate dyes (Figure 3.6). These termination agents (TAs) are synthesized from a diamine functionalized termination agent by amide coupling of fluorescein, rhodamine, or DABCYL. The DABCLY TA is synthesized by coupling two equivalents of DABCYL acid to a diamine functionalized termination agent (Figure 3.6) to

produce the final DABCYL TA in 50% yield. Rhodamine and fluorescein TAs have been synthesized in our laboratory previously and therefore will not be discussed further.[34]

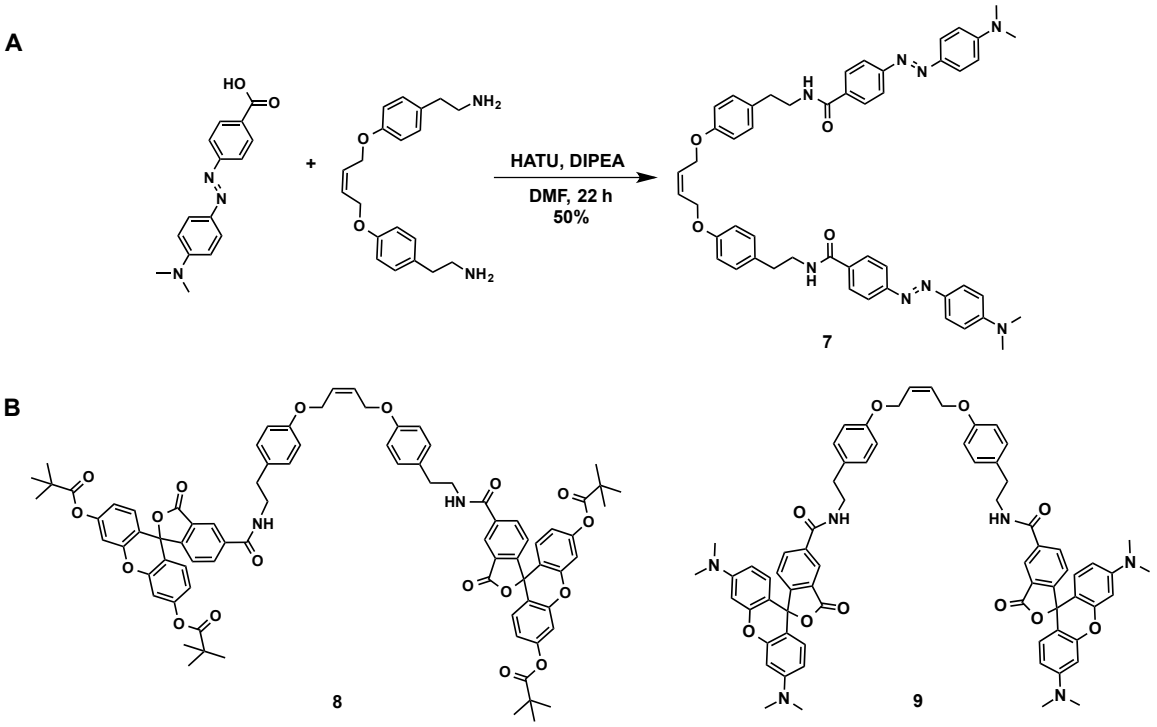

Figure 3.6 Synthetic scheme for DABCYL TA and structure for fluorescein and rhodamine TAs. A) Synthesis of DABCYL TA (**7**) by coupling of DABCYL acid to a diamine termination agent in the presence of HATU and DIPEA. B) Structure of fluorescein (**8**) and rhodamine (**9**) TAs used in this study.

To develop these novel agents for general use, the efficiency of termination was determined using a ^{1}H-NMR assay. We postulated that the ^{1}H-NMR signal corresponding to the alkylidene moiety would be useful for monitoring the termination (cross metathesis) process (Figure 3.7). ^{1}H-NMR spectra are recorded for the free initiator (Figure 3.7A-(i) and B-(i)) prior to the addition of monomer **3**, and of the living polymer 15 min after the addition of **3** (Figure 3.7A-(ii) and B-(ii)). The living polymer is then reacted with 2 equivalents

of **7** to generate species iii (Figure 3.7A-(iii)). Spectra were recorded 10 min, 45 min, and 90 min after addition of **5** (Fig. 3.7B-(iii)). As shown in Figure 3.7B, the alkylidene proton of each species has a distinct chemical shift and can be used to monitor the efficiency of termination. Addition of **5** results in a change in the chemical shift of the alkylidene proton from 18.5 ppm to 19.3 ppm (Figure 3.7B-(ii) and (iii) respectively). After 90 minutes, incomplete conversion of living polymer (ii) to terminated polymer (iii) is observed. This is attributed to the relatively poor solubility of **7**, which begins to precipitate from solution after 30 minutes. Increasing the length of time for termination and changing the solvent to DMF did not increase the efficiency of termination. The efficiencies for all TAs are determined to be quantitative via this method except for **7** (DABCYL).[34]

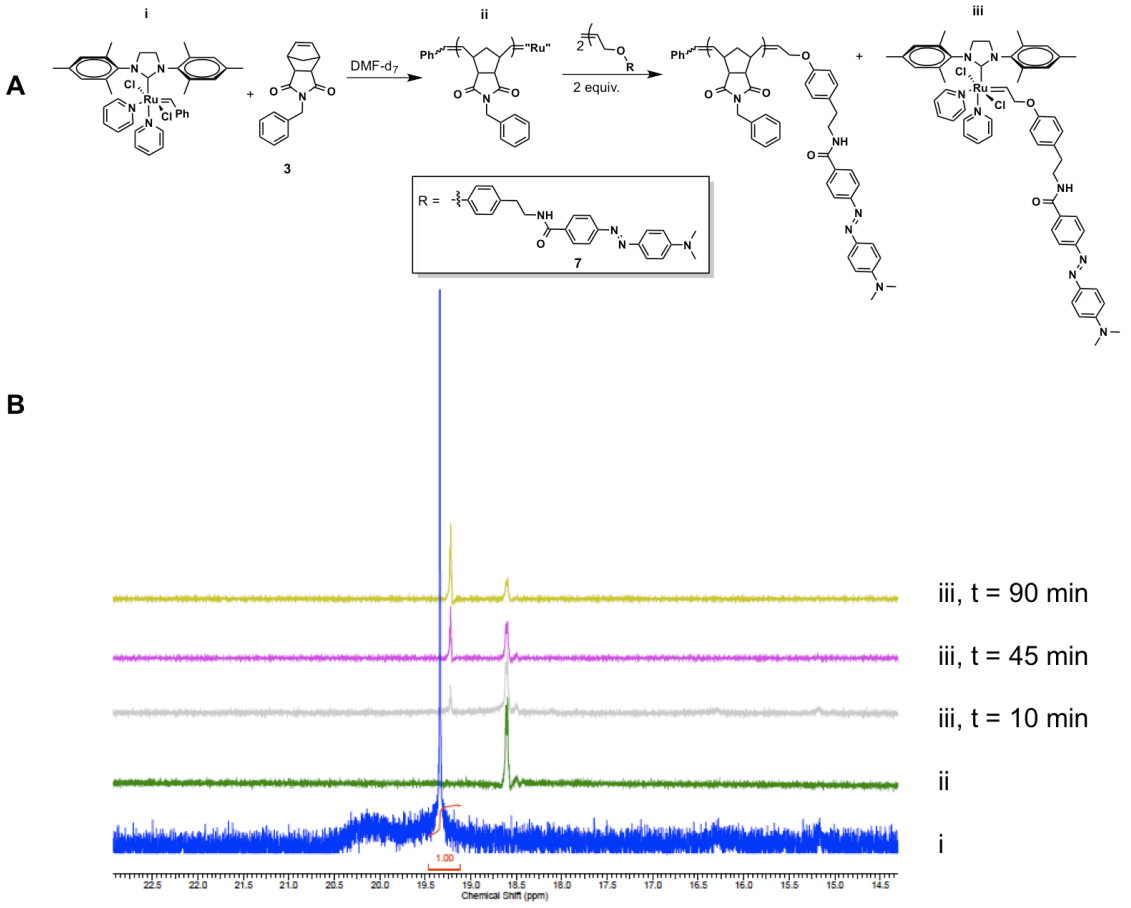

Figure 3.7 Termination efficiency for DABCYL TA **7**. A) Synthetic scheme showing addition of phenyl monomer **3** to a modified 2nd generation Grubb's catalyst (i) to generate living polymer ii. Addition of termination agent **7** produces a terminated homopolymer of **3** with termination agent **7** and a functionalized catalyst iii. B) NMR of the alkylidene proton on i (catalyst), ii (living polymer of **3**), and after addition of termination agent **7** after 10, 45, and 90 minutes (iii).

3.3.2 Polymer Synthesis and Characterization

To demonstrate the utility of tagging with functional TAs, we synthesized a set of amphiphilic block copolymers end-labeled with dyes and formulated them into micellar nanoparticles. An amphiphilic block copolymer $\mathbf{3}_{41}$-*b*-$\mathbf{4}_{23}$ was synthesized using a modified 2nd generation Grubb's catalyst, and split into 4 portions while living, followed by termination with **7**, **8**, **9**, or EVE. Similar to the

study performed as described for amphiphilic polymers containing EDANS and DABCYL monomers generated via ROMP, we chose dye TA combinations known to operate either as a quencher (DABCYL, **7**) or as a FRET acceptor (rhodamine, **9**) of the donor, fluorescein (**8**). Polymers **10 - 13** are characterized by SEC-MALS (Figure 3.8A) displaying a major peak at approximately 22 min for all four polymers. Polymers **12** and **13** display a detectable peak due to a higher molecular weight species (shoulder at earlier retention times) prevalent in the light scattering data. We postulate this is due to some aggregation or only due to small quantities of high molecular weight material as the RI signal is weak (Figure 3.8B) at 20 min retention times in comparison with the major peak observed at 22 min. Indeed, percent mass characterization by SEC-MALS indicates the peak at 22 min contains >99% of the material with a low dispersity between 1.01 and 1.09 (Table 3.3).

Table 3.3 Summary of end-group (EG) labeled polymers terminated with TAs **7** – **9**. [a] End group (i.e. termination agent) [b] Degree of polymerization of **3**. [c] Degree of polymerization of **4**. [d] No polymer number given for homopolymer synthesized. [e] Only one block was synthesized.

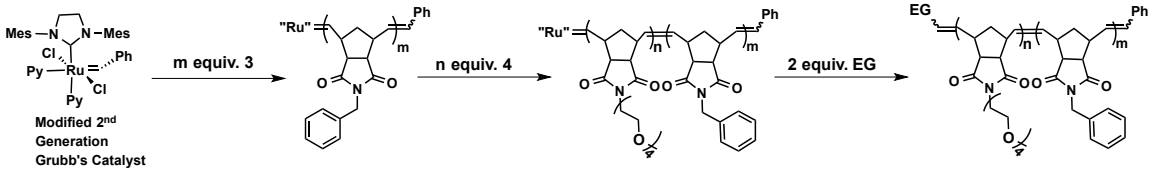

Entry	Polymer	EG[a]	DP_m (**3**)[b]	DP_n (**4**)[c]	M_n	M_w/M_n
1	-[d]	EVE	41	-[e]	10,380	1.008
2	**10**	EVE	41	23	18,460	1.009
3	**11**	**8**	41	23	18,660	1.035
4	**12**	**9**	41	23	18,730	1.033
5	**13**	**7**	41	23	21,550	1.088

To further confirm the incorporation of the dye-labeled TAs, polymers **10 – 13** were analyzed by fluorescence and UV-VIS spectroscopy (Figure 3.8C–E). The emission spectrum of fluorescein was compared to polymer **10** (terminated with EVE) by exciting both polymers **10** and **11** at 470 nm in DMF and monitoring the fluorescence intensity at 563 nm. As shown in Figure 3.8C, there is no detectable peak at 563 nm for polymer **10** as expected, with a significant increase when fluorescein is incorporated. Similarly, **12** was excited at 543 nm and the fluorescence intensity monitored at 592 nm, showing observable fluorescence with rhodamine present, compared to **10** that is lacking any fluorescent signature. Lastly, the DABCYL labeled polymer **13**, was examined via UV-Vis spectroscopy and compared to **10**. As expected, no significant absorbance was visible at 444 nm for polymer **10**, however polymer **13**

containing the DABCYL TA, shows a characteristic absorbance at 444 nm in DMF.

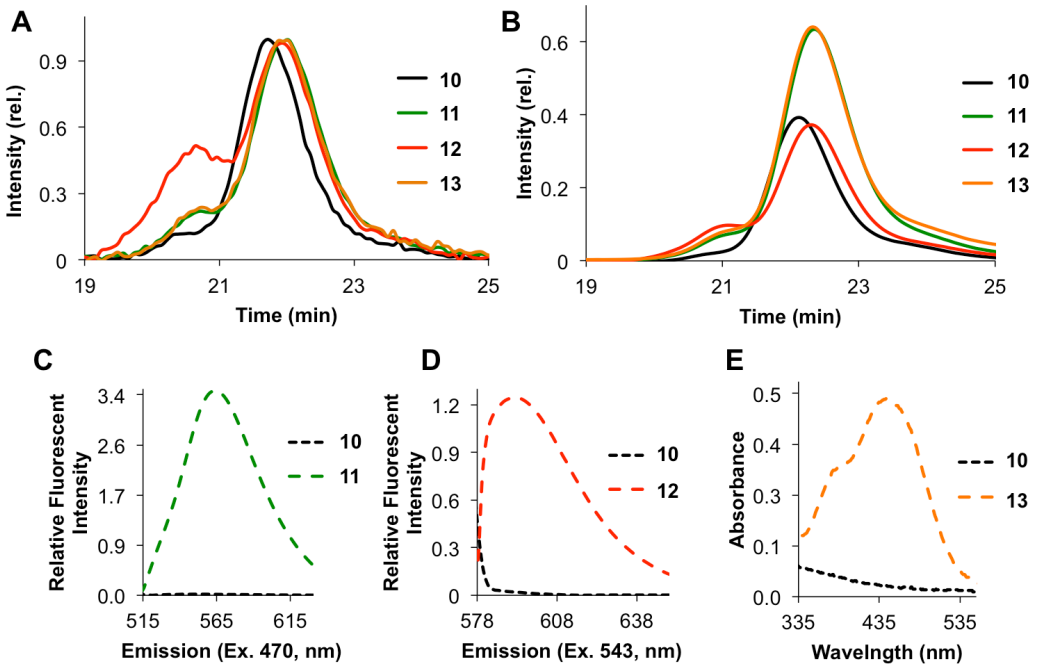

Figure 3.8 SEC and spectral characterization for polymers **10** - **13**. (A) SEC trace and scattering intensity of polymers **10** - **13**. (B) SEC trace and refractive index for polymers **10** - **13**. (C) Fluorescence emission spectra of polymers **10** and **11** with an excitation of 470 nm. (D) Fluorescence emission spectra of polymers **10** and **12** with an excitation of 543 nm. (E) UV-VIS of polymers **10** and **13**.

3.3.3 Particle Formation and Characterization

Following this initial characterization, dye-labeled block copolymers **10** - **13** were formulated into particles via slow transition into water by drop wise addition of water to a 1 mg/mL solution of polymer in DMSO followed by dialysis against water.[44] These dye combinations were chosen because fluorescein is a donor for both rhodamine and DABCYL and can be used to study the assembly

properties of resulting nanoparticles made up of given ratios of donor to acceptor carrying polymers.[11,49-55] Each of the individual polymers was dialyzed from DMSO into water (to generate **P4** – **P7**) and was analyzed by DLS and TEM (Figure 3.9A–D and Table 3.4). To account for any possible self-quenching (arising from fluorescein), a mixed particle (**P8**) containing the unlabeled **10** and fluorescein-labeled **11** was prepared (Figure 3.9E). Mixed dye particles **P9** and **P10** were prepared through dialysis by diluting the acceptor into the donor in a co-solvent (DMSO) such that the amount of acceptor is higher than that of the donor. It was determined by UV-Vis spectroscopy that **P9** contained a 1:9 ratio of donor-to-acceptor, **P10** contained a 1:1.5 ratio of fluorescein-to-DABCYL, and **P11** contained a 1:7 ratio of fluorescein-to-rhodamine. All particles **P4** – **P11** were characterized by TEM and DLS (Table 3.4 and Figure 3.9A–G). Each of these particles is spherical in morphology, although some are spherical micelles, while others are larger, and are likely vesicular (e.g. multilamellar vesicles).

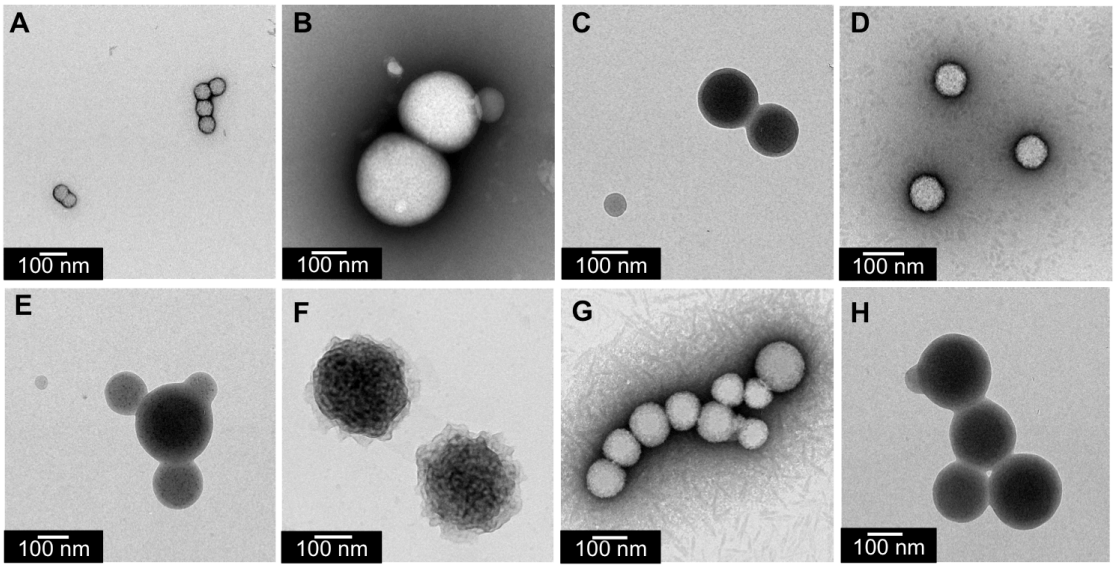

Figure 3.9 TEM of nanoparticles made of A) **P4**, B) **P5**, C) **P6**, D) **P7**, E) **P8**, F) **P9**, G) **P10**, and H) **P11**. All TEM grids are treated with a 1% uranyl acetate stain.

Table 3.4 Summary of particles synthesized from polymers **10** – **13**. [a] Polymer(s) used in the formulation of particles **P4** – **P11**. [b] End group of the polymer after termination. [c] Hydrodynamic diameter as determined by DLS. [d] Polydispersity index (PDI) as determined by DLS. [e] Concentration of donor-to-acceptor as determined by UV-Vis and used for fluorescent measurements. [f] No fluorescent label is used in this particle. [g] Only a donor or acceptor is present in this sample (i.e. not applicable, na). [h] Particle used for CMC measurements. [i] Particle used for fluorescence lifetime measurements.

Particle	Composition[a]	EG[b]	D_h[c] (nm)	PDI[d]	Conc. D:A[e] (μM)
P4	**10**	EVE	146.6	0.02489	-[f]
P5	**11**	Fluorescein	314.4	0.01418	4.15:na[g]
P6	**12**	Rhodamine	312.6	0.05280	na:36.7
P7	**13**	Dabcyl	111.5	0.08099	na:6.19
P8	**10** + **11**	EVE, Fluorescein	442.1	0.01482	4.15:na
P9[h]	**11** + **12**	Fluorescein, Rhodamine	498.8	0.02155	4.15:37.7
P10	**11** + **13**	Fluorescein, Dabcyl	204.2	0.03774	4.15:6.19
P11[i]	**11** + **12**	Fluorescein, Rhodamine	450.3	0.1109	4.15:29.7

3.3.4. Fluorescent Properties of Nanoparticles

This set of nanoparticles was analyzed by fluorescence spectroscopy and lifetime to characterize the fluorescence properties of the singly labeled particles and mixed nanoparticles. First, a fluorescence emission spectrum was measured for **P5** – **P7** while exciting at 470 nm to determine if indeed no significant fluorescence intensity was visible without fluorescein (Figure 3.10A). Figure 3.10B show the result of exciting **P8** at 470 nm, exhibiting a characteristic fluorescein maximum intensity emission at 522 nm. In mixed particles **P9** and

P10 a decrease in the overall fluorescein emission intensity was apparent due to the presence of acceptor. A decrease in the fluorescein emission intensity and an increase in rhodamine fluorescence at 569 nm were observed for **P9**, indicating that the donor and acceptor must be within the Förster radius. In the case of **P10**, it illustrates the principle by completely quenching the fluorescein signal by DABCYL, again indicating that the fluorescein and quencher are in communication.

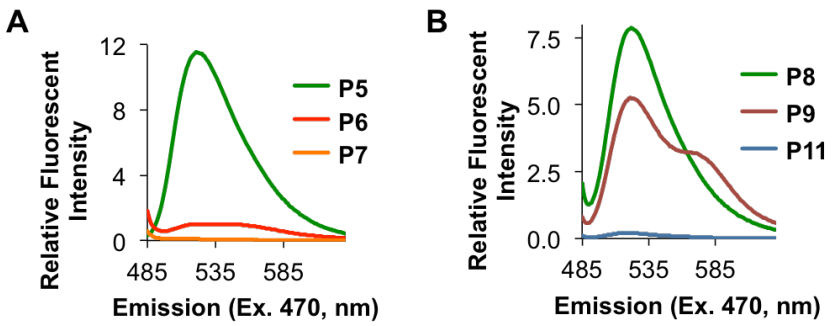

Figure 3.10 Fluorescence emission scans of **P5** – **P11**. A) Fluorescence emission spectra of **P5** (4.15 μM), **P6** (36.7 μM), and **P7** (6.19 μM), λ = 470 nm, and B) fluorescence emission spectra of **P8** (4.15 μM), **P9** (4.15 μM fluorescein, 37.7 μM rhodamine), and **P10** (4.15 μM fluorescein, 37.7 μM DABCYL), λ = 470 nm.

Although we previously have used this type of donor–acceptor interaction in determining the upper limit of the critical aggregation concentration (CAC),[54] we were unable to do so for these systems as the detection limit of fluorescein is reached before a loss in FRET-signal intensity is observed (Figure 3.11). Other common methods used to determine the CAC, including the use of solvatochromic dyes such as pyrene to observe successful micellization,[56-61]

have not yet met with considerable success in our hands for these ROMP based micelles. This is possibly due to their high stability.

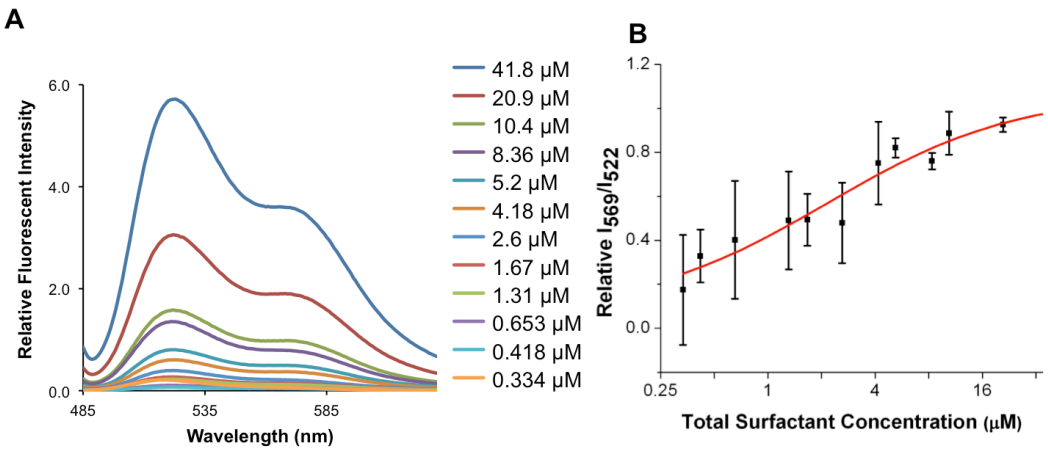

Figure 3.11 Critical aggregation concentration (CAC) for **P9**. A) Fluorescence emission spectra of **P9** at concentrations ranging from 0.3 μM to 42 μM (λ_{ex} = 470 nm). B) Maximum fluorescence intensity of rhodamine (I_{569}, λ_{em} = 569 nm) resulting from excitation of fluorescein (FRET intensity), divided by the maximum fluorescence intensity of fluorescein (I_{522}, λ_{em} = 522 nm) plotted versus total surfactant concentration. At a concentration of approximately 0.4 μM, a sharp drop is observed due to a loss in detectable signal. It is concluded that for this particular nanoparticle the CAC is less than or equal to 0.4 μM.

In addition to determining particle stability, we utilized the direct labeling strategy to elucidate structural features of the particles. The donor–acceptor (D–A) distance distribution is determined by analyzing the time-domain intensity decay of the donor (Figure 3.12A). Therefore, the data is fit as a summation of donor decays for all accessible D–A distances (Figure 3.12A). The mean distance between fluorophores, *r*, is determined by fluorescence lifetime and plotted as a probability function (Figure 3.12B and C) for both **P10** and **P11**. For **P10** (particle radius from TEM = 50 nm), the mean distance between donor and

acceptor is, r = 6.57 ± 0.14 nm, which is then converted to a decay lifetime τ_{DA} = 2.66 ± 0.23 ns (see experimental). In the case of **P11** (particle radius from TEM = 75 nm), the mean distance between donor and acceptor is, r = 6.55 ± 0.08 nm, and τ_{DA} = 2.23 ± 0.13 ns. This change in lifetime indicates that the fluorophores are interacting with one another, in positions distributed over the surface of the particles within the Förster radius.

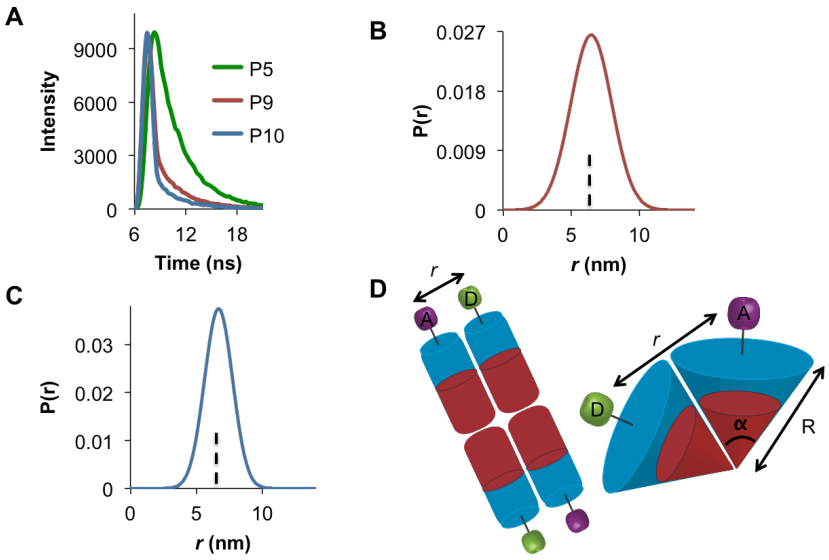

Figure 3.12 Time-domain fluorescence lifetime analysis of **P10** and **P11** and distance distribution of dyes on nanoparticle surfaces. (A) Fluorescence lifetime of **P5**, **P10**, and **P11** giving τ_D = 3.01 ± 0.22 ns for unquenched fluorescein, **P5**. (B and C) A range of distances, determined from lifetime data, between donor and acceptor in **P10** and **P11** are plotted and expressed as a probability function P(r). (B) The mean distance between fluorescein and rhodamine in **P11**, r = 6.55 ± 0.08 nm with decay lifetime τ_{DA} = 2.23 ± 0.13 ns. (C) The mean distance between fluorescein and DABCYL in **P10**, r = 6.57 ± 0.14 nm, giving τ_{DA} = 2.66 ± 0.23 ns. (D) Postulated schematic of the relationship in space between donor and acceptor (r) for a bilayer (vesicular/multilamellar) or spherical arrangement left and right respectively.

3.4 Conclusions

We have described two approaches for the incorporation of functional groups into polynorbornene via ROMP. These involve dosing in small quantities

of modified norbornene for the polymerization of dyes and the use of modified termination agents for efficient end-labeling. To demonstrate these strategies, we have prepared several new dye containing monomers and TAs. Furthermore, we have formulated a variety of the resulting polymers into labeled nanoparticles.

In summary, with an array of strategies in hand for preparing well defined, labeled polymers, materials can be synthesized that carry a diverse array of functionality. Here we have described this in the context of fluorescence, however, ongoing studies in our laboratories involve the incorporation of peptides, nucleic acids and other types of contrast agents. These studies include investigations of the utility of such systems in targeting/imaging strategies *in vivo*. We contend that it is absolutely critical to the success and progress of relatively complex nanoparticle systems that we have the ability to easily prepare and characterize them. Finally, our goal here was not to conduct an exhaustive, comprehensive study of all possible functional groups of interest, but rather to demonstrate and contrast easily utilized approaches to achieving polymer labeling via ROMP.

3.5 Experimental

3.5.1 General Methods

All reagents were purchased from commercial sources and used without further purification. Anhydrous dichloromethane was purified using a Dow-Grubbs two-column purification system (Glasscontour System, Irvine, CA).[62] Monomers **3**, **4**, amine monomer used in DABCYL monomer synthesis, diamine

termination agent, termination agents **8**, **9** and Grubb's 2nd generation catalyst, $(IMesH_2)(C_5H_5N)_2(Cl)_2Ru{=}CHPh$ were prepared as previously described.[20,34,39,63] Polymerizations were performed under dry N_2 atmospheres with anhydrous solvents. Polymer dispersity and molecular weight were determined by size-exclusion chromatography (Phenomenex Phenogel 5u 10, 1K-75K, 300 x 7.80 mm in series with a Phenomex Phenogel 5u 10, 10K-1000K, 300 x 7.80 mm (0.05 M LiBr in DMF)) or (Jordi Gel DVB 1000A, 500 • 10 mm, ($CHCl_3$)) using a Shimadzu LC-AT-VP pump equipped with a multi-angle light scattering detector (DAWN-HELIOS: Wyatt Technology), a refractive index detector (Hitachi L-2490) and a UV-Vis detector (Shimadzu SPD-10AVP) normalized to a polystyrene standard. The dn/dc values used were 0.179 (DMF) and 0.166 ($CHCl_3$) calculated by averaging several runs for homopolymers of **3** assuming 100% mass elution from the columns. ^1H and ^{13}C NMR spectra were recorded on a Varian Mercury Plus spectrometer (400 MHz) or Varian VX 500 spectrometer (500MHz). Chemical shifts (^1H) and (^{13}C) are reported in (ppm) relative to the residual solvent peak. UV-Vis experiments were conducted using a Hitachi U-2810 or a Thermo NanoDrop spectrophotometer. Fluorescent measurements were obtained using a Photon Technology International fluorescence detector or a Horiba fluorolog-3 fluorimeter system. DLS data was obtained on a Wyatt DynaPro Nanostar. TEM images were acquired on carbon grids (Ted Pella, INC.) with 1% uranyl acetate stain on a FEI Tecnai G2 Sphera at 200 KV. Fluorescent lifetime measurements were obtained on a Horiba fluorolog-3 fluorimeter system.

Mass spectra were obtained at the UCSD Chemistry and Biochemistry Molecular Mass Spectrometry Facility.

3.5.2 Monomer and Termination Agent Synthesis

Synthesis of EDANS Monomer **1**. (8 mL) and triethylamine (110 µL, 0.789 mmol) was added to a dry round bottom flask containing EDANS (200 mg, 0.751 mmol) and norbornene anhydride (118 mg, 0.716 mmol). This mixture was then stirred at 130 ºC overnight under N_2. The solvent was removed under reduced pressure to give a brown oil that was purified by flash chromatography (10% MeOH, 1% TEA, and CH_2Cl_2) resulting in 286 mg of a green solid (97% yield) ^{1}H NMR (MeOD): δ (ppm) 1.15-1.22 (dd, 2H, CH_2) 2.58 (s, 2H, 2 • CH), 3.02 (s, 2H, 2 • CH), 3.34 - 3.37 (t, 2H, CH_2), 3.74 – 3.77 (t, 2H, CH_2), 6.14 (s, 2H, HC=CH), 6.60-6.62 (d, 1H, Ar), 7.31 – 7.35 (m, 2H, Ar), 7.98 – 8.11 (m, 3H, Ar). ^{13}C NMR (MeOD): δ (ppm) 38.57, 42.90, 43.69, 49.15, 105.19, 116.69, 124.04, 125.46, 125.71, 126.79, 128.72, 131.50, 138.92, 142.43, 145.29. LRMS (ESI), 413.05 $[M+H]^+$, HRMS, expected $[M+H]^+$: 413.116, found: 413.1171.

Synthesis of DABCYL Monomer **2**. A solution of DABCYL (100 mg, 0.37 mmol), DIPEA (128 µL), and HBTU (140.83 mg, 0.37 mmol) in DMF was added to a stirred solution of the amine[44] (45.75 mg, 0.37 mmol) in DMF (1 mL). The reaction mixture was stirred under nitrogen atmosphere in the dark for 48 hrs then concentrated to dryness to give a red/orange solid. Purification by flash chromatography (3:1, hexanes:EtOAc) gave **2** as an orange solid. ^{1}H NMR ($CDCl_3$): δ (ppm) 1.40-1.50 (m, 4H, 2 • CH_2), 1.7 (m, 1H, CH), 2.70 (s, 1H, CH),

2.86 (bs, 1H, CH), 3.10 (s, 6H, 2 • CH_3), 3.40-3.55 (m, 2H, CH_2), 6.11 (m, 2H, HC=CH), 6.29 (bs, 1H, NH), 6.78 (d, 2H, 2 • CH, J = 8 Hz), 7.87-7.92 (m, 6H, 6 • CH). ^{13}C NMR ($CDCl_3$): δ (ppm) 30.96, 39.23, 40.28, 41.77, 44.39, 45.12, 45.33, 111.43, 122.22, 125.36, 127.72, 134.77, 36.24, 136.91, 143.60, 152.76, 154.98, 167.02. LRMS (ESI), 375.36 $[M+H]^+$, HRMS, expected $[M+H]^+$: 375.2179, found: 375.2181.

Synthesis of DABCYL TA **7**. DIPEA (258.5 µL, 1.48 mmol) was added to a stirred solution of the diamine[39] (205 mg, 0.371 mmol) in DMF (6.18 mL) and let stir under N_2 at room temperature. In a separate flask, a solution of DABCYL acid (200 mg, 0.743 mmol) in DMF (6.18 mL) with DIPEA (285.5 µL, 1.64 mmol) was stirred for 5 minutes. HATU (282 mg, 0.743 mmol) was added to the basic DABCYL solution and was allowed to stir for 3 minutes. The activated DABCYL solution was added to the diamine termination agent and stirred under N_2 at room temperature overnight. The orange solution was then concentrated to dryness and triturated with cold THF resulting in an orange solid (50% yield). ^{1}H NMR, (DMSO-d_6), δ (ppm): 8.65 (t, 1H), 7.97-7.79 (m, Ar, 12H), 7.18 (d, 4H), 6.91-6.83 (m, 8H), 5.84 (t, 2H), 4.69 (d, 4H), 3.47 (q, 4H), 3.07 (s, 12H), 2.80 (t, 3H). ^{13}C NMR, (DMSO-d_6), δ (ppm): 165.71, 156.72, 154.07, 153.02, 129.78, 128.68, 128.43, 125.28, 121.66, 114.78, 111.80, 63.98, 34.41 (note: some peaks are not visible due to poor solubility and are believed to be under the solvent peak of DMSO-d_6). LRMS (ESI), 829.34 $[M+H]^+$, 851.37 $[M+Na]^+$, HRMS, expected $[M+H]^+$: 829.4176, found 829.4184.

3.5.3 Polymerization Procedures

Synthesis of Polymers **5** and **6**. $(IMesH_2)(C_5H_5N)_2(Cl)_2Ru{=}CHPh$ (29.0 mg, 0.04 mmol) was added to a stirred solution of **3** (324 mg, 1.37 mmol) in dry CH_2Cl_2 (10.7 mL) at -78 ºC. The reaction was left to stir under nitrogen while warming to room temperature. An aliquot of the reaction was removed (0.1 mL) and quenched with EVE (0.09 mL). To the remaining solution, **4** (185 mg, 0.566 mmol) was added and the reaction was stirred under nitrogen at room temperature for 90 min. An aliquot of the reaction was removed (0.1 mL) and quenched with EVE (0.200 mL). The remaining solution was split into 2 aliquots (5.25 mL each) and treated with either **1** (25.0 mg, 0.061 mmol) or **2** (22.8 mg, 0.061 mmol), after 1 hr the reactions were quenched with EVE (0.20 mL), concentrated and precipitated by addition of cold ether to give block copolymers **5** and **6** respectively as powders that were characterized by SEC-MALS (Table 3.1 Main Text).

Synthesis of Polymers **10 – 13**. $(IMesH_2)(C_5H_5N)_2(Cl)_2Ru{=}CHPh$ (8.78 mg, 0.012 mmol) was added to a stirred solution of **3** (153 mg, 0.604 mmol) in dry DMF (6.7 mL). The reaction was left to stir under nitrogen at room temperature for 20 min. An aliquot of the reaction was removed (0.1 mL) and quenched with EVE (0.09 mL). To the remaining solution, **4** (213 mg, 0.604 mmol) was added and the reaction was stirred under nitrogen at room temperature for 20 min, after which the solution was split into 4 aliquots (1.65 mL each) and quenched by adding EVE (0.09 mL), **7** (4.97 mg, 0.006 mmol, 2 equiv.), **8** (8.28 mg, 0.006 mmol, 2 equiv.), or **9** (6.91 mg, 0.006 mmol, 2 equiv.). After 1 hour, each of the

respective solutions were concentrated to dryness and precipitated by addition of cold ether to give block copolymers **10, 11, 12,** and **13** respectively as glassy solids that were characterized by SEC-MALS (Table 3.3 Main Text).

Termination Efficiency Study. A ^{1}H NMR spectrum of $(IMesH_2)(C_5H_5N)_2(Cl)_2Ru{=}CHPh$ (1.9 mg, 2.6 μmoles) in DMF-d_7 was recorded. A solution of monomer **3** (10.0 mg, 39 μmoles) in DMF-d_7 (0.1 mL) was added to the NMR tube and vortexed for several seconds to ensure complete mixing. After 15 min a ^{1}H NMR was recorded of the corresponding polymer. A solution of TA **7** (3.9 mg, 4.68 μmole) in DMF-d_7 (100 μL) was added to the NMR tube and vortexed to ensure complete mixing. ^{1}H NMR spectra were recorded at various time points out to 90 minutes to monitor the reaction.

3.5.4 Particle Preparation

Preparation of **P1** and **P2**. 5 mg of polymer was dissolved in 1 mL of DMF and transferred to a 3,500 MWCO snakeskin dialysis tubing. This solution was dialyzed against 1 L of 50 mM Tris, 0.1% NaN_3 at pH 7.4 over 2 days with 2 buffer changes. The resulting opalescent solution was then concentrated by ½ the volume and centrifuged at 13,500 rpm for 5 min. The remaining supernatant was analyzed by DLS and TEM.

Preparation of **P3**. 4.1 mg of **5** and 3.6 mg of **6** were dissolved in 1 mL of DMF and transferred to a 3,500 MWCO snakeskin dialysis tubing. This solution was dialyzed against 2 L of 50 mM Tris, 0.1% NaN_3 at pH 7.4 over 2 days with 2 buffer changes (note: a small amount of orange precipitate formed during

dialysis). The orange, opalescent solution was then concentrated by ½ the volume and centrifuged at 13,500 rpm for 5 min. The remaining supernatant was analyzed by DLS and TEM.

Preparation of **P4 – P7**. 1 mg of polymer was dissolved in 1 mL of DMSO followed by addition of 1 mL of H_2O drop wise giving a final concentration of 0.5 mg/mL of polymer in 1:1 DMSO:H_2O. This solution was transferred to a 3,500 MWCO snakeskin dialysis tubing and dialyzed against 2 L of nanopure water. After 24 hrs, the solution was transferred to a 10,000 MWCO snakeskin dialysis tubing with continued dialysis against 2 L of water for 48 hrs with two water changes (note: for **P7** a small amount of orange precipitate formed during dialysis, this sample was centrifuged at 13,500 rpm for 5 min prior to analysis).

Preparation of **P8**. A solution of polymer **11** in DMSO (1.7 µL, 11mg/mL) and a solution of **10** in DMSO (220 µL, 8.5 mg/mL) were added to 1.7 mL of DMSO, giving a final polymer concentration of 1 mg/mL (DMSO). To this solution, 1.9 mL of water was added drop wise, resulting in an opalescent solution at a concentration of 0.5 mg/mL (1:1 DMSO:H_2O). This solution was transferred to a 3,500 MWCO snakeskin dialysis tubing and dialyzed against 2 L of nanopure water. After 24 hrs the solution was transferred to a 10,000 MWCO snakeskin dialysis tubing with continued dialysis for 48 hrs against 2 L of nanopure water with two subsequent water changes.

Preparation of **P9**. A solution of polymer **11** DMSO (2.3 µL, 8.3 mg/mL) and a solution of polymer **12** in DMSO (675 µL/5.6 mg/mL) was added to 3.1 mL of DMSO, resulting in a final polymer concentration of 1 mg/mL (DMSO). To this

solution was added 3.8 mL of H_2O, drop wise, followed by 30 µL of 4 M NaOH to keep the solution opalescent. This 0.5 mg/mL solution was then transferred to a 3,500 MWCO snakeskin dialysis tubing and dialyzed against 1 L of nanopure water. After 24 hrs the solution was transferred to a 10,000 MWCO snakeskin dialysis tubing with continued dialysis for 48 hrs against 1 L of nanopure water with two water changes.

Preparation of **P10**. A solution of polymer **11** in DMSO (1.7 µL, 11 mg/mL) and a solution of **13** in DMSO (553.1 µL, 6.8 mg/mL) were added to 3.2 mL of DMSO, resulting in a final polymer concentration of 1 mg/mL (DMSO). To this solution was added 3.8 mL of H_2O, drop wise. The solution was transferred to a 3,500 MWCO snakeskin dialysis tubing and dialyzed against 2 L of nanopure water. After 24 hrs the solution was transferred to a 10,000 MWCO snakeskin dialysis tubing with continued dialysis for 48 hrs against 2 L of nanopure water with two water changes (note: a small amount of orange precipitate formed during dialysis, this sample was centrifuged at 13,500 rpm for 5 min prior to analysis).

Preparation of **P11**. A solution of polymer **11** in DMSO (1.7 µL, 11 mg/mL) and a solution of **12** in DMSO (200.1 µL, 9.4 mg/mL) were added to 1.7 mL of DMSO, resulting in a final polymer concentration of 1 mg/mL in DMSO. To this solution was added 1.9 mL of H_2O dropwise. The solution was transferred to a 3,500 MWCO snakeskin dialysis tubing and dialyzed against 2 L of nanopure water. After 24 hrs the solution was transferred to a 10,000 MWCO snakeskin

dialysis tubing with continued dialysis for 48 hrs against 2 L of nanopure water with two water changes.

3.5.5 Particle Concentration Determination

P1 – P3. The concentration of each of the labeled polymers within the particle solutions was determined by UV-Vis using the following extinction coefficients: EDANS, ε_{335} = 5,900 $M^{-1}cm^{-1}$, DABCYL, ε_{453} = 32,000 $M^{-1}cm^{-1}$. **P1** = 86.4 μM, **P2 =** 23.9 μM and **P3** = 54.9 μM with respect to EDANS and 12.5 μM with respect to DABCYL.

General Procedure for **P5 – P11**. The concentration of each labeled polymers within the particle solutions was determined by UV-Vis as follows: A known volume of stock particle solution was concentrated to dryness and re-dissolved in a known volume of DMSO and/or DMSO containing 5% NH_4OH and the absorbance was measured by UV-Vis. The extinction coefficients were calculated in each of the respective solvents and determined to be the following ($M^{-1}cm^{-1}$): Rhodamine (DMSO), ε_{552} = 164.6 ± 13.4. DABCYL (5% NH_4OH/DMSO), ε_{428} = 14,035 ± 2487 and ε_{514} = 2,379 ± 283. Fluorescein (5% NH_4OH/DMSO), ε_{428} = 52.1 ± 14.93 and ε_{514} = 4322 ± 330.5 (note: no significant absorbance was measured for rhodamine in 5% NH_4OH/DMSO, or for fluorescein in DMSO).

P5 and **P7**. 400 μL of **P5** and **P7** was concentrated to dryness and re-dissolved in 150 μL of 5% NH_4OH/DMSO. [Fluorescein] in **P5 =** 27.0 μM. [DABCYL] in **P7** = 41.2 μM.

P6. 1,200 µL of **P6** was concentrated to dryness and re-dissolved in 125 µL of DMSO. [Rhodamine] = 38.6 µM.

P8. 550 µL of **P8** was concentrated to dryness and re-dissolved in 125 µL of 5% NH_4OH/DMSO. [Fluoroscein] = 6.4 µM. Since the EVE does not have a specific absorption, the concentration could not be determined by UV-Vis.

P9 and **P10**. 1,550 µL of **P9** and **P10** were concentrated to dryness and re-dissolved in 125 µL of DMSO. [Rhodamine] in **P9** = 39.7 µM, **P10** = 47.5 µM. Add 6.25 µL of 5% NH_4OH to the solutions to deprotect the fluorescein. [Fluorescein] in **P9** = 4.31 µM, **P10** = 6.64 µM.

P11. 225 µL of **P11** was concentrated to dryness and re-dissolved in 150 µL of 5% NH_4OH/DMSO. The absorbance at 428 nm and 514 nm was measured by UV-Vis and using equations 1 and 2 below. The concentration was determined to be 29.7 µM for DABCYL and 19.9 µM for fluorescein.

$$A_{428} = \varepsilon_{D428}C_D + \varepsilon_{F428}C_F \quad (1)$$

$$A_{514} = \varepsilon_{D514}C_D + \varepsilon_{F514}C_F \quad (2)$$

3.5.6 Fluorescence Measurements

Fluorescence of **P1 – P3**. Particles **P1** and **P2** were diluted to 54.9 µM and 12.5 µM respectively with 50 mM Tris buffer (pH 7.4). Emission scans of particles **P1 – P3** were performed with λ_{ex} = 335 nm (excitation of EDANS).

Fluorescence of **P5 – P11**. Dilutions of particles **P5 - P11** were made according to Table 3.4. An emission scan was measured for each of the particles

except **P11** (only used for fluorescence lifetime measurements), exciting at a wavelength of 470 nm.

Distance Distribution Analysis of **P5**, **P10**, and **P11** via Fluorescence Lifetime. A range of D–A distances are considered where the distance is expressed as a probability function P*(r)* distributed along the *r* axis. A Gaussian distribution was used to describe the distance distribution, as in the equation below:

$$P(r) = \frac{1}{\sigma\sqrt{2\pi}} \exp\left[-\frac{1}{2}\left(\frac{\bar{r}-r}{\sigma}\right)^2\right] \qquad (3)$$

In this equation $\bar{r}$ is the mean of the Gaussian with a standard deviation of σ. The distance distribution is described by two standard deviations from the mean, with the probability of finding donor and acceptor within this range as 95.4%. The donor intensity decay is a summation of the intensity decays for all accessible distances, and is written as:

$$I_{DA}(t) = \int_{r=0}^{\infty} P(r) I_{DA}(r,t)dr = I_D^0 \int_{r=0}^{\infty} P(r) \exp\left[-\frac{1}{\tau_D} - \frac{1}{\tau_D}\left(\frac{R_0}{r}\right)^6\right] dr \qquad (4)$$

This expression indicates that the intensity decay for an ensemble of flexible D–A pairs is given by the weighted average of the decays for each D–A distance. From this analysis, the distance distribution is calculated as 6.57 ± 0.14 nm for **P10** and 6.55 ± 0.08 nm for **P11** shown in Figure 3.12B and C and written as *r*.

The lifetime in **P10** and **P11** (τ_{DA}) was then calculated from the standard treatment of FRET efficiency (*E*):

$$E = \frac{R_0^6}{R_0^6 + r^6} \quad (5)$$

where R_0 is the Förster distance between donor and acceptor, applied as 47 Å for **P10** (fluorescein and DABCYL) and 55 Å for **P11** (fluorescein and rhodamine) in this work assuming that rotation of the dyes is free and therefore the orientation factor, κ^2 = 2/3. The transfer efficiency can then be used to calculate the lifetime of the donor-acceptor (τ_{DA}):

$$E = 1 - \frac{\tau_{DA}}{\tau_{DA}} \quad (6)$$

In this work, lifetimes of Fluorescein-labeled micelle (**P5**), fluorescein-DABCYL labeled micelle (**P10**) and fluorescein-rhodamine labeled micelles (**P11**) were obtained as 3.01 ± 0.22 ns, 2.66 ± 0.23 ns and 2.23 ± 0.13 ns respectively from fluorescence lifetime measurements (see Figure 3.12 in the Main text).

3.6 Acknowledgements

Chapter 3, in full, is a reprint of the material as found in Thompson, Matthew P., Randolph, Lyndsay M., James, Carrie R., Davalos, Ashley N., Hahn, Michael E., and Gianneschi, Nathan C. “Labelling polymers and micellar

nanoparticles via initiation, propagation and termination with ROMP." *Polym. Chem.* **5**, 1954-1964 (2014). The dissertation author is the secondary author of this publication.

3.7 References

(1) Aoshima, S.; Kanaoka, S. *Chem. Rev.* **2009**, *109*, 5245.

(2) Beija, M.; Charreyre, M.-T.; Martinho, J. M. G. *Prog. Polym. Sci.* **2011**, *36*, 568.

(3) Bielawski, C. W.; Grubbs, R. H. *Prog. Polym. Sci.* **2007**, *32*, 1.

(4) Broyer, R. M.; Grover, G. N.; Maynard, H. D. *Chem. Commun.* **2011**, *47*, 2212.

(5) Castle, T. C.; Hutchings, L. R.; Khosravi, E. *Macromolecules* **2004**, *37*, 2035.

(6) Guo, R.; Wang, X.; Guo, C.; Dong, A.; Zhang, J. *Macromol. Chem. Phys.* **2012**, *213*, 1851.

(7) Lele, B. S.; Murata, H.; Matyjaszewski, K.; Russell, A. J. *Biomacromolecules* **2005**, *6*, 3380.

(8) Li, M.; Li, H.; De, P.; Sumerlin, B. S. *Macromol. Rapid Commun.* **2011**, *32*, 354.

(9) Moad, G.; Rizzardo, E.; Thang, S. H. *Aust. J. Chem.* **2012**, *65*, 985.

(10) Nicolas, J.; Mantovani, G.; Haddleton, D. M. *Macromol. Rapid Commun.* **2007**, *28*, 1083.

(11) Prazeres, T. J. V.; Beija, M.; Charreyre, M.-T.; Farinha, J. P. S.; Martinho, J. M. G. *Polymer* **2010**, *51*, 355.

(12) Schaefer, M.; Hanik, N.; Kilbinger, A. F. M. *Macromolecules* **2012**, *45*, 6807.

(13) Siegwart, D. J.; Oh, J. K.; Matyjaszewski, K. *Prog. Polym. Sci.* **2012**, *37*, 18.

(14) Sumerlin, B. S. *ACS Macro Letters* **2011**, *1*, 141.

(15) Tasdelen, M. A.; Kahveci, M. U.; Yagci, Y. *Prog. Polym. Sci.* **2011**, *36*, 455.

(16) Leitgeb, A.; Wappel, J.; Slugovc, C. *Polymer* **2010**, *51*, 2927.

(17) Slugovc, C. *Macromol. Rapid Commun.* **2004**, *25*, 1283.

(18) Scholl, M.; Ding, S.; Lee, C. W.; Grubbs, R. H. *Org. Lett.* **1999**, *1*, 953.

(19) Trnka, T. M.; Grubbs, R. H. *Acc. Chem. Res.* **2000**, *34*, 18.

(20) Hahn, M. E.; Randolph, L. M.; Adamiak, L.; Thompson, M. P.; Gianneschi, N. C. *Chem. Commun.* **2013**, *49*, 2873.

(21) Kammeyer, J. K.; Blum, A. P.; Adamiak, L.; Hahn, M. E.; Gianneschi, N. C. *Polym. Chem.* **2013**, *4*, 3929.

(22) Grubbs, R. H. *Tetrahedron* **2004**, *60*, 7117.

(23) Harrity, J. P. A.; La, D. S.; Cefalo, D. R.; Visser, M. S.; Hoveyda, A. H. *J. Amer. Chem. Soc.* **1998**, *120*, 2343.

(24) Schrock, R. R.; Murdzek, J. S.; Bazan, G. C.; Robbins, J.; DiMare, M.; O'Regan, M. *J. Amer. Chem. Soc.* **1990**, *112*, 3875.

(25) Schwab, P.; France, M. B.; Ziller, J. W.; Grubbs, R. H. *Angew. Chem. Int. Ed.* **1995**, *34*, 2039.

(26) Schwab, P.; Grubbs, R. H.; Ziller, J. W. *J. Amer. Chem. Soc.* **1996**, *118*, 100.

(27) Frenzel, U.; Nuyken, O. *J. Polym. Sci., Part A: Polym. Chem.* **2002**, *40*, 2895.

(28) Sanford, M. S.; Love, J. A.; Grubbs, R. H. *Organometallics* **2001**, *20*, 5314.

(29) Sanford, M. S.; Love, J. A.; Grubbs, R. H. *J. Amer. Chem. Soc.* **2001**, *123*, 6543.

(30) Hilf, S.; Kilbinger, A. F. M. *Nat. Chem.* **2009**, *1*, 537.

(31) Kiessling, L. L.; Mangold, S. L. In *Polymer Science: A Comprehensive Reference*; Matyjaszewski, K., Möller, M., Eds.; Elsevier: Amsterdam, 2012, p 695.

(32) Nomura, K.; Abdellatif, M. M. *Polymer* **2010**, *51*, 1861.

(33) Smith, D.; Pentzer, E. B.; Nguyen, S. T. *Polym. Rev.* **2007**, *47*, 419.

(34) Thompson, M. P.; Randolph, L. M.; James, C. R.; Davalos, A. N.; Hahn, M. E.; Gianneschi, N. C. *Polym. Chem.* **2014**, *5*, 1954.

(35) Madkour, A. E.; Koch, A. H. R.; Lienkamp, K.; Tew, G. N. *Macromolecules* **2010**, *43*, 4557.

(36) Chen, B.; Metera, K.; Sleiman, H. F. *Macromolecules* **2005**, *38*, 1084.

(37) Kolonko, E. M.; Kiessling, L. L. *J. Amer. Chem. Soc.* **2008**, *130*, 5626.

(38) Mangold, S. L.; Carpenter, R. T.; Kiessling, L. L. *Org. Lett.* **2008**, *10*, 2997.

(39) Matson, J. B.; Grubbs, R. H. *Macromolecules* **2009**, *43*, 213.

(40) Owen, R. M.; Gestwicki, J. E.; Young, T.; Kiessling, L. L. *Org. Lett.* **2002**, *4*, 2293.

(41) Chien, M.-P.; Thompson, M. P.; Barback, C. V.; Ku, T.-H.; Hall, D. J.; Gianneschi, N. C. *Adv. Mater.* **2013**, *25*, 3599.

(42) Rush, A. M.; Thompson, M. P.; Tatro, E. T.; Gianneschi, N. C. *ACS Nano* **2013**, *7*, 1379.

(43) Roberts, K. S.; Sampson, N. S. *Org. Lett.* **2004**, *6*, 3253.

(44) Pontrello, J. K.; Allen, M. J.; Underbakke, E. S.; Kiessling, L. L. *J. Amer. Chem. Soc.* **2005**, *127*, 14536.

(45) Zhang, L.; Eisenberg, A. *Polym. Adv. Technol.* **1998**, *9*, 677.

(46) Blanazs, A.; Madsen, J.; Battaglia, G.; Ryan, A. J.; Armes, S. P. *J. Amer. Chem. Soc.* **2011**, *133*, 16581.

(47) Förster, T. *Ann. Phys.* **1948**, *437*, 55.

(48) Matayoshi, E. D.; Wang, G. T.; Krafft, G. A.; Erickson, J. *Science* **1990**, *247*, 954.

(49) Clegg, R. M. In *Methods in Enzymology*; David M.J. Lilley, J. E. D., Ed.; Academic Press: 1992; Vol. Volume 211, p 353.

(50) Stryer, L. *Annu. Rev. Biochem.* **1978**, *47*, 819.

(51) Selvin, P. R. *Nat. Struct. Mol. Biol.* **2000**, *7*, 730.

(52) Farinha, J. P. S.; Martinho, J. M. G. *J. Phys. Chem. C* **2008**, *112*, 10591.

(53) Schillén, K.; Yekta, A.; Ni, S.; Farinha, J. P. S.; Winnik, M. A. *J. Phys. Chem. B* **1999**, *103*, 9090.

(54) Chien, M.-P.; Thompson, M. P.; Lin, E. C.; Gianneschi, N. C. *Chem. Sci.* **2012**, *3*, 2690.

(55) Farinha, J. P. S.; Schillén, K.; Winnik, M. A. *J. Phys. Chem. B* **1999**, *103*, 2487.

(56) Acharya, K. R.; Bhattacharyya, S. C.; Moulik, S. P. *J. Photochem. Photobiol., A* **1999**, *122*, 47.

(57) Hait, S. K.; Majhi, P. R.; Blume, A.; Moulik, S. P. *J. Phys. Chem. B* **2003**, *107*, 3650.

(58) Majhi, P. R.; Mukherjee, K.; Moulik, S. P.; Sen, S.; Sahu, N. P. *Langmuir* **1999**, *15*, 6624.

(59) Turro, N. J.; Kuo, P. L. *Langmuir* **1985**, *1*, 170.

(60) Kalyanasundaram, K.; Thomas, J. K. *J. Amer. Chem. Soc.* **1977**, *99*, 2039.

(61) Aguiar, J.; Carpena, P.; Molina-Bolívar, J. A.; Carnero Ruiz, C. *J. Colloid Interface Sci.* **2003**, *258*, 116.

(62) Pangborn, A. B.; Giardello, M. A.; Grubbs, R. H.; Rosen, R. K.; Timmers, F. J. *Organometallics* **1996**, *15*, 1518.

(63) Chien, M. P.; Rush, A.; Thompson, M.; Gianneschi, N. *Angew. Chem. Int. Ed.* **2010**, *49*, 5076.

4. Labeling Polymers And Nanoparticles With MRI-Contrast Agents Via Polymerization Of Gd(III)-Based Monomers

4.1 Introduction

Magnetic resonance imaging (MRI) is a widely used noninvasive clinical imaging technique. Many of the current FDA approved MRI contrast agents are small molecule Gd-poly(aminocarboxylate) complexes such as Gd-diethylenetriaminepenta-acetic (Gd-DTPA, Magnevist^{TM}) and Gd-1,4,7,10-tetraazacyclododecane-1,4,7,10-tetraacetic acid (Gd-DOTA, Dotarem^{TM}).[1] These contrast agents enhance signal in T_1-weighted magnetic resonance (MR) images by shortening the proton relaxation time (T_1) of surrounding water molecules.[1] To increase relaxivity (r_{1p}) of contrast agents, various parameters can be optimized including the water exchange rate (k_{ex}) and the rotational correlation time (τ_R). It is well known that appending small molecule contrast agents to macromolecular scaffolds effectively increases relaxivity of contrast agents by slowing τ_R.[1] Appending Gd^{3+}-based chelates to dendrimers,[2,3] polymers,[4-6] proteins,[7,8] and nanoparticles[1,9-16] has been shown to result in large enhancements of per Gd^{3+} r_{1p} compared to analogous small molecule contrast agents. Many of these strategies involve multistep syntheses and chelation reactions performed on polymers or nanostructures. Herein we describe the synthesis of two norbornene Gd^{3+}-chelates, DTPA and DOTA, that are amenable to ring opening metathesis polymerization (ROMP). ROMP was chosen as the polymerization method due to the high functional group tolerance of the modified 2nd generation Grubb's catalyst employed.[17,18]

4.2 Synthesis and Polymerization of a DTPA Monomer

4.2.1 Synthesis of a DTPA Monomer

A novel DTPA monomer amenable to ROMP was synthesized following the synthetic scheme outlined in Figure 4.1. We set out to synthesize a DTPA analogue containing a functional group amenable to conjugation with a norbornene-containing molecule. For this reason we chose to synthesize a DTPA chelate with an amine moiety capable of amide coupling onto a norbornene containing an activated ester (Figure 4.1A). A commercial *p*-nitrophenylalanine methyl ester (**1**) was converted into an aminomethylamide (**2**) by addition of a large excess of ethylenediamine, with vigorous stirring to avoid polymerization, forming compound **2** in a 77% isolated yield. The tri-amine product (**3**) was achieved by borane reduction of the amide **2** in a 98% yield. Alkylation of the free amine was reached by an S_N2 reaction with *t*-butyl bromoacetate in DMF with KI as an additive to make the more reactive *t*-butyl iodoacetate species. This resulted in *p*-nitrobenzyl-DTPA penta-*t*-butyl ester (**4**) in a 50% yield. To finish off the synthesis to **5**, the nitro group on compound **4** was reduced under H_2 pressure with a Pd/C catalyst to afford *p*-aminobenzyl-DTPA penta-*t*-butyl ester in a 95% yield.

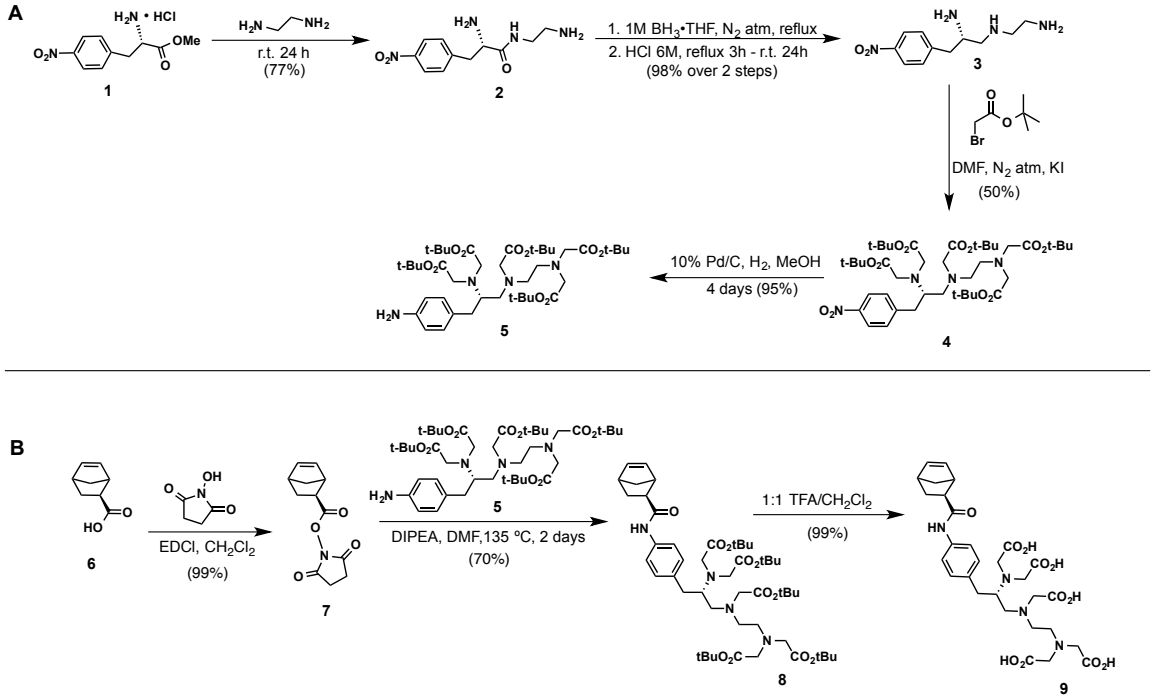

Figure 4.1 Synthesis of a norbornene modified DTPA chelate. A) Synthetic scheme for penta-*t*-butyl 1-(*S*)-(*p*-aminobenzyl)-DTPA **5**. B) Synthetic scheme for polymerizable DTPA monomer **9**.

To incorporate the amine functionalized DTPA into a polymerizable monomer, we first synthesized an activated ester onto a strained norbornene ring. *N*-hydroxysuccinimide (NHS) in the presence of EDCI was added to the commercially available exo-carboxcylic acid norbornene (**6**) to afford an exo-norbornene NHS (**7**) in a 99% yield. Next, *p*-aminobenzyl-DTPA penta-*t*-butyl ester in DMF was reacted with DIPEA and **7** at 135 ºC, allowing the production of **8** in a 70% yield. The *t*-butyl protected DTPA monomer was then deprotected with a 1:1 mixture of TFA:CH_2Cl_2 to give the DTPA monomer **9** in an overall 25% isolated yield.

4.2.2 Polymerization of DTPA Monomer

To ensure DTPA monomer **9** could be polymerized, we analyzed the polymerization reaction by NMR following the scheme outlined in Figure 4.2A. Monomer **9** was dissolved in DMF-d_7 and analyzed by NMR (Figure 4.2B, t = 0). Then, a modified 2nd generation Grubb's catalyst was added and again, analyzed by NMR at strategic time points to determine complete polymerization (Figure 4.2B). It was confirmed that after 30 minutes, all of Monomer **9** was converted to a homopolymer (Figure 4.2B). At this time the reaction was quenched by addition of ethyl vinyl ether (EVE). Next, we set out to characterize the dispersity and degree of polymerization by size exclusion chromatography coupled with multi-angle light scattering (SEC-MALS), however this was unachievable for this particular polymer in DMF or $CHCl_3$. In order to achieve our goals in a less time consuming manner, we decided to move to the synthesis of a Gd-DOTA derivative that involved less synthetic steps and eliminated the need for any post polymerization metallation with Gd^{3+}.

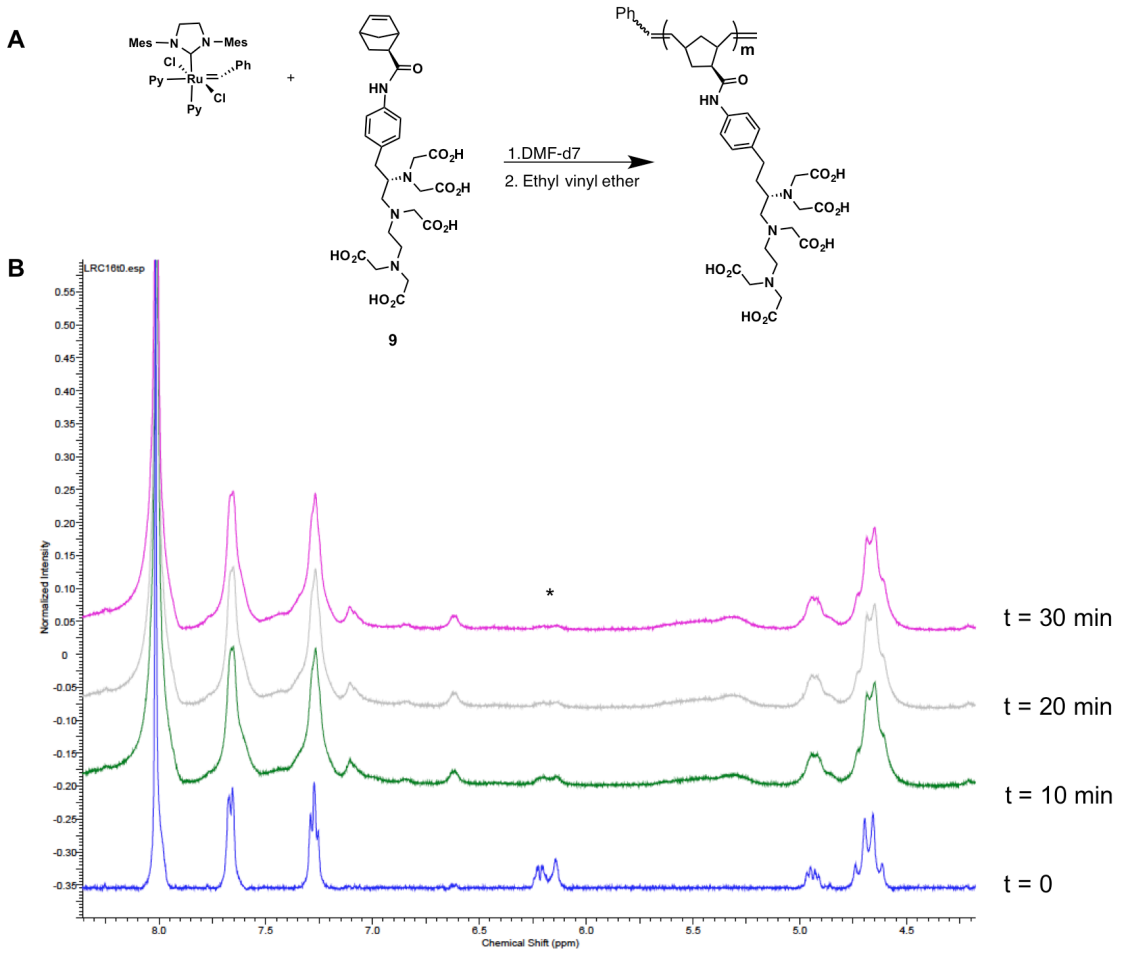

Figure 4.2 Polymerization of DTPA Monomer **9**. A) Synthetic scheme for the polymerization of **9**. B) NMR time course showing the complete polymerization of **9** after 30 minutes as indicated by the disappearance of olefin peaks, annotated by "*".

4.3. Gd-DOTA-MA Polymerization and Micellarization

4.3.1 Synthesis of Gd-DOTA-MA Monomer

Due to the ease of synthesis, we moved to the incorporation of Gd-DOTA monoamide (Gd-DOTA-MA) derivatives. In this section, we describe our approach to directly incorporate gadolinium Gd-DOTA-MA into polymers and polymeric nanoparticles. Importantly, this approach allows us to generate amphiphilic block copolymers capable of assembling into particles of different

shapes, in addition to preparing completely water-soluble polymers. First, a novel monomer amenable ROMP is synthesized (Figure 4.3A). An amine monomer (**10**) was conjugated with an NHS-modified DOTA in pyridine. Any excess amine was capped by the addition of acetic anhydride and an aliquot of norbornene-DOTA was characterized by NMR to confirm successful conjugation (see experimental). Next, chelation of $Gd(OAc)_3$ afforded paramagnetic compound **12** in a 75% overall yield. Since NMR was no longer a viable option for characterization, the Gd-DOTA-MA monomer **12** was characterized by HPLC and electrospray ionization mass spectrometry (ESI-MS) to confirm purity and correct molecular weight (Figure 4.3B-C).

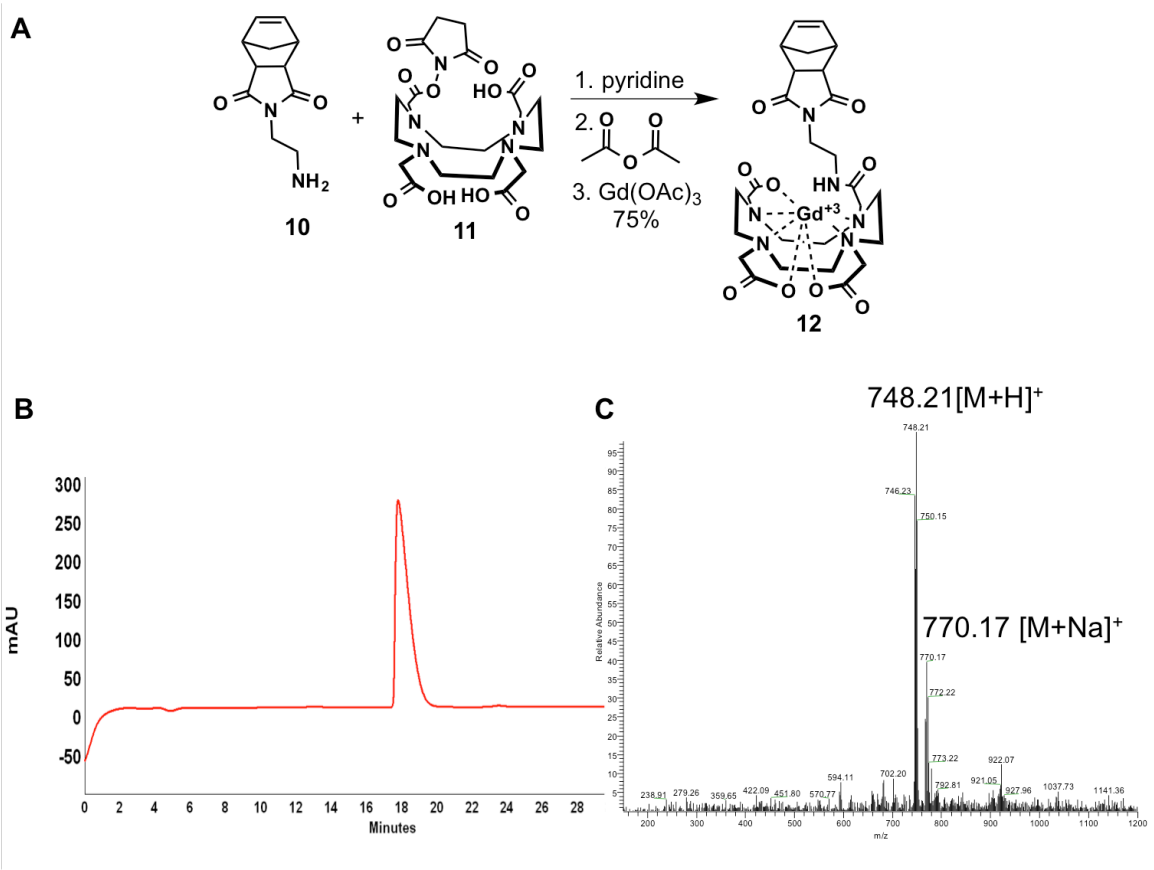

Figure 4.3 Synthesis and characterization of Gd-DOTA-MA monomer **12**. A) Synthetic scheme of Gd-DOTA-MA monomer **12**. B) Analytical RP-HPLC chromatogram of purified monomer **12** on a gradient of 8-12% ACN in H_2O with 0.1% TFA. C) ESI-MS confirming the molecular weight of **12**.

4.3.2 Synthesis of Gd-DOTA-MA Polymers

After synthesis of Gd-DOTA-MA monomer **12**, amphiphilic block copolymers were synthesized containing hydrophobic monomer **13,** with **12** incorporated as the hydrophilic block (Figure 4.4). We reasoned that varying the block sizes of amphiphilic block copolymers synthesized from monomers **12** and **13** could lead to micellar NPs of different morphologies following NP formulation.[19] Therefore, two sets of polymers with various ratios of **12** and **13**, as diblocks were prepared. In addition, to generate a fully solvated macromolecular

control as a contrast agent (i.e. a non-particle forming system), a hydrophilic polymer was synthesized as a diblock from monomer **12** and **14** (Figure 4.4). It should be noted that a homopolymer was unsuccessfully synthesized due to poor solubility during polymerization. For this reason, it was always prepared as the second block.

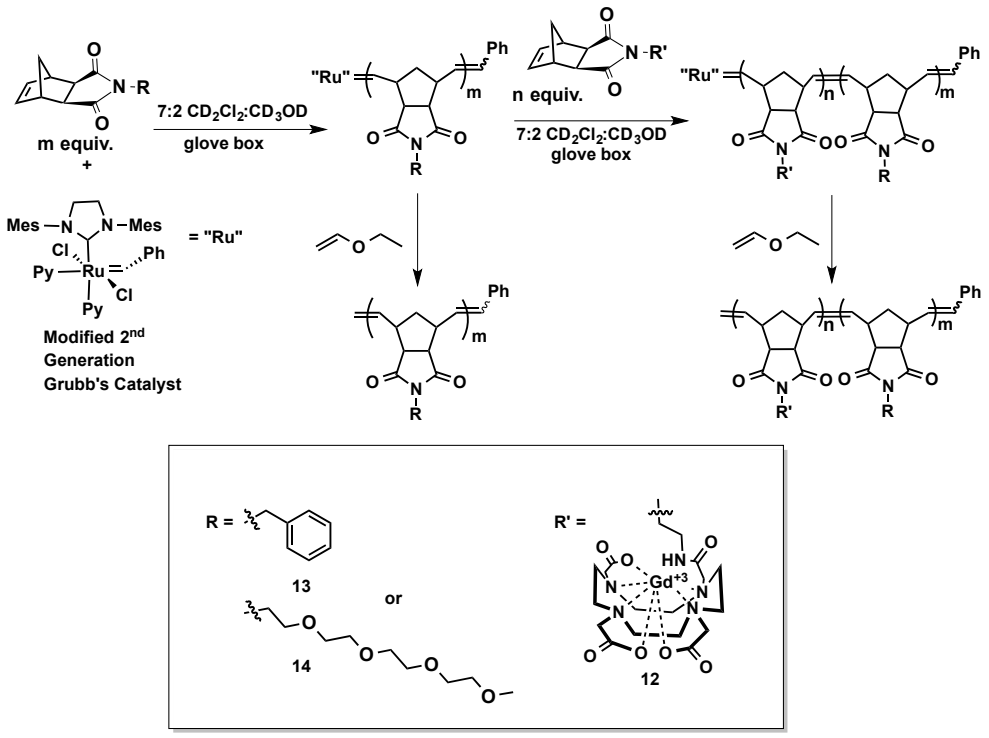

Figure 4.4 General synthetic scheme for the polymerization of block copolymers containing Gd-DOTA-MA monomer **12.**

Table 4.1 Characterization of Block Copolymers Synthesized with Gd-DOTA-MA Monomer **12**. [a] Degree of polymerization of block m of monomer **13** or **14** shown in parentheses. [b] Degree of polymerization of block n of monomer **12**. [c] Number average molecular weight as determined by SEC-MALS. [d] Dispersity as determined by SEC-MALS.

Polymer	DP_m (Mon **13** or **14**)[a]	DP_n[b] of **12**	M_n[c]	M_w/M_n[d]
15	210 (**13**)	4	55,740	1.004
16	42 (**13**)	2	11,910	1.024
17	104 (**14**)	17	49,450	1.024

To monitor the polymerization of Gd-DOTA-MA monomer **12**, NMR was no longer a viable option due to the paramagnetic nature of Gd^{3+}. For this reason, we ensured complete polymerization by utilizing RP-HPLC. After addition of the second block, we analyzed the polymers by RP-HPLC to ensure complete consumption of **12** (Figures 4.5 - 4.7). Additionally, each of the polymers was analyzed by SEC-MALS to quantify the number average molecular weight (M_n), degree of polymerization (DP) and dispersity (M_w/M_n) (Figure 4.5 – 4.7 and Table 4.1).

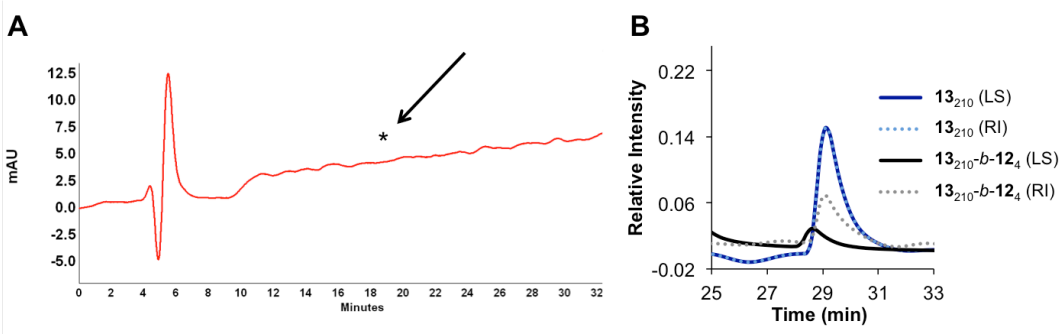

Figure 4.5 HPLC and SEC-MALS of polymer **15**. A) Analytical RP-HPLC chromatogram of reaction mixture demonstrating consumption of monomer **12**. An asterisk highlights the expected retention time of monomer **12.** B) SEC-MALS and RI analyses of a homopolymer of **13** and the final block copolymer of $\mathbf{13}_{210}$-*b*-$\mathbf{12}_4$ (i.e. Polymer **15**) in $CHCl_3$.

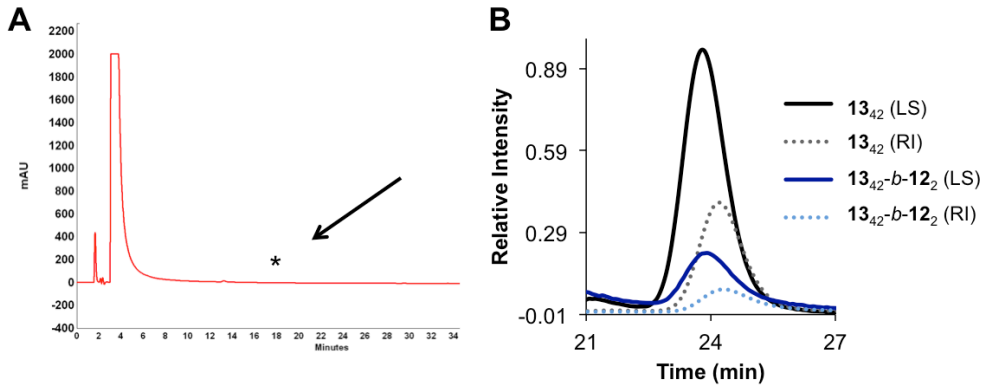

Figure 4.6 HPLC and SEC-MALS of polymer **16**. A) Analytical RP-HPLC chromatogram of reaction mixture demonstrating consumption of monomer **12**. An asterisk highlights expected retention time of monomer **12.** B) SEC-MALS and RI analyses of a homopolymer of **13** and a block copolymer of $\mathbf{13}_{42}$-*b*-$\mathbf{12}_2$ (i.e. Polymer **16**) in 50 mM LiBr in DMF.

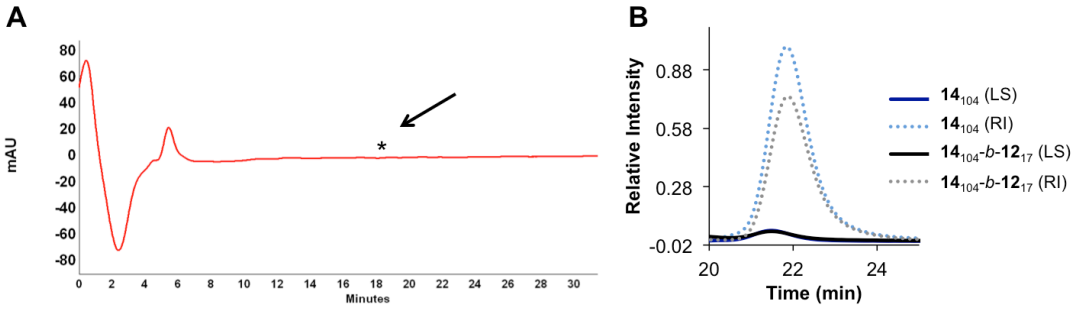

Figure 4.7 HPLC and SEC-MALS characterization of polymer **17**. A) Analytical RP-HPLC chromatogram of reaction mixture demonstrating consumption of monomer **12**. An asterisk highlights the expected retention time of monomer **12**. B) SEC-MALS and RI analyses of a homopolymer of **14** and block copolymer of $\mathbf{14}_{104}$-*b*-$\mathbf{12}_{17}$ (i.e. Polymer **17**) in 50 mM LiBr in DMF.

4.3.3 Nanoparticle Formulation

The synthetic strategy outlined in the previous section allowed us to target three structures: 1) a hydrophilic, solvated polymer (**SP**) with composition $\mathbf{14}_{104}$-*b*-$\mathbf{12}_{17}$ (polymer **17**), 2) spherical micellar nanoparticles (**SMN**s) formulated from $\mathbf{13}_{210}$-*b*-$\mathbf{12}_4$ (Polymer **15**), and 3) fibril-shaped micellar nanoparticles (**FMN**s)

formulated from **13**$_{42}$-*b*-**12**$_2$ (Polymer **16**). In the case of Polymer **15**, slow transition from DMSO into water results in the formation of monodisperse **SMN**s as evidenced by negative stain transmission electron microscopy (TEM) and dynamic light scattering (Figure 4.8A, Table 4.2). Bright field scanning transmission electron microscopy (BF-STEM) (Figure 4.8B) shows close packing of nanoparticles with dark rings around the coronas, indicative of a heavy element (Gd^{3+}). High angle annular dark field (HAADF)-STEM coupled with energy dispersive X-ray spectroscopy (EDS) (Figure 4.8 C-E) further confirms the presence of Gd^{3+} in the shell of the micelle indicated by the bright halos around the outer edges and characteristic X-ray scattering from Gd^{3+}.

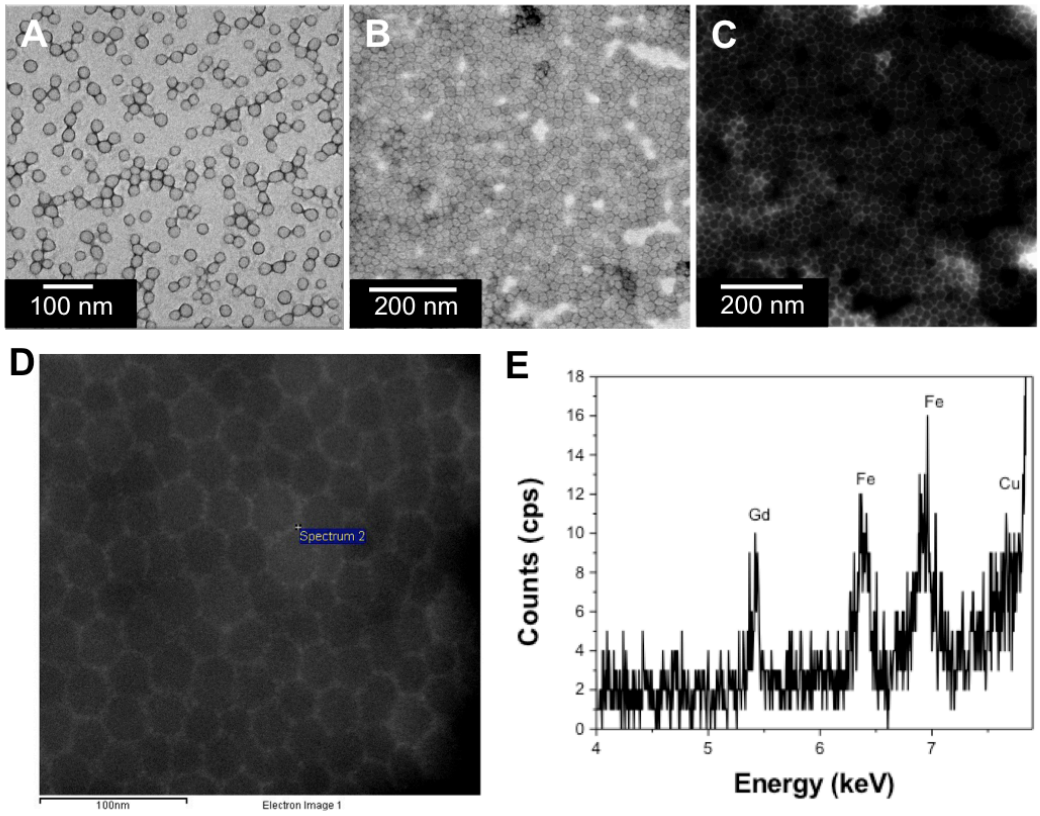

Figure 4.8 Particle characterization by electron microscopy of spherical micellar nanoparticles (**SMN**s). A) Negative stain TEM of **SMN**. B) BF-STEM of **SMN**. C) HAADF-STEM of **SMN**. D) STEM-HAADF of **SMN** with area chosen for EDS analysis (annotated as spectrum 2). E) EDS of **SMN** from the area selected in (D). Iron and copper signals are artifacts from the specimen holder and copper grid.

Table 4.2. Dynamic Light Scattering (DLS) Characterization of **SMN** and **FMN**. [a] Hydrodynamic diameter as determined by DLS. [b] Polydispersity index (PDI) as determined by DLS.

Sample	D_h (nm)[a]	PDI[b]
SMN	36.8	0.02257
FMN	151.4; 1913.6	0.0228; 0.1818

In a similar fashion, polymer **16** was slowly transitioned into water from DMSO via dialysis to generate **FMN**s (Figure 4.9A and Table 4.2). BF- and HAADF-STEM coupled with EDS revealed the presence of a heavy metal (Figure

4.9B-E). The **FMN** formulation is not an entirely homogeneous phase, but rather contains a minor component of spherical structures consistent with the findings of others, indicating that pure cylindrical phases are rather rare (Figure 4.9A-C).[20] However, we assign this formulation to be predominately **FMN** based on the shape populations visualized by TEM and STEM analysis (see Figure 4.9A-D). In the case of **SP**, as expected, there are no visible NP structures via DLS or TEM due to the hydrophilic nature of the polymer (data not shown). We note that the NP formulations are stable as **SMN** or **FMN** for periods in excess of 12 months in aqueous media.

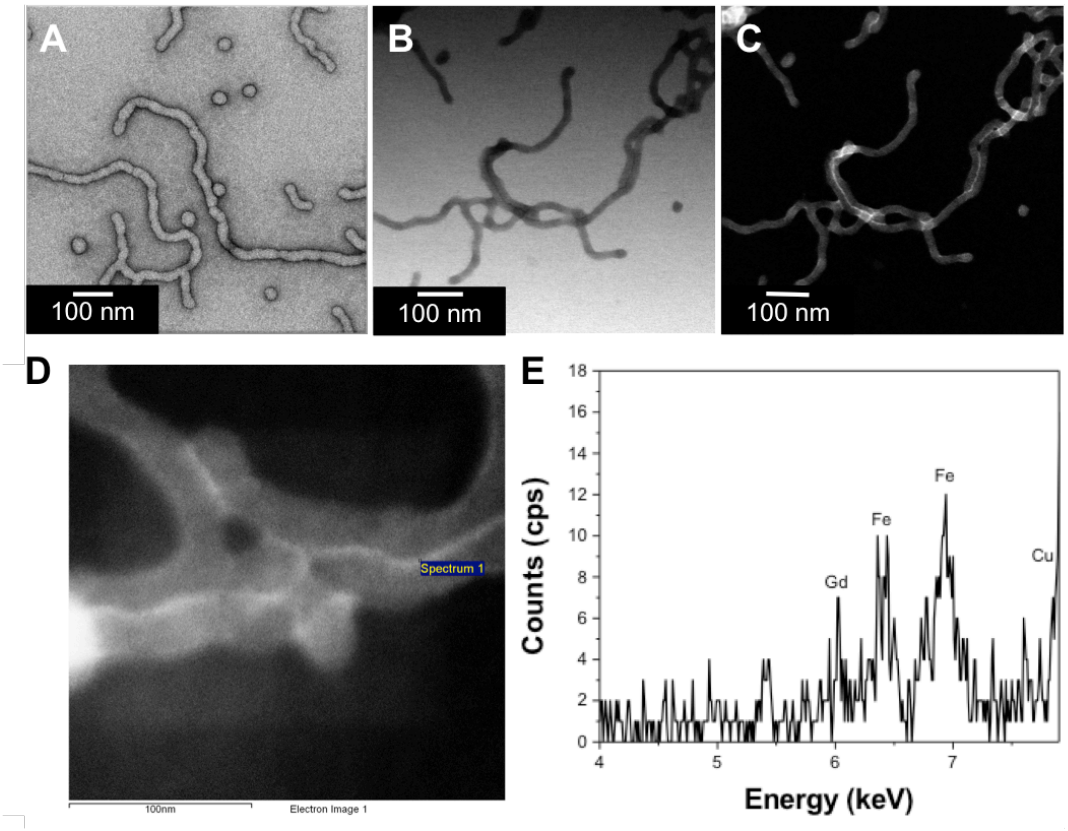

Figure 4.9 Particle characterization by electron microscopy of fibril micellar nanoparticles (**FMN**s). A) Negative stain TEM of **FMN**. B) BF-STEM of **FMN**. C) HAADF-STEM of **FMN**. D) STEM-HAADF of **FMN** with area chosen for EDS analysis (annotated as spectrum 1). E) EDS of **FMN** from the area selected in (D). Iron and copper signals are artifacts from the specimen holder and copper grid.

4.3.4 Relaxivity Measurements

To accurately determine the concentration of Gd^{3+} in **SP**, **SMN**, and **FMN**, an NMR assay was developed, taking advantage of the paramagnetic properties of Gd^{3+}. A standard curve was produced with free Gd^{3+} at various known concentrations of nitric acid and D_2O. Using inversion recovery NMR experiments, the ^1H relaxation time (T_1) was determined using NMR at each of the pre-determined concentrations in order to obtain the standard curve shown in

Figure 4.10. The inverse of T_1 ($1/T_1$) is plotted against known concentrations of Gd^{3+} to give a linear slope (r_{1p}) of 13.84 $mM^{-1}sec^{-1}$.

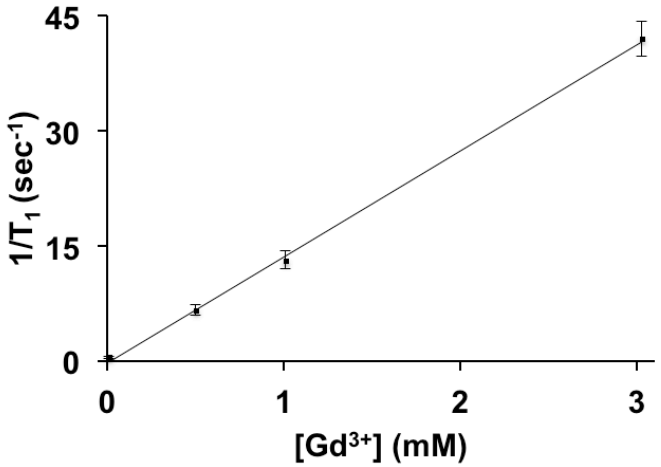

Figure 4.10 Standard curve of $1/T_1$ vs $[Gd^{3+}]$. Slope of the line is 13.84 ± 0.830 $mM^{-1}sec^{-1}$ with an R^2 value of 0.9992.

With this standard curve, we could determine the Gd^{3+} concentration of **SP**, **SMN**, and **FMN**. Each sample was digested separately in nitric acid and inversion recovery analysis by NMR determined the T_1 time. From the standard curve in Figure 4.10, it was possible to obtain the concentration of Gd^{3+} in each of the samples and is given in Table 4.3.

Table 4.3 Gd^{3+} concentration of **SP**, **SMN,** and **FMN.**

Sample	T_1 (sec)	Gd^{3+} Concentration (mM)
SP	1.086	0.267
SMN	0.701	0.408
FMN	0.6543	0.444

With these Gd^{3+} displaying polymers and NPs in hand, we set out to study the basic relaxometric properties of the three contrast agents: **SP**, **SMN**, and **FMN** (Figure 4.11, Table 4.4, Table 4.5). At 25 ºC and 37 ºC, the nuclear magnetic resonance dispersion (NMRD) profile of all three systems show the characteristic shape for macromolecular structures due to a reduction in rotational tumbling rate.[21,22] The data points in Figure 4.11 were fit using equations for outer hydration sphere (OS) and inner hydration sphere (IS) contributions to relaxivity based on classical Solomon-Bloembergen-Morgan (SBM) theory, incorporating the Lipari-Szabo model for rotational dynamics.[21] This model differentiates the local and global tumbling motions of the chelate, allowing the effect of local molecular motion on r_{1p} to be considered. Notable features in the NMRD profile show a region of constant relaxivity at low field strengths (~0.01 MHz – 0.5 MHz, 0.0002 – 0.01 T) for all three structures with a slightly elevated per Gd^{3+} relaxivity at all field strengths for **FMN**. Most interesting is a large maximum relaxivity centered at 20 MHz (0.5 T) followed by a steep decrease at higher frequencies. The NMRD profiles at 25 ºC for **SP** and **SMN** are almost identical with a maximum per Gd^{3+} r_{1p} at 20 MHz (~0.5 T) of 13.7 $mM^{-1}sec^{-1}$, while **FMN** demonstrates an elevated r_{1p} of 16.6 $mM^{-1}sec^{-1}$. When the temperature is increased to a physiologically relevant temperature of 37 ºC, a noticeable rise in relaxivity is apparent for **SMN** and **FMN** but not for **SP**, indicative of either different rates of water exchange in the inner hydration sphere ($k_{ex} = 1/\tau_M$) and/or a different degree of local rotational flexibility (τ_{RL}).[23]

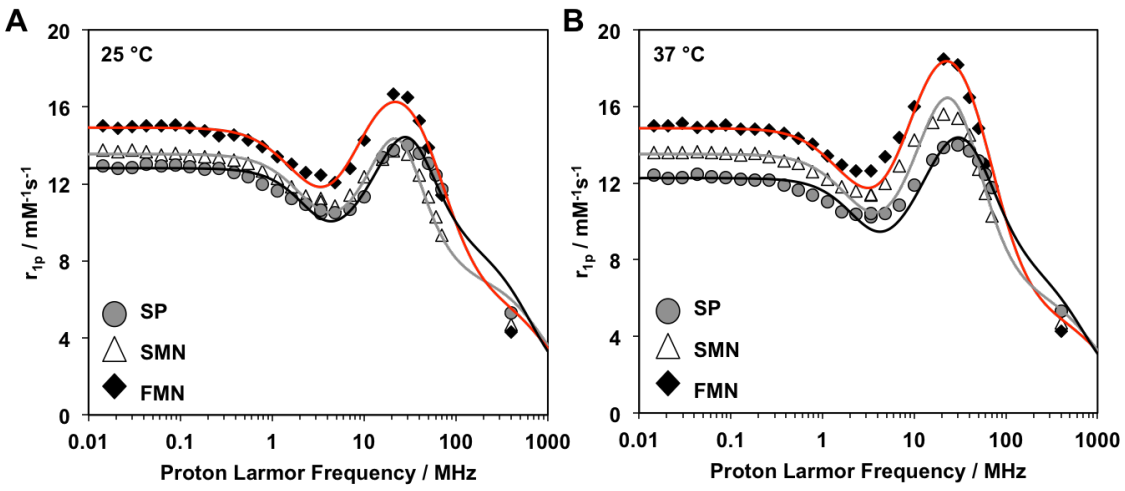

Figure 4.11 ^{1}H NMRD profiles for: A) **SP**, **SMN**, and **FMN** at 25 ºC; B) **SP**, **SMN**, and **FMN** at 37 ºC.

The small differences in relaxivity between **SP**, **SMN**, and **FMN** can be further understood by evaluating the parameters that define relaxivity. It has been shown that when the residence lifetime (τ_M) is long (≥500 ns at 25 ºC, Table 4.4), this may significantly limit relaxivity, especially in the case of macromolecules that have a reduced global rotation (τ_{RG}).[24,25] As shown in Table 4.4, each of the three systems has a τ_M that is greater than 500 ns, which limits the relaxivity enhancement. These values are comparable with those reported for corresponding Gd-DOTA-MA analogues.[22] However, at 37 ºC this is not the case for **FMN** (Table 4.5). Another limiting factor of the relaxivity of these systems is the local rotational flexibility of Gd^{3+} compared to the global rotation of the polymer or nanostructure. In general, τ_{RL} tends to be much faster than τ_{RG}, likely limiting the possible maximum enhancement in r_{1p}.[26,27] For **SP**, **SMN**, and **FMN**, all have a τ_{RL} an order of magnitude less than τ_{RG}, further confirming the

limitation of this type of chelate in polymer and polymeric nanostructures. The degree of correlation between τ_{RL} and τ_{RG} is described by the order parameter S^2 such that $0 < S^2 < 1$. The other two parameters for electronic relaxation listed in Table 4.4 and Table 4.5 (Δ^2, τ_v) are empirical fitting parameters and do not assume a clear physical meaning for these slowly tumbling nano-sized systems.[23] We note that elevated per Gd^{3+} relaxivities of **SP**, **SMN**, and **FMN** as compared to the mononuclear Gd-DOTA at 20 MHz (r_{1p} = 4.2 $mM^{-1}sec^{-1}$, 25 ºC) are similar to those seen for other nanoparticle and polymer-based systems.[1,11] Additionally, at 9.4T (400 MHz) all three of these systems converge to almost identical r_{1p} but at the same time contain enhanced r_{1p} compared to the small molecule analogues.

Table 4.4 Relaxation parameters obtained from the analysis of ^{1}H NMRD profiles reported in Figure 4.11A. The parameters are ^{298}D, q and r with values of 4.0 Å, 2.24×10^{-5} cm^2 s^{-1}, 1 and 3.0 *Å*, respectively; [a] let to vary between 400 and 900 ns.

	$^{20}r_{1p}$ (mM^{-1} s^{-1})	Δ^2 (10^{19} s^{-2})	τ_V (ps)	τ_{RL} (ns)	τ_{RG} (ns)	S^2	τ_M (ns)[a]
SP	13.7	1.5	37	0.30	4.6	0.17	700
SMN	13.7	0.9	44	0.21	7.0	0.14	700
FMN	16.6	0.7	50	0.18	3.0	0.25	600

Table 4.5 Relaxation parameters obtained from the analysis of NMRD profiles reported in Figure 4.11B. The parameters are ^{310}D, q and r with values of 4.0 Å, 3.10×10^{-5}cm^2 s^{-1}, 1 and 3.0 *Á*, respectively; [a] let to vary between 200 and 900 ns.

	$^{20}r_{1p}$ (mM^{-1} s^{-1})	Δ^2 (10^{19} s^{-2})	τ_V (ps)	τ_{RL} (ns)	τ_{RG} (ns)	S^2	τ_M (ns)[a]
SP	13.9	1.5	36	0.27	3.2	0.21	620
SMN	15.6	0.9	42	0.19	5.9	0.20	560
FMN	18.5	0.7	49	0.15	2.8	0.25	350

4.4 Conclusions

We have developed a synthetic strategy that allows us to directly polymerize norbornene based DTPA and Gd-DOTA analogues. While we successfully polymerized norbornene-DTPA, the lengthy synthesis motivated us to move toward Gd-DOTA-MA analogues. Polymers containing Gd-DOTA-MA can be formulated into polymeric and micellar materials of various morphologies. Our strategy offers the advantage of allowing the formulation of chemically similar structures via a direct polymerization process leading to well-defined materials. In the case of nanoparticles, STEM-EDS analysis reveal that Gd^{3+} is present in the corona of NPs, allowing access to water and therefore rendering them capable of being effective T_1 contrast agents. Cyclic NMRD profiles reveal that at low field strength (~0.5 – 1T) and at 37 ^{o}C, **SP**, **SMN**, and **FMN** have maximum r_{1p} values of 13.9, 15.6, and 18.5 mM^{-1}sec^{-1} respectively. These values are larger than that observed for the mononuclear Gd-DOTA chelate. On going studies in our laboratory are analyzing the function of different polymerizable MRI contrast agents for the purpose of enhanced relaxivity. Additionally, we are

looking into the relaxivity differences between polymerized monomers containing MRI contrast agents and polymers terminated with MRI contrast agents.

4.5 Experimental

4.5.1 General Methods

Monomer and Polymer Synthesis and Characterization. All reagents were purchased from Sigma-Aldrich or Macrocyclics and used without further purification. Molecules **1 – 5** were prepared as previously described.[28] 2,5-dioxopyrrolidin-1-yl-(2*S*)-bicyclo[2.2.1]hept-5-ene-2-carboxylate (**7**) was prepared as previously described.[29] 2-(2-aminoethyl)-3a,4,7,7a-tetrahydro-1*H*-4,7-methanoisoindole-1,3(2*H*)-dione (**10**) was prepared as previously described.[30] (N-Benzyl)-5-norbornene-*exo*-2,3-dicarboximide (**13**) was prepared as described previously.[31] Oligoethyleneglycol monomer (**14**) was prepared as previously described.[32] $(IMesH_2)(C_5H_5N)_2(Cl)_2Ru{=}CHPh$ was prepared as described by Sanford *et al*.[33] Polymerizations were performed under a dry dinitrogen atmosphere with anhydrous, degassed solvents in a glove box. RP-HPLC analyses were performed on a Jupiter 4m Proteo 90Å Phenomenex column (150 x 4.60 mm) with a binary gradient at a flow rate of 1 mL/min using a Hitachi-Elite LaChrom L-2130 pump equipped with UV-Vis detector (Hitachi- Elite LaChrom L-2420). For purification, a semi-preparative Phenomenex Jupiter 4m Proteo 90Å column (250 x 10.0mm) was utilized at a flow rate of 4 mL/min. For both analytical and semi-preparative RP-HPLC, the following mobile phases were used: Eluant A = 0.1% TFA in water; Eluant B = 99.9% acetonitrile, 0.1% TFA. ^1H

(300 and 400 MHz) and ^{13}C (100 MHz) NMR spectra were recorded on a Varian Mercury Plus spectrometer. ^{1}H and ^{13}C chemical shifts are reported in δ (ppm) relative to the residual proton peaks. Mass spectra were obtained at the UCSD Chemistry and Biochemistry Molecular Mass Spectrometry Facility. Polymer dispersity and molecular weight were determined by size-exclusion chromatography (Phenomenex Phenogel 5m **10**, 1K-75K, 300 x 7.80 mm in series with a Phenomex Phenogel 5m **10**, 10K-1000K, 300 x 7.80 mm (0.05 M LiBr in DMF or HPLC grade $CHCl_3$) using a Shimatzu pump equipped with a multi-angle light scattering detector (DAWN-HELIOS: Wyatt Technology) and a refractive index detector (Hitachi L-2490) normalized to a 30,000 MW polystyrene standard using dn/dc of 0.179 for polymers containing monomer **13** and 0.100 for polymers containing monomer **14**.

Nanomaterial Formulation and Characterization. Snakeskin^{TM} dialysis tubing was purchased from thermoscientific with a molecular weight cut off (MWCO) of 3,500 or 10,000 g/mol. Hydrodynamic diameter (D_h) was determined by DLS using a Wyatt Dynapro NanoStar. TEM was performed on a FEI Sphera microscope operating at 200 keV. TEM grids were prepared by depositing small (3.5 µl) aliquots of sample onto grids (~ 2 min, Formvar stabilized with carbon (5-10 nm) on 400 copper mesh, Ted Pella Inc.) that had previously been glow discharged using an Emitech K350 glow discharge unit and plasma-cleaned for 90 s in an E.A. Fischione 1020 unit. The sample grid was then stained with 1% uranyl acetate solution, rinsed with water (~5 µL), and excess liquid was removed. Micrographs were recorded on a 2K X 2K Gatan CCD camera. STEM

and STEM-EDS analysis were acquired on a JEOL JEM 2100F TEM equipped with an INCA (Oxford) EDS detector at the University of Pittsburgh, PA. Samples were prepared by drop-casting 5 μL of sample onto TEM grids (ultrathin 5 nm A-type carbon with 400 mesh Copper) followed by slow drying covered on the bench top for at least 3 hours. Samples were then dried under vacuum for 24-48 hours to remove contamination that would interfere with STEM-EDS. STEM-EDS data was collected for 180 - 600 s at specific points, using the largest probe size (1.5 nm electron beam diameter) with a 200 kV accelerating voltage. Images were collected in bright field (BF) and high-angle annular dark field (HAADF) modes.

^{1}H NMRD Profiles. Proton $1/T_1$ NMRD profiles were measured on a Fast Field-Cycling Stelar SMARTracer NMR Relaxometer (Stelar, Mede (PV), Italy) over a continuum of magnetic field strengths from 0.00024 to 0.25 T (corresponding to 0.01-10 MHz proton Larmor frequencies). The relaxometer operates under computer control with an absolute uncertainty in $1/T_1$ of ± 1%. Additional data points in the range 20-70 and 400 MHz were obtained on a Bruker WP80 NMR electromagnet adapted to variable-field measurements (15-80 MHz proton Larmor frequency) Stelar Relaxometer and Jeol ECP spectrometer (9.39 T), respectively. The ^{1}H T_1 relaxation times were acquired by the standard inversion recovery method with typical 90° pulse width of 3.5 ms, 16 experiments of 4 scans. The temperature was controlled with a Stelar VTC-91 airflow heater equipped with a calibrated copper–constantan thermocouple

(uncertainty of ±0.1 ℃). The temperature was determined by previous calibration with a Pt resistance temperature probe.

4.5.2 Monomer Synthesis

Synthesis of Norbornene-Penta-*t*-Butyl 1-(*S*)-(*p*-Aminobenzyl)-DTPA (**8**). Penta-*t*-Butyl 1-(*S*)-(*p*-Aminobenzyl)-DTPA (**5**, 700 mg, 0.898 mmol) and Norbornene-NHS (**7**, 211 mg, 0.898 mmol) were dissolved in DMF (22 mL, 0.04 M). DIPEA (311 µL, 1.79 mmol) was added to this stirred solution, placed under a N_2 atmosphere and heated to 120 ºC following addition of a condenser head. After 48 hours, the reaction was cooled to room temperature and purified by flash chromatography eluting with 1% triethylamine in 1:1 Hexane:Ethyl Acetate resulting in 590 mg of an amber oil (73% yield). ^{1}H NMR (CDCl3): ∂ (ppm) 1.40 (s, 9 H, 3 x CH_3), 1.42-1.46 (2 s, 36H, 12 x CH_3), 2.028-2.04 (m, 2H, CH_2), 2.12 – 2.16 (dd, 2H, CH_2), 2.45 – 2.50 (dd, 2H, CH_2), 2.61 – 2.70 (m, 5H, 2 x CH_2, 1 x CH), 2.77 – 2.86 (m, 3H, 2 x CH_2, 1 x CH), 2.96 (m, 1H, CH), 3.30 – 3.49 (m, 11H, 5 x CH_2, 1 x CH), 6.15 – 6.18 (dd, 2H, HC=CH), 7.15 – 7.19 (m, 3H, 1 x NH, 2 x CH), 7.38 – 7.41 (d, 2H, 2 x CH). ^{13}C NMR ($CDCl_3$): ∂ (ppm) 28.16, 30.59, 41.63, 45.91, 46.32, 47.29, 52.56, 52.96, 53.59, 55.83, 55.92, 56.02, 56.21, 63.20, 80.78, 119.59, 129.75, 135.93, 138.51, 170.72, 171.32. LRMS (ESI) 899.31 $[M+H]^+$, 921.25 $[M+Na]^+$. HRMS, expected $[M+H]^+$: 899.5740, found: 899.5743

Synthesis of Norbornene-DTPA (**9**). Norbornene-Penta-*t*-Butyl 1-(*S*)-(*p*-Aminobenzyl)-DTPA (**8**, 100 mg, 0.111 mmol) was dissolved in CH_2Cl_2 (1 mL,

0.111M). Trifluoroacetic acid (1 mL, 13.5 mmol) was then added to the protected DTPA monomer **8** and stirred at room temperature overnight. The solution was concentrated to dryness resulting in a gold oil (>99% yield). ^{1}H NMR (CD_3OD): ∂ (ppm) 1.94-1.98 (m, 2H, CH_2), 2.30– 2.32 (dd, 2H, CH_2), 2.56 – 2.61 (dd, 2H, CH_2), 2.88 – 2.92 (m, 5H, 2 x CH_2, 1 x CH), 3.05 – 3.10 (m, 3H, 2 x CH_2, 1 x CH), 3.17 (m, 1H, CH), 3.51 – 3.72 (m, 11H, 5 x CH_2, 1 x CH), 6.18 (s, 2H, HC=CH), 7.20 – 7.22 (d, 2H, 2 x CH), 7.49 – 7.54 (m, 2H, 2 x CH). LRMS (ESI) 619.34 $[M+H]^+$, 641.33 $[M+Na]^+$.

Synthesis of Norbornene-DOTA-MA.**10** (25 mg, 0.0788 mmol) and DOTA-NHS•HPF_6•CF_3CO_2H (**11**, 50 mg, 0.0656 mmol) were dissolved in pyridine (0.328 mL) and placed on a vortex overnight. Acetic anhydride (0.1547 mL, 1.64 mmol) was added and the reaction mixture was placed back on the vortex for 10 min. The reaction mixture was concentrated to dryness resulting in a highly viscous translucent yellow oil. The product was purified by semi-preparative RP-HPLC over a 50 minute linear gradient from 8% to 15% eluant B in eluant A (18 mg, 70%). ^{1}H NMR (C_5D_5N): ∂ (ppm) 1.29 (s, 2H, CH_2), 2.84, (s, 2H, 2 x CH), 3.15-3.40 (m, 18H, 2 x CH, 16 x CH_2), 3.69-3.70 (m, 2H, CH_2), 3.88-3.92 (m, 2H, CH_2), 4.04-4.17 (m, 8H, 8 x CH_2), 6.05 (s, 2H, CH=CH), 8.54 (b.s., 1H, NH), 9.70 (s, 3H, 3 x COOH). ^{13}C NMR (C_5D_5N): δ (ppm) 38.29, 43.69, 45.85, 48.87, 51.62, 52.67, 53.04, 56.78, 138.43, 170.34, 173.61, 179.04. LRMS (ESI) 593.37 $[M+H]^+$, 615.33 $[M+Na]^+$, 631.26 $[M+K]^+$, HRMS, expected $[M+H]^+$: 593.2929, found: 593.2930.

Synthesis of Norbornene-[Gd-DOTA-MA] **12**. **10** (50 mg, 0.158 mmol) and DOTA-NHS•HPF_6•CF_3CO_2H (**11**, 100 mg, 0.131 mmol) were dissolved in pyridine (0.655 mL) and placed on a vortex overnight. Acetic anhydride (0.309 mL, 3.28 mmol) was added and the reaction mixture was placed back on the vortex for 10 min. $Gd(OAc)_3$ (160 mg, 0.393 mmol) was then added to the remaining solution and placed back on the vortex overnight. The reaction was concentrated to dryness to give a light brown residue. The product was then purified by semi-preparative RP-HPLC over a 50 minute linear gradient from 8% to 15% eluant B in eluant A (50 mg, 75%). LRMS (ESI) 748.21 $[M+H]^+$, 770.17 $[M+Na]^+$, HRMS, expected $[M+H]^+$: 748.1936, found: 748.1932.

4.5.3 Polymerization Procedures

Time Course Polymerization of Norbornene-DTPA (**9**). Norbornene-DTPA (**9**, 10 mg, 0.0162 mmol) was dissolved in DMF-d_7 (500 µL) and analyzed by ^1H NMR. This solution was cooled in an isopropanol/dry ice bath and the initiator ($(IMesH_2)(C_5H_5N)_2(Cl)_2Ru=CHPh$) (0.785 mg, 0.00108 mmol) in DMF-d_7 (171 µL) was added. A time course ^1H NMR analysis was performed at strategic time points until complete disappearance of norbornene protons was achieved. Please see Figure 4.2 for time course ^1H NMR.

Synthesis of Polymer **15**. The initiator ($(IMesH_2)(C_5H_5N)_2(Cl)_2Ru=CHPh$) (2.44 mg, 0.00335 mmol) in anhydrous 7:2 CH_2Cl_2:CH_3OH (0.129 mL) was added to a stirred solution of **13** (68 mg, 0.268 mmol) in same solvent mixture (2.97 mL). The reaction was left to stir in a glove box for 20 min, after which an

analytical aliquot (approximately 32% by volume) was removed and mixed with an excess of ethyl vinyl ether for 30 min, then dried under high vacuum to give a homopolymer of **13** as a solid. Immediately following analytical aliquot removal, a solution of **12** (25 mg, 0.0335 mmol) in anhydrous 7:2 CH_2Cl_2:CH_3OH (0.08 mL) was added. The reaction was monitored by analytical RP-HPLC (using the same conditions described above for compound **12**) to ensure complete consumption of **12**. The mixture was left to stir in the glove box for 90 min and then quenched with excess ethyl vinyl ether (0.0251 mL) for 20 minutes, which was concentrated to dryness to give a greenish solid. This was used without further purification until particle formation. The homopolymer and block-copolymer were analyzed by SEC-MALS (Figure 4.5, Table 4.1).

Synthesis of Polymer **16**. The initiator ($(IMesH_2)(C_5H_5N)_2(Cl)_2Ru$=CHPh) (3.9 mg, 0.005 mmol) in anhydrous CH_2Cl_2 (0.8 mL) was added to a stirred solution of monomer **13** (61 mg, 0.24 mmol) in anhydrous CH_2Cl_2 (1.4 mL). The reaction was left to stir in a glove box for 20 min, after which an analytical aliquot (approximately 20% by volume) was removed and mixed with an excess of ethyl vinyl ether for 30 min, then dried under high vacuum to give a homopolymer of **13** as a solid. To the remaining reaction mixture, a solution of monomer **12** (25 mg, 0.033 mmol), in anhydrous CH_3OH (0.625 mL) was added immediately following aliquot removal. The reaction was monitored by analytical RP-HPLC (using the same conditions described above for compound **12**) to ensure complete consumption of monomer **12**. The mixture was left to stir in the glove box for 90 min, and then quenched with excess ethyl vinyl ether for 30 minutes. A small

aliquot was removed for subsequent analysis. This material was carried on without further purification until particle formation. The homopolymer and block-copolymer were analyzed by SEC-MALS (Figure 4.6, Table 4.1).

Synthesis of Polymer **17**. Initiator ($(IMesH_2)(C_5H_5N)_2(Cl)_2Ru{=}CHPh$) (2.44 mg, 0.00335 mmol) in anhydrous 7:2 CH_2Cl_2:CH_3OH (0.1291 mL) was added to a stirred solution of **14** (95 mg, 0.268 mmol) in a mixture of anhydrous 7:2 CH_2Cl_2:CH_3OH (2.98 mL). The reaction was left to stir under nitrogen for 20 min, after which an analytical aliquot (approximately 32% by volume) was removed and mixed with an excess of ethyl vinyl ether for 30 min, and then dried under high vacuum to give a homopolymer of **14** as a solid. To the remaining reaction mixture, a solution of **12** (25 mg, 0.0335 mmol) in anhydrous 7:2 CH_2Cl_2:CH_3OH (0.08 mL) was added, immediately following analytical aliquot removal. The reaction was monitored by analytical RP-HPLC to ensure complete consumption of monomer **12**. The mixture was left to stir under nitrogen for 90 min and then quenched with ethyl vinyl ether (0.025 mL). The polymer was used without further purification until dialysis. The solution was concentrated to dryness to give a glassy solid. The homopolymer and block-copolymer were analyzed by SEC-MALS (Figure 4.7, Table 4.1).

4.5.4 Dialysis and Particle Formation

SMN (derived from **15**). **15** (75 mg, 1.35 μmol) was dissolved in DMSO (2.5 mL) and the solution was sonicated until fully dissolved. A solution of 1:1 DMSO:H_2O (2.5 mL) was added drop wise. The cloudy polymer mixture was

sonicated for 15 minutes, then transferred to a 3,500 MWCO snakeskin dialysis tubing (Pierce) and dialyzed against a 1:1 DMSO:H_2O solution (2L). After 24 hours, the milky solution was removed from dialysis and H_2O was added drop wise (2.5 mL) to the polymer mixture. This mixture was then transferred to a 10,000 MWCO snakeskin dialysis tubing and dialyzed against 2L of H_2O. After 24 hours, H_2O (2.5 mL) was added to the dialysis bag and the dialysate was refreshed with 2L of H_2O. Dialysis was allowed to continue for 24 hours. The sample was removed from dialysis and the tubing was rinsed with H_2O (3 x 1mL) into the polymer sample. An additional 25 mL of H_2O was added to further solubilize the milky solution and then sonicated for 9 hours. The solution was placed in a centrifuge at 4000 rcf for 6 min and decanted the solution away from residual particulate. The decanted solution was used for all further analysis.

FMN (derived from Polymer **16**). Half of the reaction volume from the synthesis of **16** was diluted to 2 mg/mL with respect to the starting materials with 7:2 CH_2Cl_2:CH_3OH. This solution was placed into a 3,500 MWCO snakeskin dialysis tubing and dialyzed against DMSO for 4 hours. The sample was then dialyzed against 4:1 DMSO:H_2O for 4 hours, followed by 3:2 DMSO:H_2O for 4 hours, followed by 2:3 DMSO:H_2O for 4 hours, followed by 1:4 DMSO:H_2O for 4 hours, then 2 x H_2O for 4 hours each to yield a milky suspension.

SP (derived from Polymer **17**). CH_3OH was added to **17** (112 mg, 2.26 μmol) to give a final concentration of 0.602 mM in 2.5 mL. A solution of 1:1 DMSO:H_2O (2.5 mL) was added to this solution, which remained brown and translucent. The solution was transferred to a 3,500 MWCO snakeskin dialysis

tubing and dialyzed against 1:1 DMSO:H_2O (2L). After 24 hours, the solution in the dialysis tubing had become cloudy. Then 2.5 mL of H_2O was added, which resulted in a clear mixture. The mixture was transferred to a 10,000 MWCO snakeskin dialysis tubing and dialyzed against 2 x 2L of H_2O for 24 hours. The solution in the tubing remained clear. The aqueous polymer solution was removed from dialysis and centrifuged at 4,000 rcf for 6 min. To the supernatant was added 10 mL of H_2O. The solution was then sonicated for 5 hours prior to analysis.

4.5.5 Determination of Gd^{3+} Concentration

Standard Curve for Gd^{3+} Concentration Determination. A 0.1 M stock solution of $GdCl_3$ in H_2O was prepared. From this stock, concentrations of 3.0, 1.0, 0.5, and 0.01 mM of Gd^{3+} in 2:3:5 HNO_3:H_2O:D_2O were made. T_1 relaxations were determined for each concentration of Gd^{3+} using inversion recovery experiments on a 300 MHz Varian NMR instrument. $1/T_1$ were averaged for three separate samples at the same concentration, then plotted to give the standard curve shown in Figure 4.10. Relaxivity of free Gd^{3+} was found to be 13.8 $mM^{-1}sec^{-1}$ at the given conditions.

General Procedure to Determine Concentration of Gd^{3+} for **SP**, **SMN**, and **FMN**. In order to determine Gd^{3+} concentration, the metal was first stripped from the chelate using the following procedure. A solution of 80% HNO_3 in water (115 µL) was added to an aliquot of each sample (115 µL). Each mixture was then heated at 65 ºC for approximately 12 hours. The sample was diluted with 230 µL

of D_2O and T_1 was determined using an inversion recovery experiment on a 300 MHz Varian NMR. Based on r_1 data obtained from the standard curve described above (Figure 4.10), the concentration of Gd^{3+} could be calculated. The concentration of stock solutions can be found in Table 4.3.

4.6 Acknowledgements

Chapter 4, in part, has been submitted for publication: Randolph, Lyndsay M., LeGuyader, Clare L. M., Hahn, Michael E., Andolina, Christopher M., Mattrey, Robert F., Millstone, Jill E., Botta, Mauro, Scadeng, Miriam, and Gianneschi, Nathan C. "*In vivo* MRI reveals Morphology Dependent Biodistribution of Nanoparticles Versus Small Molecule Contrast Agents." *submitted* (2014). The dissertation author is the primary author of this manuscript.

4.7 References

(1) Villaraza, A. J.; Bumb, A.; Brechbiel, M. W. *Chem. Rev.* **2010**, *110*, 2921.

(2) Jaspers, K.; Versluis, B.; Leiner, T.; Dijkstra, P.; Oostendorp, M.; van Golde, J. M.; Post, M. J.; Backes, W. H. *PLoS One* **2011**, *6*, e16159.

(3) Langereis, S.; Dirksen, A.; Hackeng, T. M.; van Genderen, M. H. P.; Meijer, E. W. *New J. Chem.* **2007**, *31*, 1152.

(4) Allen, M. J.; Raines, R. T.; Kiessling, L. L. *J. Amer. Chem. Soc.* **2006**, *128*, 6534.

(5) Grogna, M.; Cloots, R.; Luxen, A.; Jerome, C.; Desreux, J.-F.; Detrembleur, C. *J. Mater. Chem.* **2011**, *21*, 12917.

(6) Xu, Q.; Zhu, L.; Yu, M.; Feng, F.; An, L.; Xing, C.; Wang, S. *Polymer* **2010**, *51*, 1336.

(7) Dumas, S.; Jacques, V.; Sun, W. C.; Troughton, J. S.; Welch, J. T.; Chasse, J. M.; Schmitt-Willich, H.; Caravan, P. *Invest. Radiol.* **2010**, *45*, 600.

(8) Li, S.; Jiang, J.; Zou, J.; Qiao, J.; Xue, S.; Wei, L.; Long, R.; Wang, L.; Castiblanco, A.; White, N.; Ngo, J.; Mao, H.; Liu, Z.-R.; Yang, J. J. *J. Inorg. Biochem.* **2012**, *107*, 111.

(9) Guodong Zhang, R. Z., Xiaoxia Wen, Li Li, Chun Li *Biomacromolecules* **2008**, *9*, 36.

(10) Besenius, P.; Heynens, J. L.; Straathof, R.; Nieuwenhuizen, M. M.; Bomans, P. H.; Terreno, E.; Aime, S.; Strijkers, G. J.; Nicolay, K.; Meijer, E. W. *Contrast Media Mol. Imaging* **2012**, *7*, 356.

(11) Liu, Y.; Zhang, N. *Biomaterials* **2012**, *33*, 5363.

(12) Vaccaro, M.; Accardo, A.; Tesauro, D.; Mangiapia, G.; Lof, D.; Schillen, K.; Soderman, O.; Morelli, G.; Paduano, L. *Langmuir* **2006**, *22*, 6635.

(13) Turner, J. L.; Pan, D.; Plummer, R.; Chen, Z.; Whittaker, A. K.; Wooley, K. L. *Adv. Funct. Mater.* **2005**, *15*, 1248.

(14) Liu, T.; Qian, Y.; Hu, X.; Ge, Z.; Liu, S. *J. Mater. Chem.* **2012**, *22*, 5020.

(15) Ratzinger, G.; Agrawal, P.; Korner, W.; Lonkai, J.; Sanders, H. M.; Terreno, E.; Wirth, M.; Strijkers, G. J.; Nicolay, K.; Gabor, F. *Biomaterials* **2010**, *31*, 8716.

(16) Grogna, M.; Cloots, R.; Luxen, A.; Jerome, C.; Passirani, C.; Lautram, N.; Desreux, J.-F.; Detrembleur, C. *Polym. Chem.* **2010**, *1*, 1485.

(17) Bielawski, C. W.; Grubbs, R. H. *Prog. Polym. Sci.* **2007**, *32*, 1.

(18) Leitgeb, A.; Wappel, J.; Slugovc, C. *Polymer* **2010**, *51*, 2927.

(19) Jain, S.; Bates, F. S. *Science* **2003**, *300*, 460.

(20) Blanazs, A.; Madsen, J.; Battaglia, G.; Ryan, A. J.; Armes, S. P. *J. Amer. Chem. Soc.* **2011**, *133*, 16581.

(21) Aime, S.; Botta, M.; Terreno, E. In *Advances in Inorganic Chemistry*; Academic Press: 2005; Vol. Volume 57, p 173.

(22) Caravan, P.; Ellison, J. J.; McMurry, T. J.; Lauffer, R. B. *Chem. Rev.* **1999**, *99*, 2293.

(23) Cittadino, E.; Botta, M.; Tei, L.; Kielar, F.; Stefania, R.; Chiavazza, E.; Aime, S.; Terreno, E. *ChemPlusChem* **2013**, *78*, 712.

(24) Botta, M.; Tei, L. *Eur. J. Inorg. Chem.* **2012**, *2012*, 1945.

(25) Helm, L.; Nicolle, G. M.; Merbach, R. E. In *Advances in Inorganic Chemistry*; Academic Press: 2005; Vol. Volume 57, p 327.

(26) Kielar, F.; Tei, L.; Terreno, E.; Botta, M. *J. Amer. Chem. Soc.* **2010**, *132*, 7836.

(27) Zhang, Z.; Greenfield, M. T.; Spiller, M.; McMurry, T. J.; Lauffer, R. B.; Caravan, P. *Angew. Chem. Int. Ed.* **2005**, *44*, 6766.

(28) Corson, D. T.; Meares, C. F. *Bioconjugate Chem.* **2000**, *11*, 292.

(29) Pontrello, J. K.; Allen, M. J.; Underbakke, E. S.; Kiessling, L. L. *J. Amer. Chem. Soc.* **2005**, *127*, 14536.

(30) Thompson, M. P.; Randolph, L. M.; James, C. R.; Davalos, A. N.; Hahn, M. E.; Gianneschi, N. C. *Polym. Chem.* **2014**, *5*, 1954.

(31) Chien, M. P.; Rush, A.; Thompson, M.; Gianneschi, N. *Angew. Chem. Int. Ed.* **2010**, *49*, 5076.

(32) Hahn, M. E.; Randolph, L. M.; Adamiak, L.; Thompson, M. P.; Gianneschi, N. C. *Chem. Commun.* **2013**, *49*, 2873.

(33) Sanford, M. S.; Love, J. A.; Grubbs, R. H. *Organometallics* **2001**, *20*, 5314.

5. *In Vivo* MRI Reveals Morphology Dependent Biodistribution of Nanoparticles Versus Small Molecule Contrast Agents

5.1 Introduction

The basic physical properties of nanoparticles (NPs), including particle morphology, can greatly influence their behavior *in vivo*. For example, Discher and colleagues demonstrated that fibril shaped NPs have longer circulation times as compared with spherical and vesicular morphologies when introduced intravenously into mice.[1] This observation led to the conclusion that particle shape may be used to control delivery of therapeutic and diagnostic agents *in vivo* following intravenous (IV) injection.[1,2] We hypothesized that NP morphology would contribute to the biodistribution and retention of NPs introduced through intraperitoneal (IP) injection rather than IV injection.[3] This mode of administration has been exploited for efficient introduction of diagnostic and therapeutic agents meant for systemic delivery via uptake in the highly vascularized IP space and in some cases have proven to be superior for NP uptake.[4-6] Additionally, IP injection of NPs is proven to be advantageous to IV injection in mouse models of ovarian cancer.[7,8] Moreover, direct delivery of chemotherapeutic agents to the IP space is a well-established therapeutic paradigm in the treatment of metastatic ovarian,[9-11] pancreatic[12] and gastric malignancies.[9,13] The work presented here is motivated by the rationale that extended retention of nanoscale materials in the IP space may have significant implications for IP therapeutic strategies.

Live animal imaging following injection of materials is useful for determining the mode of retention and biodistribution of NPs; for this reason we turned to magnetic resonance imaging (MRI). MRI is commonly used for noninvasive clinical imaging. Herein, we describe our approach to track Gd-

DOTA based polymeric and polymeric nanoparticles *in vivo* via MRI of live mice (see Figure 5.1 for chemical structures). Importantly, this approach allowed us to compare water-soluble polymers and polymeric nanoparticles of different shapes with their small molecule Gd-DOTA analogues via *in vivo* studies.

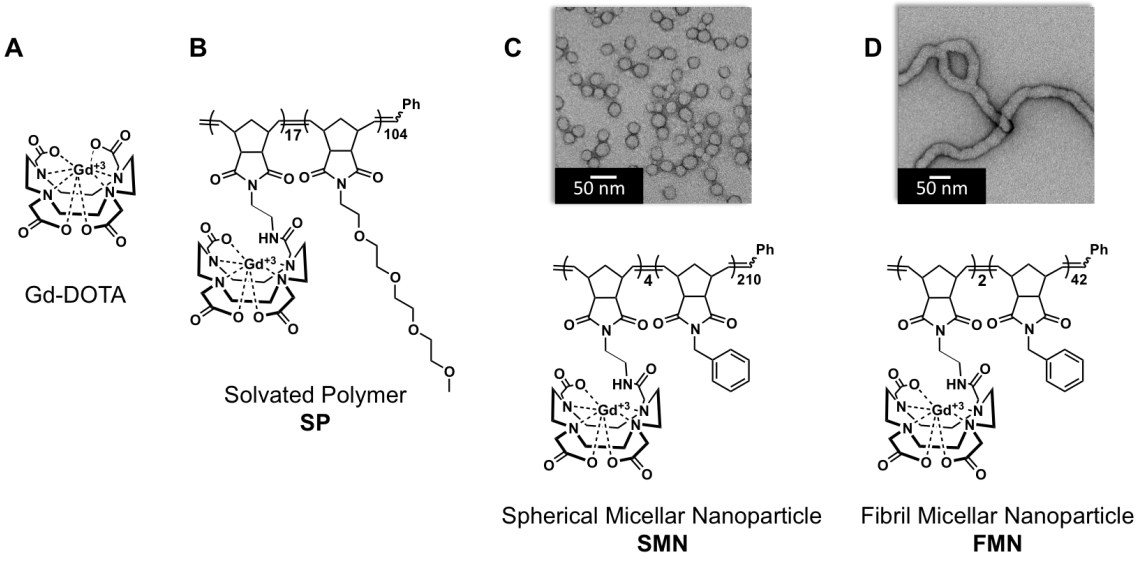

Figure 5.1 Chemical structures and morphology of Gd^{3+}-based materials for IP Injections into healthy mice. A) Chemical structure of FDA approved small molecule Gd-DOTA. B) Chemical structure of solvated polymer (**SP**). C) Chemical structure and transmission electron microscopy (TEM) image of spherical micellar nanoparticles (**SMN**s). D) Chemical structure and TEM of fibril micellar nanoparticles (**FMN**s).

5.2 MRI of Gd-DOTA, SP, SMN, and FMN

*5.2.1 In Vitro MRI of Gd-DOTA, **SP**, **SMN**, and **FMN***

We assessed the relaxivity of Gd-DOTA, **SP, SMN,** and **FMN** via 7T MRI prior to injection of C57Bl/6 mice with these samples. Each sample was analyzed in triplicate at a concentration of 0.267 mM of Gd^{3+}. Contrast enhancement was visually achieved when compared to water, as shown in Figure 5.2 for Gd-DOTA,

SP, **SMN**, and **FMN**. Analysis of T_1 results in a relaxivity (r_{1p}, $mM^{-1}sec^{-1}$) of Gd-DOTA, **SP, SMN,** and **FMN** as 4.0, 5.4, 4.6, and 5.2, respectively, at this field strength (Table 5.1). While the relaxivity differences are minimal, this is still an enhancement with respect to water, allowing this to be an optimal tool to visualize the effect of morphology on pharmacokinetics and biodistribution.

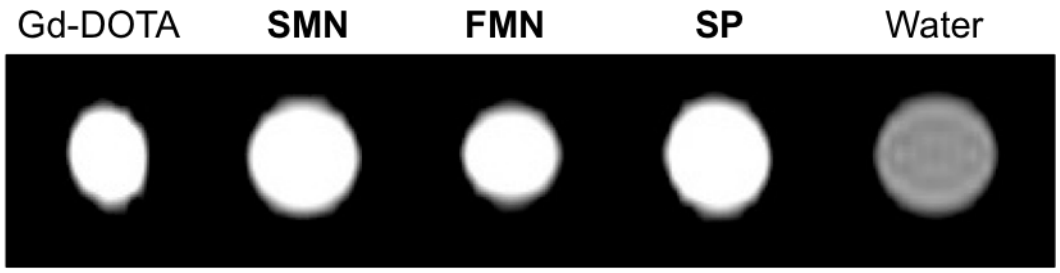

Figure 5.2 Phantoms of Gd-DOTA, **SMN**, **FMN**, **SP** and water at 7T.

Table 5.1 Relaxivity of **SP**, **SMN**, and **FMN** at 7T.

Sample	r_1 ($mM^{-1}sec^{-1}$)	Std. Dev. (± $mM^{-1}sec^{-1}$)
Gd-DOTA	3.97	1.515
SP	5.45	0.191
SMN	4.57	0.208
FMN	5.21	0.170

*5.2.2 IP Injections of Gd-DOTA, **SP**, **SMN**, and **FMN***

We hypothesize that an increase in molecular weight and/or size of a Gd-DOTA containing material will allow for longer IP retention and varied biodistribution. We employed MRI to assess the differences in biodistribution of

Gd-DOTA, **SP**, **SMN**, and **FMN** following IP injection into healthy C57Bl/6 mice. These agents were readily imaged with T_1-weighted MRI via contrast enhancement by their pendant Gd^{3+}, as shown in Figure 5.2.

Mice were anesthetized and imaged on a 7T MRI instrument prior to injection, then further imaged at multiple time points following administration of each contrast agent. A volume of 550 μL Gd-DOTA, **SP**, **SMN**, or **FMN** was injected into IP cavities at a concentration of 0.4 mM (concentration with respect to Gd^{3+} content in aqueous media; three mice per material for a total of twelve mice). Each animal was imaged continuously for two hours post injection while under anesthesia then at additional time points under anesthesia with imaging terminating after one week. Successful IP injections were confirmed in each case via MR scan immediately following injection (Figure 5.3). Animals were monitored to determine the *in vivo* biodistribution and mode of clearance by tracking any increase in contrast (decrease in T_1) in the urinary bladder, kidneys, and liver compared to pre-injection images.

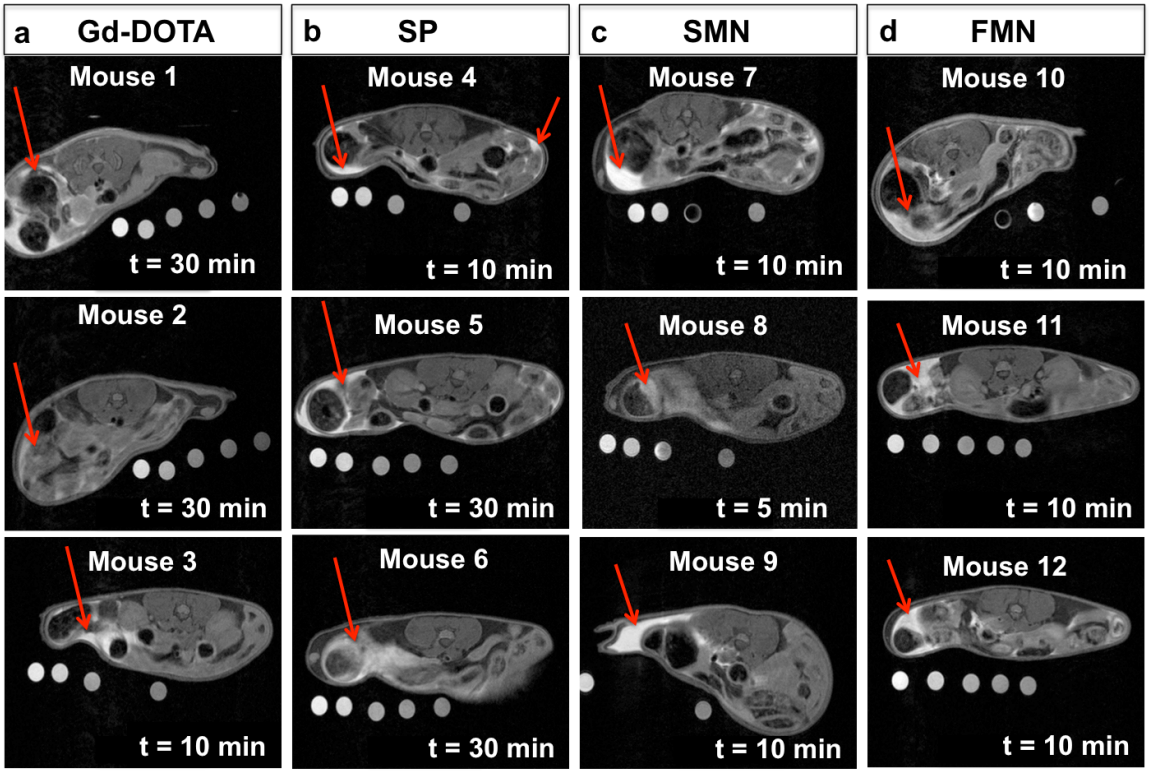

Figure 5.3 Anatomical MRI post-injection of contrast agent showing successful introduction of materials IP. Red arrows indicate contrast surrounding the bowl loops. A) Anatomical images of mice 1 – 3, 10 – 30 minutes post-IP injection of Gd-DOTA. B) Anatomical images of mice 4 – 6, 10 – 30 minutes post-IP injection of **SP**. C) Anatomical images of mice 7 – 9, 5 – 10 minutes post-IP injection of **SMN**. D) Anatomical image of mice 10 – 12, 10 minutes post-IP injection of **FMN**.

*5.2.3 Biodistribution of Gd-DOTA, **SP**, **SMN**, **FMN***

First, a volume of 550 µL Gd-DOTA was injected into peritoneal cavities of three mice at a concentration of 0.4 mM Gd^{3+}. As an internal standard, the mice were placed atop phantoms containing various concentrations of Gd-DOTA ranging from 0.003 to 0.4 mM Gd^{3+}. As expected, clearance into the urinary bladder was seen immediately following injection (Figure 5.4A)[14] as indicated by an intensity increase in anatomical scans. To account for any scan-to-scan variability, T_1 was normalized to the pre-scan phantoms. As shown in Figure

5.4A, there is a noticeable T_1 decrease in the lumen of this organ. Additionally, this clearance mechanism was further supported by an increase in intensity and T_1 decrease in the kidneys (Figure 5.5A and Figure 5.6A). Mice were unable to urinate during the first two hours of scan time due to a constant administration of anesthesia.

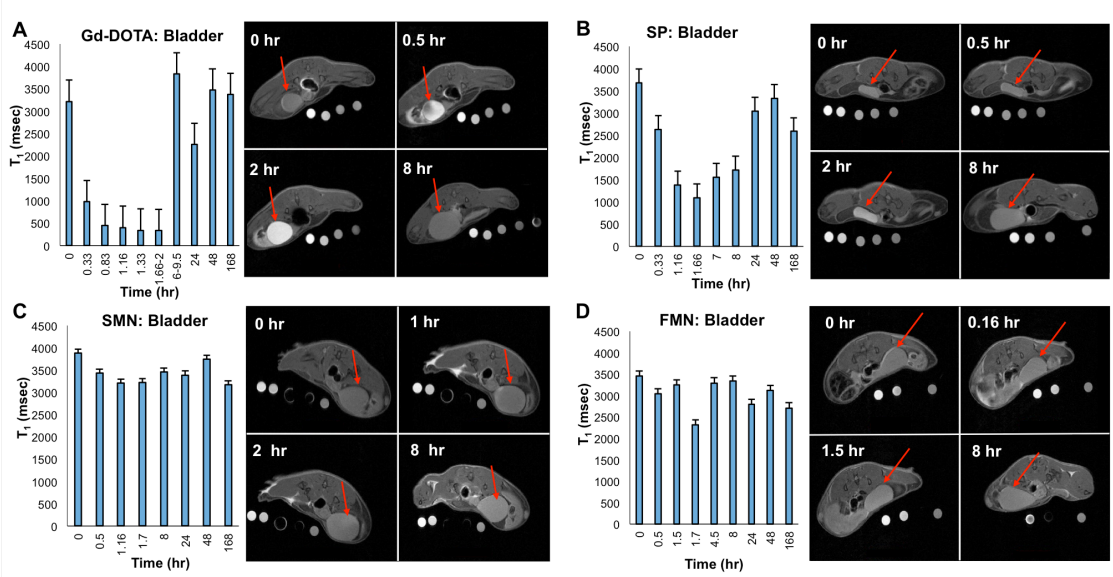

Figure 5.4 Time progression of contrast enhancement, quantified as T_1, and corresponding axial T_1-weighted images of the bladder after IP-injection of A) Gd-DOTA, B) **SP**, C) **SMN**, and D) **FMN**. For mice 1-12, multiple regions of interest (ROI) are sampled, normalized by comparing the relaxivity of phantoms for each scan to the pre-injection phantom relaxivity, averaged over the organ in the scan, then converted back to T_1 (see experimental for full analysis and description). For sampled time points of each material, T_1 times are averaged, and standard error is generated for n = 3 mice. Anatomical scans are from Mouse 1, Mouse 5, Mouse 9, and Mouse 10 for Gd-DOTA, **SP**, **SMN** and **FMN**, respectively. Red arrows indicate the urinary bladder.

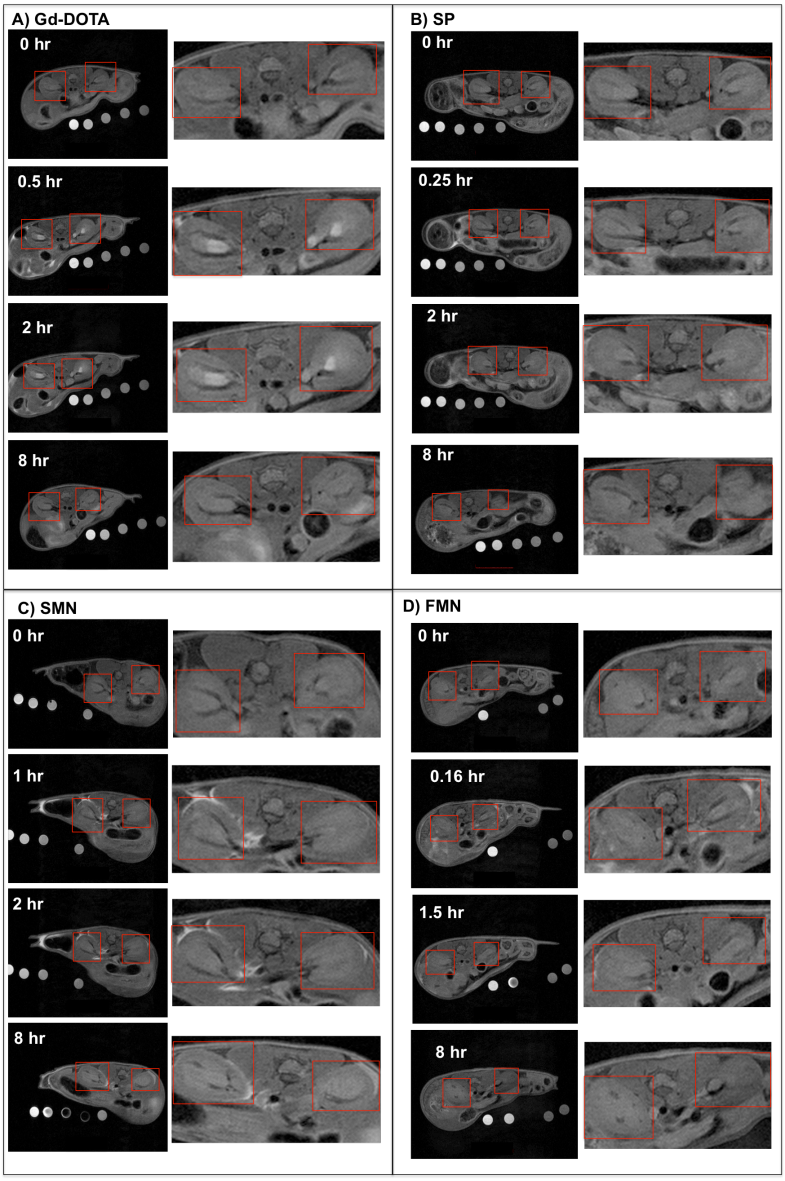

Figure 5.5 Time point anatomical images of kidneys. Left hand image shows full slice and the right hand image is magnified to highlight the kidneys (red boxes). A) Kidney data of mouse 1 injected with Gd-DOTA at t = 0, 0.5, 2, and 8 hours. B) Kidney data of mouse 5 injected with **SP** at t = 0, 0.5, 2 and 8 hours. C) Kidney data of mouse 9 injected with **SMN** at t = 0, 1, 2, and 8 hours. D) Kidney data of mouse 10 injected with **FMN** at t = 0, 0.16, 1.5 and 8 hours.

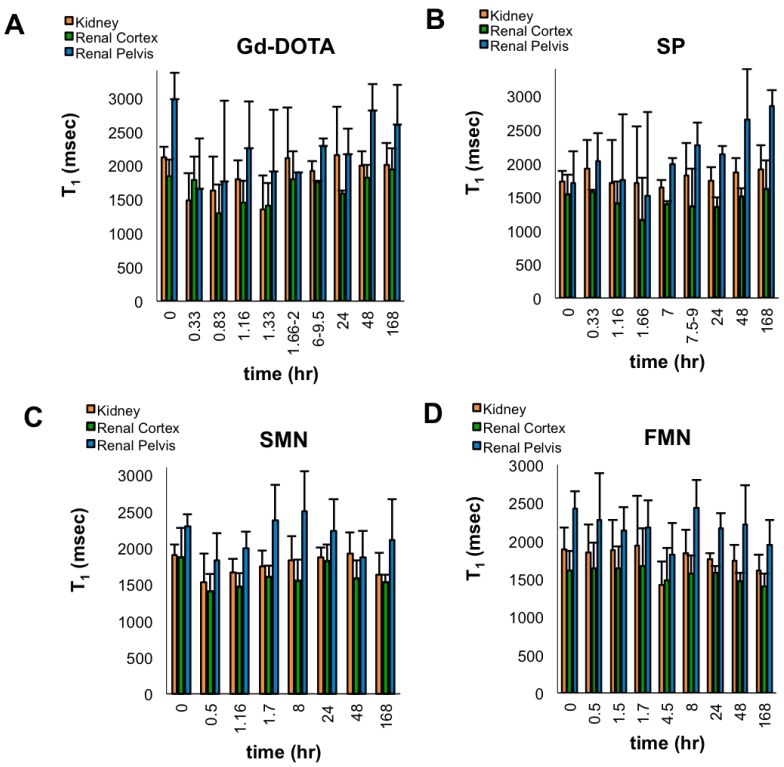

Figure 5.6 Time progression of contrast enhancement, reported as T_1 of kidneys after IP-injection. A) Gd-DOTA, B) **SP**, C) **SMN**, D) **FMN**.

After demonstrating that a concentration of 0.4 mM Gd^{3+} is visible *in vivo* with Gd-DOTA, we next investigated the biodistribution and clearance pathway of water-soluble polymer **SP**. Similarly to Gd-DOTA, clearance of **SP** into the urinary bladder was observed, albeit at a slower rate than the small molecule analogue (Figure 5.4B). Maximum contrast enhancement observed in anatomical images and minimum T_1 was achieved 2 hours following IP administration, as with Gd-DOTA, however in the case of **SP**, material continued to clear as observed by the slow recovery back to baseline over the following eight hours (Figure 5.4B). Specifically, after the animal was allowed to urinate (i.e. recover

from anesthesia), contrast enhancement was again identified in the bladder via a clear reduction in T_1 out to eight hours following injection of the water-soluble polymer (Figure 5.4B). We conclude that renal elimination of **SP** was delayed when compared to Gd-DOTA, presumably due to increased molecular weight of the former species. Renal clearance is also consistent with contrast enhancement in the kidneys (Figure 5.5B and Figure 5.6B). Retention of polymer in the IP cavity is further demonstrated by the observation that visible contrast enhancement persisted at 2 hours post injection; this phenomenon however is not observed for Gd-DOTA (Figure 5.7A,B).

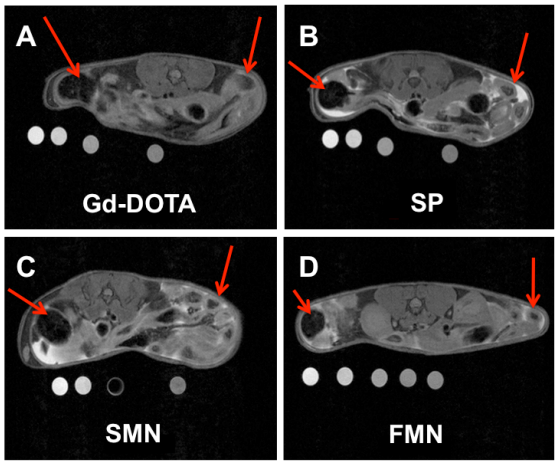

Figure 5.7 Axial T_1-weighted images of the abdomen approximately 2 hours following IP injection of A) Gd-DOTA into mouse 3, B) **SP** into mouse 6, C) **SMN** into mouse 7, and D) **FMN** into mouse 11. Red arrows indicate bowel loops of mice lying prone atop five phantoms. See Figure 5.3 for images that confirm successful IP injection of each material and each mouse.

Next, nanoparticle formulations of Gd-DOTA-MA were evaluated. **SMN** and **FMN** were injected separately into the intraperitoneal cavity of mice (three mice per material) and each of the previously described organs was monitored

for contrast enhancement and decreased T_1. Conversely to Gd-DOTA and **SP**, minimal contrast enhancement and concomitant decrease in T_1 was seen in the urinary bladder lumen (Figure 5.4C-D). Additionally, the kidneys did not display any observable contrast enhancement (Figure 5.5C-D and Figure 5.6C-D). These findings are consistent with the observation of sustained and significant contrast enhancement in the IP cavity, remaining robust at 2 hours following injection (Figure 5.7C-D). In the case of **SP**, **SMN**, and **FMN**, all three mice displayed a significant amount of contrast in the intraperitoneal cavity 2 hours post IP injection, presumably from the injection of polymer and polymeric nanomaterials bearing Gd^{3+}. This apparent retention of nanomaterials out to two hours is in stark contrast to the seemingly complete disbursement of visual material from the IP cavity less than two hours after injection of the small molecule contrast agent.

Although a slight decrease of T_1 in the urinary bladder is visible following IP injection of **SMN** and **FMN**, it is not enough to conclude this to be the singular, or dominant mechanism of excretion. An observed decrease of T_1 in the liver reveals that this is perhaps the organ where these NPs are accumulating (Figure 5.8C-D). This mode of accumulation is consistent with other studies examining IP injection of NPs.[6,15] Additionally, in the case of **FMN**, it is less clear if biodistribution is limited to the liver and bladder. Previous studies by others of different NP systems suggest that IP injected NPs demonstrate delayed uptake by macrophages followed by uptake in the liver.[16] Further studies will be required to definitively conclude how these materials are cleared *in vivo*.

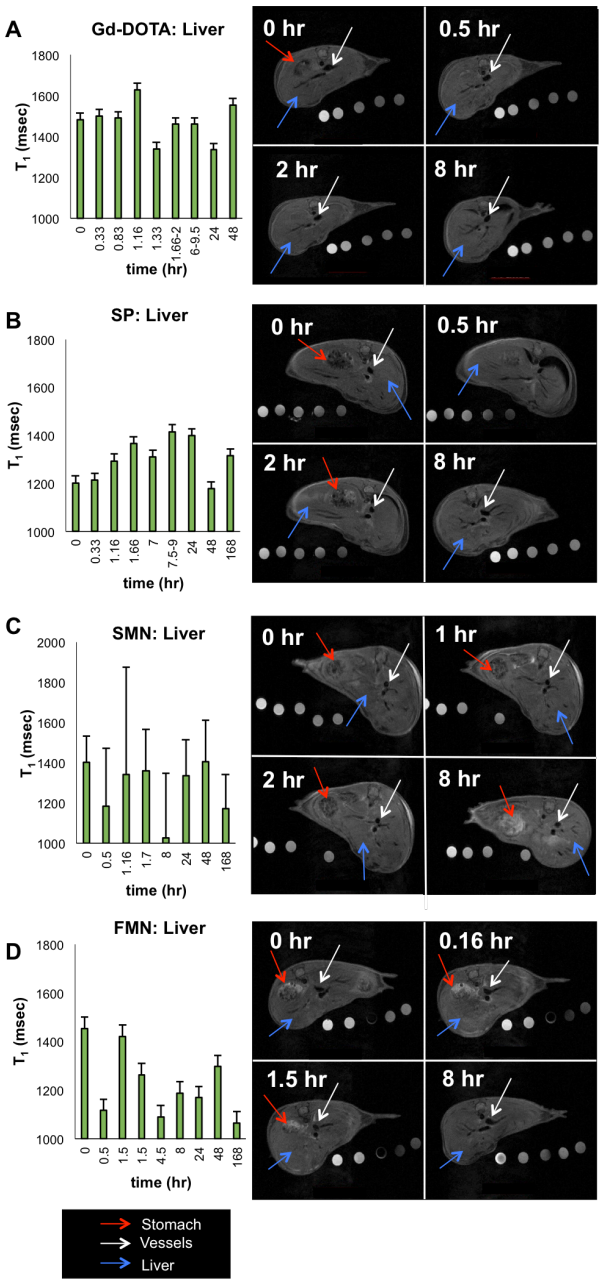

Figure 5.8 Time progression of contrast enhancement, reported as T_1, and corresponding axial anatomical scans of the liver after IP-injection. Any contrast enhancement in the stomach is due to food, not injected material. Red arrows indicate the stomach, white arrows indicate a vessel, and blue arrows indicate a ROI in the liver. A) Gd-DOTA. B) **SP**. C) **SMN**. D) **FMN**.

Lastly, the brain of each mouse was analyzed for any T_1-weighted enhancement. Contrast agents containing Gd^{3+} have not been reported to pass

an intact blood-brain barrier.[17] Indeed, Gd-DOTA proceeded with out contrast enhancement in the brain or a significant decrease in T_1 (Figure 5.9A). The same is true for **SP** and **SMN**, with only a small fluctuation in T_1 and no visual contrast enhancement. **FMN** shows more variance in T_1 when compared to Gd-DOTA, **SP**, and **SMN**. However, the change is minimal and can be attributed to the small sampling size and mouse-to-mouse discrepancies. Further studies *in vivo* with a larger sampling size are needed to confirm that these materials do not pass the blood brain barrier.

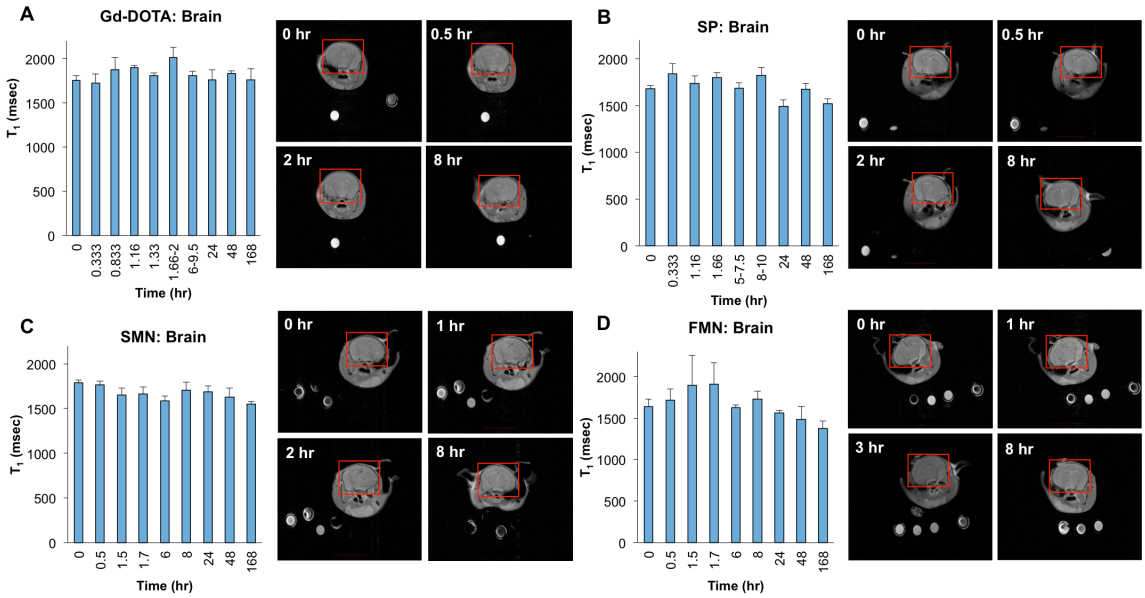

Figure 5.9 Time progression of contrast enhancement, quantified as T_1, and corresponding axial T_1-weighted images of the brain after IP-injection of A) Gd-DOTA, B) **SP**, c) **SMN**, and d) **FMN**. For mice 1-12, multiple regions of interest (ROI) are sampled, normalized by comparing the relaxivity of phantoms for each scan to the pre-injection phantom relaxivity, averaged over the organ in the scan, then converted back to T_1 (see experimental for full analysis and description). For sampled time points of each material, T_1 times are averaged, and standard error is generated for n = 3 mice. Anatomical scans are from Mouse 1, Mouse 5, Mouse 9, and Mouse 10 for Gd-DOTA, **SP**, **SMN** and **FMN**, respectively. Red boxes outline the brain.

5.2.4 Ex-Vivo ICP-MS Analysis

One-week post-injection, each mouse was imaged via MRI to determine if any contrast enhancement was still visible. After confirmation that contrast had returned to baseline, each mouse was sacrificed and various fluids and organs were harvested (urine, bladder, gut, kidneys, liver, lungs, and heart). Each sample was digested in acid and evaluated by ICP-MS to determine Gd^{3+} content. Figure 5.10 shows minimal Gd^{3+} remains in the harvested organs when compared to the initial amount of Gd^{3+} injected. This indicated that although each of the materials has a longer circulation time and retention in the IP space when compared to Gd-DOTA, each is significantly cleared over a 1-week time frame.

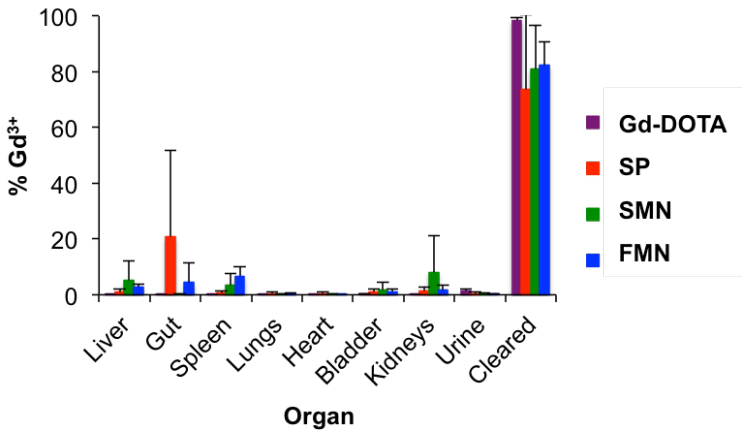

Figure 5.10 Concentration of Gd^{3+} determined by ICP-MS found for different organs and/or fluids excised from mice one week post-injection with Gd-DOTA, **SP**, **SMN**, or **FMN**. Error bars indicate standard deviation for n = 3 mice except for the urine sample of **FMN** where n = 1. Cleared indicates amount injected (64 ppm) subtracted from the total amount of Gd^{3+} accounted for by ICP-MS.

5.3 Conclusions

Investigation of the *in vivo* biodistribution of polymeric and polymeric nanomaterials in healthy C57Bl/6 mice following IP injection demonstrate that a water-soluble polymer, **SP**, has a slightly delayed but similar pathway of renal elimination when compared to the FDA approved small molecule Gd-DOTA. Importantly, we found that the NP formulations of **SMN** and **FMN** are retained significantly longer in the IP space as compared to the small molecule Gd-DOTA. In all cases, after one week post-injection, Gd^{3+} is undetectable by MRI and significantly eliminated one-week post injection as determined by ICP-MS. The exact mechanism of elimination remains unclear at present but preliminary data show that hepatobiliary pathways may play a role. A detailed analysis of these pathways is the subject of ongoing investigations in our laboratory in addition to analogous intravenous studies.

Critically, these results show that particle morphology can greatly influence the behavior of IP administered materials. This is consistent with other research studying the behavior of intravenously injected NPs.[1] We conclude that macromolecular and/or NP formulation is a promising strategy for prolonged retention in the IP-space, which offers potential advantages in the treatment of IP-space malignancies such as metastatic ovarian, pancreatic, and gastric cancers. Current studies in our laboratory aim to determine circulation half lives of these materials as well as biodistribution when injected IP and IV. Through these studies we intend to further define and investigate whether nanoscale

shape is a viable and tunable parameter for optimization of imaging and therapeutic agents meant for *in vivo* use.

5.4 Experimental

5.4.1 General Methods

Gd-DOTA was purchased from Macrocyclics and used without any further purification. **SP**, **SMN**, and **FMN** were prepared as described in Chapter 4. MR images were acquired on a Bruker 7.0 T magnet with Avance II hardware equipped with a 72 mm quadrature transmit/receive coil. Axial MR images were acquired using a standard T_1-weighted sequence with a repetition time of 3249.2 ms, time to echo of 7.6 ms, with fat suppression, a matrix of 256 x 256, field of view (FOV) of 4.00 x 3.00 cm, resolution of 156 x 117 microns, slice thickness of 1.00 mm, inter-slice distance of 1.00 mm, 80 slices. T_1 contrast was determined by selecting regions of interest (ROI) using Software ParaVision Version 5.1 from T_1-T_2 map with the following parameters: Times to echo of 11, 33, 55, 77, and 99 ms and 6 repetition times of 5000, 3000, 2500, 2000, 1500, and 1200 ms, and a flip angle of 180º. Female C57Bl/6 mice weighing 18 grams were purchased from Harlan Sprague Dawley. Animals were anesthetized using a 0.5 – 3 % isofluorane in oxygen solution. All animal procedures were approved by University of California, San Diego's institutional animal care and use committee, protocol S10145. Exova performed ICP-MS analysis.

5.4.2 Analysis of T_1 Data

To correct for scan-to-scan abnormalities in different mice over 7 days, T_1 was normalized to pre-injection phantom relaxivities. Phantoms, consisting of 5 concentrations (0.41, 0.12, 0.033, 0.0095, and 0.0027 mM of Gd^{3+} in H_2O) of Gd-DOTA, **SP**, **SMN** or **FMN**, were included in each scan corresponding to the material injected. Pre-injection relaxivities were generated for each mouse by averaging $1/T_1$ (r_1) values (sec^{-1}) for each phantom concentration over selected slices of the mouse (The selected slices were those in which the organs of interest were visible). Then, for each scanning time point after injection, an average $1/T_1$ for 5 phantoms were calculated and compared to the pre-injection relaxivity value to generate an adjustment factor for the scan of interest. Relaxivity values generated from phantoms for each scan were within (+/-) 1 - 20% of the pre-injection phantom relaxivity. After organ ROI T_1 was converted to $1/T_1$, each was multiplied by the adjustment factor. $1/T_1$ were averaged over each organ and then converted back to T_1 (msec). Normalized T_1 were averaged over three mice for each time point sampled and each material. Error for urinary bladder, liver and brain are standard errors, over three mice for each material, using normalized T_1 for each specific time point sampled. Error for the kidneys, renal cortex and renal pelvis are standard deviation in the average of three mice for the respective organ and time point.

5.4.3 Ex-Vivo ICP-MS Analysis

One week post injection, each mouse was sacrificed using a lethal overdose of >5% isofluorane and selected organs harvested (see Figure 5.10). Nitric acid (900 µL) was added to a measured weight of organ or volume (in the case of urine) and placed on a shaker overnight, vented. After 12 hours, concentrated H_2O_2 (50 µL) was added to each of the organ solutions and placed back on the shaker, vented, for approximately 30 min. An aliquot (200 µL) of the digested organs was added to distilled DI water (800 µL) and submitted to Exova for ICP-MS analysis to determine Gd^{3+} concentration. The final concentration of Gd^{3+} in each organ is shown if Figure 5.10.

5.5 Acknowledgements

Chapter 5, in full, has been submitted for publication: Randolph, Lyndsay M., LeGuyader, Clare L. M., Hahn, Michael E., Andolina, Christopher M., Mattrey, Robert F., Millstone, Jill E., Botta, Mauro, Scadeng, Miriam, and Gianneschi, Nathan C. "*In vivo* MRI reveals Morphology Dependent Biodistribution of Nanoparticles Versus Small Molecule Contrast Agents." *submitted* (2014). The dissertation author is the primary author of this manuscript.

5.6 References

(1) Geng, Y.; Dalhaimer, P.; Cai, S.; Tsai, R.; Tewari, M.; Minko, T.; Discher, D. *Nat. Nanotechnol.* **2007**, *2*, 249.

(2) Christian, D. A.; Cai, S.; Garbuzenko, O. B.; Harada, T.; Zajac, A. L.; Minko, T.; Discher, D. E. *Mol. Pharm.* **2009**, *6*, 1343.

(3) Reddy, L. H.; Murthy, R. S. *Biomed Pap Med Fac Univ Palacky Olomouc Czech Repub* **2004**, *148*, 161.

(4) Howard, K. A.; Paludan, S. R.; Behlke, M. A.; Besenbacher, F.; Deleuran, B.; Kjems, J. *Mol. Ther.* **2009**, *17*, 162.

(5) Jacquet, P.; Averbach, A.; Stuart, O. A.; Chang, D.; Sugarbaker, P. H. *Cancer Chemother. Pharmacol.* **1998**, *41*, 147.

(6) Jung, C.; Kaul, M. G.; Bruns, O. T.; Dučić, T.; Freund, B.; Heine, M.; Reimer, R.; Meents, A.; Salmen, S. C.; Weller, H.; Nielsen, P.; Adam, G.; Heeren, J.; Ittrich, H. *Circ. Cardiovasc. Imaging* **2013**.

(7) Di Pasqua, A. J.; Yuan, H.; Chung, Y.; Kim, J.-K.; Huckle, J. E.; Li, C.; Sadgrove, M.; Tran, T. H.; Jay, M.; Lu, X. *J. Nucl. Med.* **2013**, *54*, 111.

(8) Toraya-Brown, S.; Sheen, M. R.; Baird, J. R.; Barry, S.; Demidenko, E.; Turk, M. J.; Hoopes, P. J.; Conejo-Garcia, J. R.; Fiering, S. *Integr. Biol.* **2013**, *5*, 159.

(9) Markman, M. *Crit. Rev. Oncol. Hemat.* **1999**, *31*, 239.

(10) Xie, Y.; Long, Q.; Wu, Q.; Shi, S.; Dai, M.; Liu, Y.; Liu, L.; Gong, C.; Qian, Z.; Wei, Y.; Zhao, X. *RSC Adv.* **2012**, *2*, 7759.

(11) Di Pasqua, A. J.; Huckle, J. E.; Kim, J. K.; Chung, Y.; Wang, A. Z.; Jay, M.; Lu, X. *Small* **2012**, *8*, 997.

(12) Basel, M. T.; Balivada, S.; Wang, H.; Shrestha, T. B.; Seo, G. M.; Pyle, M.; Abayaweera, G.; Dani, R.; Koper, O. B.; Tamura, M.; Chikan, V.; Bossmann, S. H.; Troyer, D. L. *Int. J. Nanomedicine* **2012**, *7*, 297.

(13) Ishigami, H.; Kitayama, J.; Kaisaki, S.; Hidemura, A.; Kato, M.; Otani, K.; Kamei, T.; Soma, D.; Miyato, H.; Yamashita, H.; Nagawa, H. *Ann. Oncol.* **2010**, *21*, 67.

(14) Morcos, S. K. *Eur. J. Radiol.* **2008**, *66*, 175.

(15) Abdelhalim, M.; Mady, M. *Lipids Health Dis.* **2011**, *10*, 1.

(16) Sadauskas, E.; Wallin, H.; Stoltenberg, M.; Vogel, U.; Doering, P.; Larsen, A.; Danscher, G. *Part. Fibre Toxicol.* **2007**, *4*, 10.

(17) Villaraza, A. J.; Bumb, A.; Brechbiel, M. W. *Chem. Rev.* **2010**, *110*, 2921.